Doctoral Thesis

Quantification of Linear and Non-Linear Flow Behaviours in a Rock Fracture with Complex Void Geometry

Zhihe Wang

Under supervision of

Associate Professor **Chaoshui Xu**

Professor **Peter Dowd**

School of Civil, Environmental and Mining Engineering

Faculty of Engineering, Computer and Mathematical Sciences

The University of Adelaide

August 2019

Content

Publications Included

[1] **Wang, Z.**, C. Xu, P. Dowd, F. Xiong, and H. Wang (2019), A non-linear version of the Reynolds equation for flow in rock fractures with complex void geometries, submitted to *Water Resources Research.*

[2] **Wang, Z.**, C. Xu, and P. Dowd (2019), Perturbation solutions for flow in a slowly varying fracture and the estimation of its transmissivity, *Transport in Porous Media*, 128(1), 97–121.

[3] **Wang, Z.**, C. Xu, and P. Dowd (2018), A modified cubic law for single-phase saturated laminar flow in rough rock fractures, *International Journal of Rock Mechanics and Mining Sciences*, 103, 107–115.

Abstract

Understanding the process of fluid flow through fractured rock in subsurface engineering applications has been an active field of research for decades. Accurate modelling of the process is essential to providing guidance for the development of underground projects and reduction of associated risks. This work focuses on the study of flow behaviours in a single rock fracture with complex void geometry, which is fundamental to larger scale flow-related problems in fractured rocks.

In this research, the effects of aperture variation, tortuosity and local roughness of fracture surfaces are quantified over segmented areas to develop a more accurate modified cubic law that improves flow prediction in rock fractures with rough walls. To account for the flow non-linearity when inertial effects become significant, new approximate analytical solutions of two-dimensional (2D) Navier-Stokes equations are derived under both the pressure boundary condition (PBC) and flow rate boundary condition (FBC) using the perturbation method. Considering the slowly varying feature of fracture apertures, the ratio of aperture variation to fracture length, instead of the commonly used ratio of mean aperture to fracture length, is used as the perturbation parameter in our solutions. The derived solutions are applied to 2D symmetric wedges and sinusoidal fractures, and it is found that the FBC solution provides more accurate flow estimations, due to a more precise quantification of inertial effects. The derived FBC solution is then extended to asymmetric geometries for more realistic representations of fracture voids at pore-scale. A non-linear Reynolds equation is then developed based on the derived FBC solution for rough rock fractures and results have shown a close agreement with both experiments and flow simulations in capturing the non-linear feature of flow through the fracture.

Declarations

I certify that this work contains no material that has been accepted for the award of any other degree or diploma in my name, in any university or other tertiary institution and, to the best of my knowledge and belief, contains no material previously published or written by another person, except where due reference has been made in the text. In addition, I certify that no part of this work will, in the future, be used in a submission in my name, for any other degree or diploma in any university or other tertiary institution without the prior approval of the University of Adelaide and where applicable, any partner institution responsible for the joint-award of this degree.

I acknowledge that copyright of published works contained within this thesis resides with the copyright holder(s) of those works.

I also give permission for the digital version of my thesis to be made available on the web, via the University's digital research repository, the Library Search and also through web search engines, unless permission has been granted by the University to restrict access for a period of time.

Acknowledgements

I would like to first express my gratitude to my supervisors Associate Professor Chaoshui Xu and Professor Peter Dowd for taking me as their PhD student and teaching me how to do proper research. Four years of studying alongside them in Adelaide has been the most important and memorable experience and I will always carry it with me for the rest of my destinations.

I wish to thank group members/great friends Dr Changtai Zhou and Miss Hang Wang for the enormous help I received during my PhD journey and their overly-frequent company, which has obviously prevented me from publishing at least one extra piece of high quality research work.

Many thanks to the colleagues in our school for all those interesting conversations and discussions that have nothing to do with research at all. I want to thank Associate Professor Murat Karakus for his kind help, especially when I had just started the PhD. I also want to thank IT technician Mark Innes for installing COMSOL multiple times for me to ensure that I can always have the latest version. I acknowledge Dr Alison-Jane Hunter for spending time on improving my writing skills and one should note that she will take full responsibility for any inappropriate statements in this acknowledgement.

I thank my basketball mates for those great games and for making sure I get some proper physical exercise every week. I thank all my friends in Adelaide for giving me a true taste of home here. I also thank all my friends in China for keeping me informed about everything that is happening there.

Special thanks to Zona and Dora for letting me feed, pet and play with them, and also for making all my clothes as fluffy as they are.

I share my gratitude to my parents for being consistently supportive of my life-changing decisions.

Lastly, I wish to thank Miss Yusha Li for sharing her life with me. There are definitely more great things ahead of us.

Chapter 1: Introduction

This section presents a brief description of the research background, a review of the current literature, a summary of research objectives and research findings, and finally an outline of the thesis. The work presented in this thesis aims to address the problem of fluid flow in a rock fracture with the complex void geometry and provides conceptual flow models using semi-analytical and analytical approaches. Note this introduction is closely related to the presented work and does not mean to provide a comprehensive review of research that covers the whole area of the problem. Other important aspects related to this problem, not covered in this thesis, include techniques for measuring fracture void geometry, aperture distribution analysis, experimental laboratory work and etc.

1.1 Fluid flow in rock fractures

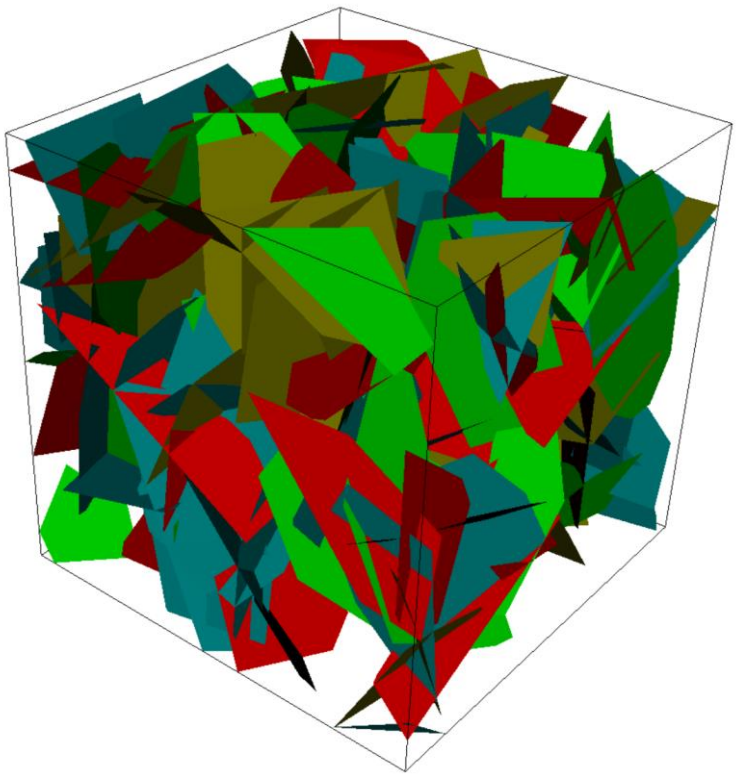

Figure 1.1 A randomly generated DFN model using FracSim3D (Xu and Dowd 2010).

For decades, the process of fluid flowing through subsurface fractured rock masses has interested and puzzled engineers and researchers in different fields. The process is critical for a wide range of applications from the extraction of natural resources to hazardous waste disposal. These underground engineering applications require an in-depth knowledge of the

process to achieve maximal performance with minimal risk (Berkowitz 2002; Hunt and Sahimi 2017; Jing and Stephansson 2007; Pyrak-Nolte et al. 1988; Tsang and Tsang 1989; Zimmerman and Bodvarsson 1996). The difficulty of predicting flow in fractured rocks is strongly associated with the anisotropic behaviour of rocks as a result of natural or man-made fractures on varying scales (Berkowitz 2002; Xu et al. 2015). Rock fractures often have a dominant impact on the hydraulic properties of rock masses due to the large gap between their permeability and matrix permeability, especially for low permeability rocks such as granite. In theory, each fracture of a fracture network system should be considered when working on the problem of flow in fractured rocks (Jing and Stephansson 2007), which leads to the discrete fracture network (DFN) approach (see Figure 1.1). Therefore, as a basic element, understanding the flow behaviours in a single rock fracture is fundamental to studying flow problems in fractured rock masses (Brush and Thomson 2003; Zimmerman 2005).

1.1.1 Fracture void geometry

When a rock fracture is considered bounded by two surfaces as shown in Figure 1.2, the fracture void is essentially the gap between the top and bottom surfaces that provides the space for fluid to pass through under a given pressure gradient. The hydraulic properties of the fracture are thus controlled by the behaviours of flow when travelling within the fracture void. In general, surface roughness and contact are widely considered to have significant impact on the fracture hydraulic properties, although contact areas can be seen as a result of the variable aperture field due to surface roughness (Brown 1987; Zimmerman and Bodvarsson 1996).

For rock fractures, both surfaces are mostly rough with relatively small-scale asperities (Oron and Berkowitz 1998; Patir and Cheng 1978; Zimmerman et al. 1991). These roughness and asperities contribute to a variable aperture field located on an uneven mid-surface, and provide additional resistance to flow and reduce progressively the overall fracture permeability as the surface roughness increases (Brush and Thomson 2003; Lee et al. 2014). The well-known parabolic velocity profile for flow within two perfectly smooth and parallel surfaces breaks down when the surface roughness is introduced; increasingly more eddies are formed near the asperities as the velocity increases to enhance the inertial effects (Zou et al. 2017). Different quantifications of surface roughness have been used to study surface properties such as friction and light reflection, in which surface profiles are statistically characterized using, for example, root mean square (RMS), the first derivative of the *RMS*, the second derivative of the *RMS*, Z_4, structure function and fractal dimension (Sayles and Thomas 1977; Yu and

Vayssade 1991). In the field of rock engineering, the joint roughness coefficient (*JRC*) is widely used to quantify the effect of roughness on the shear strength of fractures and is also correlated with the hydraulic properties of fractures (Barton 1982; Barton 1973). For hydraulic properties of fractures, a perhaps more commonly used parameter to describe fracture surface roughness is the relative roughness, defined as the ratio of the aperture standard deviation to mean aperture (Brush and Thomson 2003; Zimmerman et al. 1991).

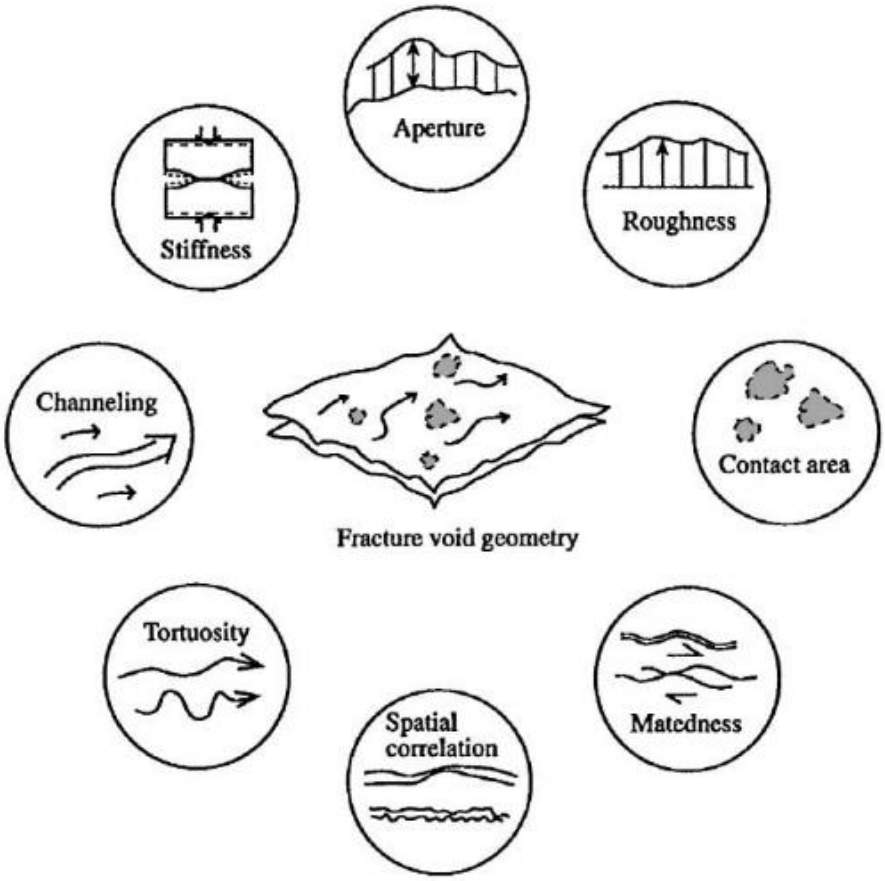

Figure 1.2 Fracture void geometry and associated fracture properties, after Hakami (1995).

Contact can be defined as the fracture areas where the aperture equals zero or a defined value (Hakami 1995; Walsh 1981). Since the matrix permeability is considered negligible compared with the fracture permeability, fracture contact areas can effectively block and alter flow pathways. With the increase of fracture contact areas, flow is more suppressed to limited tortuous pathways with less available space for fluid to pass, and hence the fracture permeability is reduced accordingly (Zimmerman et al. 1992). Walsh (1981) applied the effective medium approach to derive an analytical solution for the effective permeability of a fracture with uniformly-distributed circular contact areas. A later extension by Obdam and Veling (1987) considered the contact areas to be elliptical. However, contact areas in a real

rock fracture usually have irregular shapes and complex spatial distributions, the practical applications of these analytical expressions are therefore limited (Zimmerman et al. 1992).

1.1.2 Governing equations

The process of single-phase saturated incompressible flow in a rock fracture at steady-state is governed by the three-dimensional (3D) Navier-Stokes equations (NSE) (Brush and Thomson 2003; Zimmerman and Bodvarsson 1996). With mass conservation, they can be expressed as:

$$\rho(\boldsymbol{u} \cdot \nabla)\boldsymbol{u} = -\nabla P + \mu \nabla^2 \boldsymbol{u} \tag{1.1}$$

$$\nabla \cdot \boldsymbol{u} = 0 \tag{1.2}$$

where $\boldsymbol{u}$ is the velocity, P is the pressure and μ is the dynamic viscosity. The first term on the left-hand sides of equations (1.1) is the advective term that accounts for inertia forces, the second term represents the pressure gradient and the last term describes the viscous forces. The NSE become Stokes equations (SE) when the inertial terms are negligibly small compared to the viscous terms (i.e., Reynolds number Re=0), which is common to many subsurface applications where flow travels very slowly within the fractures (Oron and Berkowitz 1998; Zimmerman et al. 1991). The SE can be expressed as:

$$\nabla P = \mu \nabla^2 \boldsymbol{u} \tag{1.3}$$

An exact analytical solution to NSE is restricted to a few special cases e.g. Poiseuille flow through planar plates and the Jeffery-Hamel problem (Nicholl et al. 1999; Oron and Berkowitz 1998). However, the complexity of 3D fracture void geometry obviously prohibits any direct use of these solutions. There are many numerical approaches to solving the 3D NSE in variable aperture fields that are randomly generated or measured directly from real rock fractures (Brush and Thomson 2003; Nazridoust et al. 2006; Zimmerman et al. 2004). These approaches include the finite difference method (FDM), the finite volume method (FVM), and the finite element method (FEM). Although numerical solutions of the NSE provide accurate flow predictions, the current computational costs have constrained the application to small-scale problems (Brush and Thomson 2003; Xiong et al. 2018).

1.2 Traditional approaches to modelling fluid flow in a single rock fracture

When studying the process of fluid flow in fractured rocks, compromises are often made in the representation of fracture geometry and/or selection of flow governing equations to enable a reasonable and applicable approach to the problem. The choices made for the fracture

representation and flow governing equation are often interconnected to some extent. The parallel planar plates representation of fracture geometry is used in the derivation of the well-known cubic law (Snow 1969; Witherspoon et al. 1980), as shown in Figure 1.3. The Reynolds equation can be obtained if the fracture geometry is assumed to vary slowly over the aperture field (Brown 1987; Zimmerman et al. 1991). A number of asymptotic solutions to the NSE have been derived for apertures that vary in a sinusoidal fashion (Hasegawa and Izuchi 1983; Kitanidis and Dykaar 1997; Sisavath et al. 2003). Each of these approaches has its own merits when applied to the same problem, although emphases are placed upon different aspects.

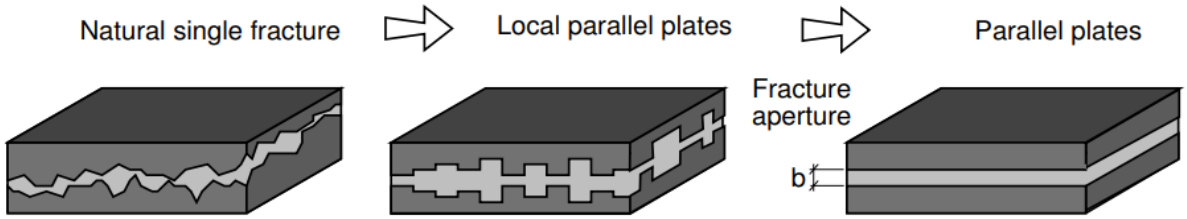

Figure 1.3 Illustration of the concept of the parallel plates assumption, after Dietrich et al. (2005).

1.2.1 Cubic law

The cubic law (CL) is arguably the most well-known model for flow in rock fractures (Dippenaar and Van Rooy 2016; Zimmerman 2005). Since the fracture aperture is normally on a much smaller scale relative to fracture length and width, a fairly reasonable simplification is to neglect the aperture variability and assume that the rock fracture is bounded by two parallel planar walls with a constant aperture (Snow 1969). With no-flux and no-slip boundary for the walls, the CL can be analytical derived from the NSE in the form (Brush and Thomson 2003):

$$Q = -\frac{b^3 W}{12\mu}\frac{\Delta P}{L} \tag{1.4}$$

where Q is the volumetric flow rate, b is the fracture aperture, W is the fracture width and L is the fracture length. The application of equation (1.4) is straight-forward. Dynamic viscosity (μ) is a known parameter for the chosen fluid for most of the practices regarding flow in subsurface fractured rocks; length, width and aperture are the dimensions of the fracture; with a known pressure boundary condition, the volumetric flow rate can be easily obtained from equation (1.4). The hydraulic properties of the fracture, e.g. permeability and transmissivity, can also be assessed as shown in Table 1.1. In general, all these parameters are used to describe how well flow can pass through rock fractures under a given pressure gradient. The validity of the CL

has been previously evaluated by straight flow experiments in tension fractures within granite samples, with a deviation factor varying from 1.05 to 1.21 (Witherspoon et al. 1980).

Table 1.1 Definitions of various fracture hydraulic properties

Terms	Definitions	References
Transmissivity	$T = \frac{b^3}{12\mu}$	(Nicholl et al. 1999)
Permeability	$k = \frac{b^2}{12}$	(Zimmerman et al. 1991)
Conductivity	$C = \frac{\rho g b^2}{12\mu}$	(Witherspoon et al. 1980)
Resistance	$R = \frac{12\mu L}{\rho g b^3 W}$	(Yang et al. 1995)
Frictional factor	$F = \frac{2\Delta P \cdot b^3}{\rho L Q^2}$	(Nazridoust et al. 2006)

1.2.2 Reynolds equation

The CL assumption breaks down for rock fractures with rough surfaces where the aperture can no longer be considered constant throughout the fracture plane (Basha and El-Asmar 2003). As a further extension to CL, the Reynolds equation (RE) is commonly used to model flow in rock fractures with a variable aperture field (Zimmerman et al. 1991), and is given by

$$\frac{\partial}{\partial x}\left[b^3(x,y)\frac{\partial P}{\partial x}\right] + \frac{\partial}{\partial y}\left[b^3(x,y)\frac{\partial P}{\partial y}\right] = 0 \tag{1.5}$$

The RE can be derived from the NSE under certain geometrical and kinematical conditions (Zimmerman 2005). It can also be derived simply by assuming that the CL is applicable at each local position and therefore, the RE is also referred as the local cubic law (Zimmerman et al. 1991). Oron and Berkowitz (1998) concluded that the RE is valid when the following geometrical and kinematical conditions are met:

$$\varepsilon \ll 1, \qquad \delta^2 \ll 1, \qquad Re \cdot Max(\varepsilon, \delta) \ll 1$$

where ε and δ are, respectively, the local roughness parameter and aspect ratio defined in Oron and Berkowitz (1998), their mathematical expressions can also be found in Section 2.2.1. These conditions essentially define a slowly varying aperture field (i.e., gradual aperture variation

along the flow direction) and negligible inertial effects relative to viscous effects, which, in practice, can be considered to hold for flow in rock fractures. More specifically for the creeping flow condition, Brush and Thomson (2003) found that, compared with the SE, the error produced by using the RE is within ±10% when the following geometrical conditions are met

$$\sigma_b/b_m < 1, \qquad \sigma_b/\lambda_b < 0.2, \qquad b_m/\lambda_b < 0.5$$

where b_m is the mean aperture, σ_b is the aperture standard deviation and λ_b is the aperture correlation length. The RE enables the incorporation of aperture variation along both directions of the fracture plane and in-plane tortuosity, which are not considered in the CL. It also agrees qualitatively with the laboratory observation that the fracture hydraulic properties depend mainly on the variability of the aperture field and extent of fracture surface contact (Brush and Thomson 2003; Konzuk and Kueper 2004). An over-estimation of 20% in the flow rate was found when comparing the RE with flow tests in fracture replicas in Yeo et al. (1998). Similar flow over-estimation is also observed in Brush and Thomson (2003); Nicholl et al. (1999).

1.2.3 Approximate analytical solution

In principle, the RE uses the same fundamental assumption of flow between planar plates, only the CL relationship is applied locally at each position of the fracture rather than globally. As a result of the one-dimensional (1D) Poiseuille flow assumption, the flow component perpendicular to the fracture plane is assumed negligible in the RE and inertial effects are ignored (Basha and El-Asmar 2003; Oron and Berkowitz 1998). To account for the neglected flow features, approximate analytical solutions to the two-dimensional (2D) NSE are derived as further extensions to the CL assumption.

Wang (1978) derived an approximate analytical solution to Stokes flow using the perturbation method for a 2D fracture with a periodic variation geometry, and the ratio of mean aperture to fracture length was used as the perturbation parameter. Hasegawa and Izuchi (1983) used the same perturbation parameter to obtain a perturbation solution to the 2D NSE under the pressure boundary condition (PBC) for a channel with a sinusoidal top wall and a flat bottom wall. Kitanidis and Dykaar (1997) conducted a similar perturbation analysis of Stokes flow in a fracture bounded by two sinusoidal walls, where the dissipated energy due to the viscous force is balanced by the work done by the surface force. Basha and El-Asmar (2003) conducted and evaluated perturbation solutions for flow in fractures with various geometrical configurations (Figure 1.4) using the same perturbation parameter. Sisavath et al. (2003) applied a different perturbation parameter, the ratio of aperture amplitude to fracture length,

and derived the perturbation solution to the problem of two-dimensional Stokes flow in a fracture with two sinusoidal walls under a flow rate boundary condition (FBC). The PBC and FBC solutions generally take these forms respectively:

$$Q = Q_0 + \epsilon Q_1 + \epsilon^2 Q_2 + \cdots \tag{1.6}$$

$$\Delta P = \Delta P_0 + \epsilon \Delta P_1 + \epsilon^2 \Delta P_2 + \cdots \tag{1.7}$$

Apparently, the derived 2D solutions cannot directly solve flow problems in realistic 3D rock fractures (Zimmerman 2005). However, these solutions can provide theoretical understanding of the phenomena including the permeability reduction and generation of immobile zones due to surface roughness (Kitanidis and Dykaar 1997; Sisavath et al. 2003). In addition, the validity of the CL and RE are often examined using these analytical solutions as references (Yeo et al. 1998). These derived expressions can also potentially be extended to develop conceptual models for solving more realistic flow problems in fracture networks (Basha and El-Asmar 2003).

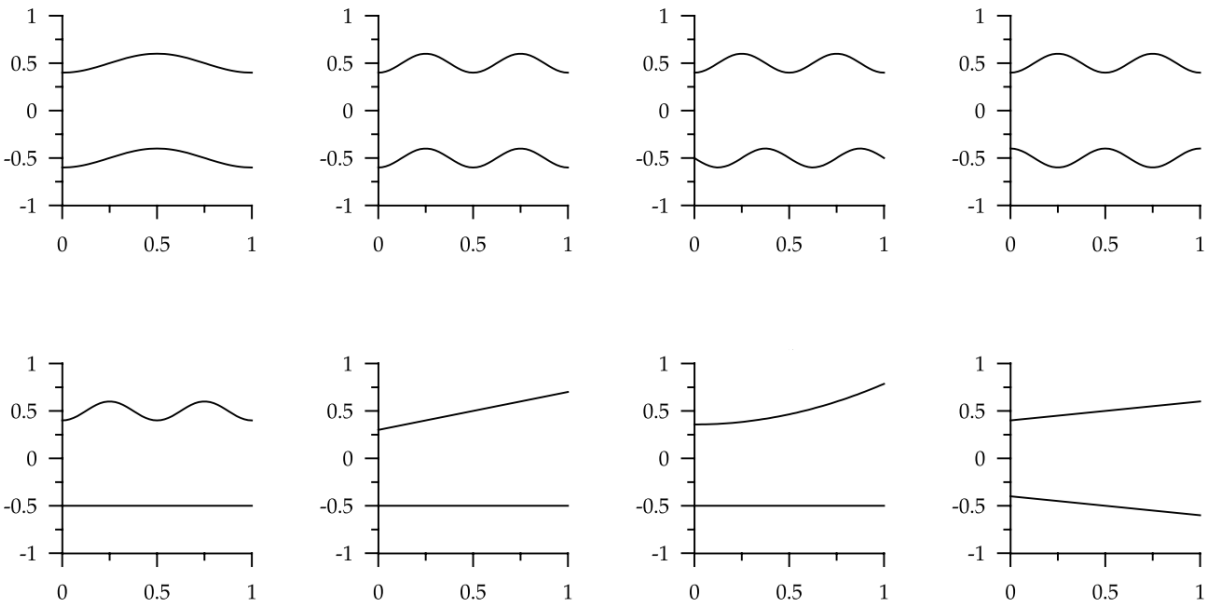

Figure 1.4 Fracture geometry configurations, after Basha and El-Asmar (2003).

1.3 Recent development in cubic law based models

The limitations of the CL and RE in quantifying the hydraulic properties of fractures with complex void geometries have long been recognized from theoretical analyses and experimental studies (Hasegawa and Izuchi 1983; Nicholl et al. 1999; Oron and Berkowitz 1998; Zimmerman and Bodvarsson 1996). More recently, solving the NSE and SE by

numerical approaches has also shown that both the CL and RE tend to over-estimate the overall flow, even with the same measured aperture fields (Brush and Thomson 2003; Xiong et al. 2011). Further modifications and improvements have been attempted to 'correct' both the CL and RE for more accurate flow prediction in rough rock fractures. These approaches generally include modifications at the scale of a single fracture and at the local pore-scale (Konzuk and Kueper 2004).

1.3.1 Modification at the scale of a single facture

Table 1.2. Summary of typical formulas for equivalent hydraulic aperture b_H.

Notations	Expressions	References
AM	$b_H = \frac{1}{WL}\int_0^W \int_0^L b(x,y)dxdy$	(Brown 1987)
GM	$b_H = b_M\left[1+\left(\frac{\sigma_b}{b_m}\right)^2\right]^{-0.5}$	(Renshaw 1995)
ZRF	$b_H = b_M\left(\frac{1-\alpha}{1+\alpha}\right)^{1/3}$	(Walsh 1981)
PC	$b_H = b_m\left(1-0.9e^{-0.56\langle b\rangle/\sigma_b}\right)^{1/3}$	(Patir and Cheng 1978)
BA	$b_H = \frac{{b_M}^2}{JRC^{2.5}}$	(Barton 1982)
NA	$b_H = \frac{b_m-\sigma_b}{(1+\theta)^{1/3}}$	(Nazridoust et al. 2006)

For the application of the CL in fractures with non-planar surfaces, an extra factor f is often introduced to account for the additional geometrical effect. The modified version of the CL is then given by:

$$Q = -\frac{b^3 W\Delta P}{12\mu L}f = -\frac{{b_H}^3 W\Delta P}{12\mu L} \tag{1.8}$$

where b_H is the equivalent hydraulic aperture. b_H can be formulated using statistical approaches, empirical approaches or a combination of both to include parameters such as mechanical aperture b_M, mean aperture b_m, aperture standard deviation σ_b, contact ratio α, *JRC* and tortuosity θ. Some typical formulas are listed in Table 1.2. The incorporation of geometrical effects on the flow behaviours provides a direct approach for the correction of the CL. However,

both statistical and empirical approaches fail to consider accurately the mid-surface undulation and flow channelling effects (Brush and Thomson 2003). The application of these approaches is therefore limited to fractures with little flow tortuosity and/or insignificant surface contact. For example, Konzuk and Kueper (2004) conducted a flow experiment in a rough single rock fracture and found that AM, GM and ZRF can over-estimate flow by a factor over 1.5.

1.3.2 Modification at the pore-scale

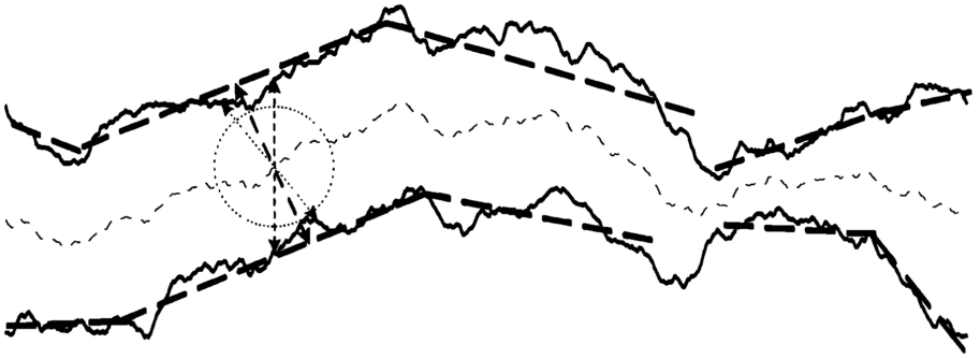

Figure 1.5 Different definitions of fracture aperture with the short-dashed arrow representing vertical aperture, the dotted arrow representing the aperture perpendicular to the cell centreline (Ge 1997) and the bold dashed arrow representing segment aperture, after Oron and Berkowitz (1998).

The overall fracture hydraulic properties depend on the geometrical and topological manner in which the pore-scale cells are located, as measured from rock fractures (Zimmerman and Bodvarsson 1996). To account for the hydraulic properties of local pore-scale cells, several alternative definitions of aperture have been developed based on the measured vertical aperture that represents the separation distance between top and bottom surfaces. Ge (1997) suggested that the flow direction follows mainly the direction of the average angle of top and bottom surfaces between adjacent measured vertical apertures and hence the aperture should be measured perpendicular to the local flow direction (see Figure 1.5). Brush and Thomson (2003) have defined the aperture in a similar way, with the difference that the flow direction is assumed to follow the direction of the local mid-surface, which connects the centre points of two measured apertures. Under the required geometrical conditions, aperture can also be defined over a segment that represents the average undulation of the top and bottom surfaces at a predefined scale, as suggested in Oron and Berkowitz (1998). When an aperture definition is selected, the link transmissivity T_L ($T_L=b_L^3$) between adjacent apertures can be obtained using established averaging schemes (Nicholl et al. 1999), which include:

Arithmetic average:

$$b_L{}^3 = \frac{b_i{}^3 + b_j{}^3}{2} \tag{1.9}$$

Harmonic average:

$$b_L{}^3 = \frac{2b_i{}^3 b_j{}^3}{b_i{}^3 + b_j{}^3} \tag{1.10}$$

Midpoint average:

$$b_L{}^3 = \left(\frac{b_i + b_j}{2}\right)^3 \tag{1.11}$$

Harmonic average:

$$b_L{}^3 = \sqrt{b_i{}^3 b_j{}^3} \tag{1.12}$$

where b_L is the approximated local aperture, b_i and b_j are adjacent apertures of the local cell. Considering the geometrical effect at local pore-scale, a modified version of the RE can then be derived as given by

$$\frac{\partial}{\partial x}\left[T_L(x,y)\frac{\partial P}{\partial x}\right] + \frac{\partial}{\partial y}\left[T_L(x,y)\frac{\partial P}{\partial y}\right] = 0 \tag{1.13}$$

For different aperture definitions, modified versions of the CL can also be formulated accordingly. The improvements to the standard CL and RE with additional pore-scale modifications are evident. Konzuk and Kueper (2004) found that using the perpendicular aperture and GM approximation method, the error associated with the modified CL was reduced by over 30%; and for the modified RE, around 18% of error reduction was observed when similar pore-scale modifications were incorporated. However, many of these modifications are incorporated based on assumed local flow direction and/or subjective choice of averaging scheme, and their performance can sometimes be affected by the resolution of aperture fields (Oron and Berkowitz 1998).

1.4 Research objectives and contributions

The main objective of this work is to broaden the understanding of the geometrical and kinematical impacts on fracture hydraulic properties and establish mathematical models to quantify accurately the flow behaviour in rock fractures with complex void geometries. This work has contributed to knowledge of the field in the following aspects:

1. Quantification of aperture variation, tortuosity and local roughness effects on flow behaviours at segment-scale to improve the overall flow prediction at single-fracture-scale under the linear flow condition.
2. Derivation of approximate analytical solutions to the two-dimensional Navier-Stokes equations using the perturbation method to extend the scope of application with more accurate quantification of inertial effects.
3. Establishment of geometrical and kinematical criteria for the validity evaluation of the cubic law and Reynolds approximation based on the derived perturbation solutions.
4. Development of a non-linear model for flow in a rock fracture with complex void geometry considering both geometrical and kinematical effects.

1.5 Thesis outline

In Chapter 2, an improved version of the cubic law is proposed by incorporating the effects of flow tortuosity, aperture variation and local roughness. The model development starts using proper assumptions for the characteristic flow direction over a fracture segment under given geometrical criteria from previous studies. The flow tortuosity and aperture variation are then quantified according to the assumed flow direction throughout the fracture area. The local roughness of top and bottom surfaces is approximated statistically by considering the fact that greater pressure drops always take place in smaller apertures. Finally, a modified cubic law is proposed by incorporating all these geometrical effects. The proposed model is validated against numerical solution of the three-dimensional Navier-Stokes equations using synthetically generated fractures with different surface roughness quantified by Z_2 and *JRC*.

Approximate analytical solutions are derived in Chapter 3 using the perturbation method for more accurate quantification of the geometrical and kinematical effects on flow in two-dimensional symmetric fractures. The ratio of aperture variation to length is used as the perturbation parameter, instead of the commonly used ratio of mean aperture to length. This allows a less strict geometrical requirement for the application of the perturbation solutions, hence extending the scope of application to a wider range of fracture cases. The perturbation solutions are derived for both the pressure boundary condition (PBC) and flow rate boundary solution (FBC); the solutions are evaluated by flow simulation using the Navier-Stokes equations. Compared with the PBC solution, the FBC solution demonstrates a closer agreement with flow simulation due to its more accurate quantification of inertial effects.

For Chapter 4, the FBC perturbation solution derived in Chapter 3 is extended to asymmetric cases to quantify more realistically the flow behaviours in fractures at pore-scale. The effects of aperture variation, aspect ratio, fracture asymmetry and Reynolds number on the hydraulic properties of local cells are quantified and discussed. A non-linear flow model is developed based on the extended FBC solution and its validity has been verified with flow experiments and simulations in rock fractures with different degrees of relative roughness and contact ratios. Results show that the proposed model demonstrates a non-linear flow behaviour similar to that from simulations as the Reynolds number increases. This non-linear feature is not seen in previously developed cubic law based models. The developed non-linear flow model can be used as an alternative to the standard Reynolds equation to study flow-related problems in fractured rocks, particularly when inertial effects cannot be ignored.

Finally, Chapter 5 summarizes the overall work presented in the thesis, in terms of major findings, limitations and potential follow-up work in the future.

The developed models and derived solutions all start with the attempt to quantify flow behaviours in two-dimensional fracture geometries. Therefore, to avoid any confusion, one may note that for such a two-dimensional geometry, the vertical and horizontal axes considered in the remaining chapters follow, respectively, the fracture aperture and flow directions.

References

Barton, N.: Review of a new shear-strength criterion for rock joints. Eng. Geol. 7, 287–332 (1973). doi:10.1016/0013-7952(73)90013-6

Barton, N.: Modelling rock joint behaviour from in situ block tests: implications for nuclear waste repository design. Office of Nuclear Waste Isolation, Columbus, OH, ONWI-308 (1982)

Basha, H.A., El-Asmar, W.: The fracture flow equation and its perturbation solution. Water Resour. Res. 39, 1365 (2003). doi:10.1029/2003WR002472

Berkowitz, B.: Characterizing flow and transport in fractured geological media: A review. Adv. Water Resour. 25, 861–884 (2002). doi:10.1016/S0309-1708(02)00042-8

Brown, S.R.: Fluid flow through rock joints: the effect of surface roughness. J. Geophys. Res. 92, 1337–1347 (1987). doi:10.1029/JB092iB02p01337

Brush, D.J., Thomson, N.R.: Fluid flow in synthetic rough-walled fractures: Navier-Stokes, Stokes, and local cubic law simulations. Water Resour. Res. 39, 1085 (2003). doi:10.1029/2002WR001346

Dietrich, P., Helmig, R., Sauter, M., Hötzl, H., Köngeter, J., Teutsch, G.: Flow and Transport in Fractured Porous Media. Springer, Berlin, Heidelberg (2005)

Dippenaar, M.A., Van Rooy, J.L.: On the cubic law and variably saturated flow through discrete open rough-walled discontinuities. Int. J. Rock Mech. Min. Sci. 89, 200–211 (2016). doi:10.1016/j.ijrmms.2016.09.011

Ge, S.: A governing equation for fluid flow in rough fractures. Water Resour. Res. 33, 53–61 (1997). doi:10.1029/96WR02588

Hakami, E.: Aperture distribution of rock fractures. Ph.D. Thesis, (1995)

Hasegawa, E., Izuchi, H.: On Steady Flow through a Channel Consisting of an Uneven Wall and a Plane Wall Part 1. Case of No Relative Motion in Two Walls. Bull. JSME. 26, 532–542 (1983). doi:10.1248/cpb.37.3229

Hunt, A.G., Sahimi, M.: Transport and Reaction in Porous Media: Percolation Scaling, Critical-Path Analysis, and Effective-Medium Approximation. Rev. Geophys. (2017). doi:10.1002/2017RG000558

Jing, L., Stephansson, O.: Discrete Fracture Network (DFN) Method. Dev. Geotech. Eng. 85, 365–398 (2007). doi:10.1016/S0165-1250(07)85010-3

Kitanidis, P.K., Dykaar, B.B.: Stokes flow in a slowly varying two-dimensional periodic pore. Transp. Porous Media. 26, 89–98 (1997). doi:10.1023/A:1006575028391

Konzuk, J.S., Kueper, B.H.: Evaluation of cubic law based models describing single-phase flow through a rough-walled fracture. Water Resour. Res. 40, 1–17 (2004). doi:10.1029/2003WR002356

Lee, S.H., Lee, K.K., Yeo, I.W.: Assessment of the validity of Stokes and Reynolds equations for fluid flow through a rough-walled fracture with flow imaging. Geophys. Res. Lett. 41, 4578–4585 (2014). doi:10.1002/2014GL060481

Nazridoust, K., Ahmadi, G., Smith, D.H.: A new friction factor correlation for laminar, single-

phase flows through rock fractures. J. Hydrol. 329, 315–328 (2006). doi:10.1016/j.jhydrol.2006.02.032

Nicholl, M.J., Rajaram, H., Glass, R.J., Detwiler, R.: Saturated flow in a single fracture: Evaluation of the Reynolds equation in measured aperture fields. Water Resour. Res. 35, 3361–3373 (1999). doi:10.1029/1999WR900241

Obdam, A.N.M., Veling, E.J.M.: Elliptical inhomogeneities in groundwater flow - An analytical description. J. Hydrol. 95, 87–96 (1987). doi:10.1016/0022-1694(87)90117-X

Oron, A.P., Berkowitz, B.: Flow in rock fractures: The local cubic law assumption reexamined. Water Resour. Res. 34, 2811–2825 (1998). doi:10.1029/98WR02285

Patir, N., Cheng, H.S.: An Average Flow Model for Determining Effects of Three-Dimensional Roughness on Partial Hydrodynamic Lubrication. J. Lubr. Technol. 100, 12–17 (1978). doi:10.1115/1.3453103

Pyrak-Nolte, L.J., Cook, N.G.W., Nolte, D.D.: Fluid percolation through single fractures. Geophys. Res. Lett. 15, 1247–1250 (1988). doi:doi:10.1029/GL015i011p01247

Renshaw, C.E.: On the relationship between mechanical and hydraulic apertures in rough-walled fractures. J. Geophys. Res. 100, 24629–24636 (1995). doi:10.1029/95JB02159

Sayles, R.S., Thomas, T.R.: The spatial representation of surface roughness by means of the structure function: A practical alternative to correlation. Wear. 42, 263–276 (1977). doi:10.1016/0043-1648(77)90057-6

Sisavath, S., Al-Yaaruby, a., Pain, C.C., Zimmerman, R.W.: A Simple Model for Deviations from the Cubic Law for a Fracture Undergoing Dilation or Closure. Pure Appl. Geophys. 160, 1009–1022 (2003). doi:10.1007/PL00012558

Snow, D.T.: Anisotropie Permeability of Fractured Media. Water Resour. Res. 5, 1273–1289 (1969). doi:10.1029/WR005i006p01273

Tsang, Y.W., Tsang, C.F.: Flow channeling in a single fracture as a two-dimensional strongly heterogeneous permeable medium. Water Resour. Res. 25, 2076–2080 (1989). doi:10.1029/WR025i009p02076

Walsh, J.B.: Effect of pore pressure and confining pressure on fracture permeability. Int. J. Rock Mech. Min. Sci. Geomech. Abstr. 18, 429–435 (1981). doi:http://dx.doi.org/10.1016/0148-9062(81)90006-1

Wang, C.-Y.: Drag due to a striated boundary in slow Couette flow. Phys. Fluids. 21, 697 (1978). doi:10.1063/1.862279

Witherspoon, P.A., Wang, J.S.Y., Iwai, K., Gale, J.E.: Validity of Cubic Law for fluid flow in a deformable rock fracture. Water Resour. Res. 16, 1016–1024 (1980). doi:10.1029/WR016i006p01016

Xiong, F., Jiang, Q., Ye, Z., Zhang, X.: Nonlinear flow behavior through rough-walled rock fractures: The effect of contact area. Comput. Geotech. 102, 179–195 (2018). doi:10.1016/j.compgeo.2018.06.006

Xiong, X., Li, B., Jiang, Y., Koyama, T., Zhang, C.: Experimental and Numerical Study of the Geometrical and Hydraulic Characteristics of a Single Rock Fracture during Shear. Int. J. Rock Mech. Min. Sci. 48, 1292–1302 (2011). doi:10.1016/B978-0-12-408083-6.00022-2

Xu, C., Dowd, P.: A new computer code for discrete fracture network modelling. Comput. Geosci. 36, 292–301 (2010). doi:10.1016/j.cageo.2009.05.012

Xu, C., Dowd, P.A., Tian, Z.F.: A simplified coupled hydro-thermal model for enhanced geothermal systems. Appl. Energy. 140, 135–145 (2015). doi:10.1016/j.apenergy.2014.11.050

Yang, G., Myer, L.R., Brown, R., Cook, G.W.: Microscopic analysis of macroscopic transport properties of single natural fractures using graph theory alogrithms. Geophys. Res. Lett. 22, 1429–1432 (1995)

Yeo, I.W., De Freitas, M.H., Zimmerman, R.W.: Effect of shear displacement on the aperture and permeability of a rock fracture. Int. J. Rock Mech. Min. Sci. 35, 1051–1070 (1998). doi:10.1016/S0148-9062(98)00165-X

Yu, X., Vayssade, B.: Joint profiles and their roughness parameters. Int. J. Rock Mech. Min. Sci. 28, 333–336 (1991). doi:10.1016/0148-9062(91)90598-G

Zimmerman, R., Bodvarsson, G.: Hydraulic conductivity of rock fractures. Transp. Porous Media. 23, 1–30 (1996). doi:10.1007/BF00145263

Zimmerman, R.W.: Fluid Flow in Rock Fractures. In: Proc. 11th Int. Conf. on Computer Methods and Advances in Geomechanics. pp. 89–107. , Turin, Italy (2005)

Zimmerman, R.W., Al-Yaarubi, A., Pain, C.C., Grattoni, C.A.: Non-linear regimes of fluid flow in rock fractures. Int. J. Rock Mech. Min. Sci. 41, 1–7 (2004). doi:10.1016/j.ijrmms.2004.03.036

Zimmerman, R.W., Chen, D.W., Cook, N.G.W.: The effect of contact area on the permeability of fractures. J. Hydrol. 139, 79–96 (1992). doi:10.1016/0022-1694(92)90196-3

Zimmerman, R.W., Kumar, S., Bodvarsson, G.S.: Lubrication theory analysis of the permeability of rough-walled fractures. Int. J. Rock Mech. Min. Sci. 28, 325–331 (1991). doi:10.1016/0148-9062(91)90597-F

Zou, L., Jing, L., Cvetkovic, V.: Shear-enhanced nonlinear flow in rough-walled rock fractures. Int. J. Rock Mech. Min. Sci. 97, 33–45 (2017). doi:10.1016/j.ijrmms.2017.06.001

Chapter 2: A Modified Cubic Law for Single-Phase Saturated Laminar Flow in Rough Rock Fractures

Statement of Authorship

Title of Paper	A modified cubic law for single-phase saturated laminar flow in rough rock fractures
Publication Status	☑ Published ☐ Accepted for Publication ☐ Submitted for Publication ☐ Unpublished and Unsubmitted w ork w ritten in manuscript style
Publication Details	Wang, Z., C. Xu, and P. Dowd (2018), A modified cubic law for single-phase saturated laminar flow in rough rock fractures, International Journal of Rock Mechanics and Mining Sciences, 103, 107–115.

Principal Author

Name of Principal Author (Candidate)	Zhihe Wang
Contribution to the Paper	Development of the methods, conduct of the analysis, validation and drafting the manuscript.
Overall percentage (%)	70%
Certification:	This paper reports on original research I conducted during the period of my Higher Degree by Research candidature and is not subject to any obligations or contractual agreements with a third party that would constrain its inclusion in this thesis. I am the primary author of this paper.
Signature	Date 22/08/2019

Co-Author Contributions

By signing the Statement of Authorship, each author certifies that:

i. the candidate's stated contribution to the publication is accurate (as detailed above);

ii. permission is granted for the candidate in include the publication in the thesis; and

iii. the sum of all co-author contributions is equal to 100% less the candidate's stated contribution.

Name of Co-Author	Chaoshui Xu
Contribution to the Paper	Supervision, design of the work and reviewing the manuscript.
Signature	Date 22/08/2019

Name of Co-Author	Peter Dowd
Contribution to the Paper	Supervision, design of the work and reviewing the manuscript.
Signature	Date 21/8/2019

Please cut and paste additional co-author panels here as required.

Abstract

The purpose of the study is to develop a modified cubic law (MCL) for single-phase saturated laminar flow in rough rock fractures. Based on the fundamental assumptions made for the cubic law (CL), the proposed MCL incorporates modifications to the aperture field by considering flow tortuosity, aperture variation and local roughness effects. We assess the performance of the MCL by applying it to synthetic fractures with different surface roughness and compare the outputs to numerical simulation results from solving the Navier-Stokes equations and previous versions of CL-based models. In general, the MCL performs well in predicting the volumetric flow rate in synthetic fractures with deviations (*D)* from simulation results ranging from -11.13% to 8.35% and an average effective deviation ($\overline{|D|}$) of 4.72%. The proposed model retains the simplicity of CL-based models and improves the accuracy of flow prediction in terms of single-phase saturated laminar flow in rough rock fractures and it can be extended to analyse other hydro-related problems.

2.1 Introduction

Rock masses commonly include fractures or faults resulting from either tectonic activities or human disturbances. These fractures, at different scales, often act as active conduits for fluid flow (e.g. water). A sound knowledge of the controlling mechanism of fluid flow in rock fractures is of interest in various research fields and engineering applications including groundwater flow, solute transport, enhanced geothermal systems and hazardous waste disposal (Xu et al. 2015; Yeo et al. 1998; Zimmerman and Bodvarsson 1996). Modelling the complex behaviour of flows in fractured rock masses requires a fundamental understanding of the hydraulic behaviour of discrete single fractures.

The Navier-Stokes equations (NSE) are widely accepted as the governing equations for steady-state incompressible flow in rock fractures (Zimmerman 2005; Zou et al. 2015). By considering mass conservation, they can be written as:

$$\rho(\boldsymbol{u}\cdot\nabla)\boldsymbol{u} = -\nabla P + \mu\nabla^2\boldsymbol{u} \tag{2.1}$$

$$\nabla\cdot\mathbf{u} = 0 \tag{2.2}$$

where $\boldsymbol{u}$ is the velocity and P is the pressure. Although in theory the NSE provide an exact description of three-dimensional flow in rock fractures, the computational cost required to solve the three-dimensional partial differential equations is prohibitive for applications beyond microscopic scale (Brush and Thomson 2003).

The common approach to modelling fluid flow through rock fractures is to assume that a fracture consists of two smooth parallel plates separated by a constant aperture (Snow 1969). Under this assumption, the cubic law (CL) can be derived (Zimmerman and Yeo 2000) and has the following form:

$$Q = -\frac{W\rho g b^3}{12\mu}\frac{\Delta H}{L} \tag{2.3}$$

where Q is the volumetric flow rate, W is the fracture width, ρ is the fluid density, g is the gravitational acceleration, b is the fracture aperture, μ is the dynamic viscosity, H is the hydraulic head and L is the fracture length.

The CL is widely used for flow prediction in rock fractures in many fields due to its simplicity. However, real fractures are often formed by two surfaces with anisotropic roughness and varying aperture, which lead to a three-dimensional non-uniform tortuous flow

field rather than the one-dimensional Poiseuille flow assumed by the CL (Brown 1987; Brush and Thomson 2003). Numerous laboratory experiments indicate that the CL may produce significant errors in the prediction of flow through rock fractures (Tsang 1984; Witherspoon et al. 1980). Another approach is to account for the spatial variability of the fracture aperture by assuming that a particular CL applies at each explicit location. This is known as the local cubic law (LCL) and can be derived from the NSE using lubrication theory (Zimmerman et al. 1991); it is also called the Reynolds equation and takes the form:

$$\nabla \cdot \left[\frac{\rho g b^3}{12\mu} \nabla H\right] = 0 \tag{2.4}$$

The validity of the LCL has been questioned in previous studies. It assumes a flat plane for the fracture mid-surface, whereas rough fractures are more likely to have a tortuous mid-surface (Ge 1997; Wang et al. 2015), which is incompatible with the assumption of a parabolic velocity profile and can result in an over-estimation of the flow rate by a factor of at least 1.75 (Konzuk and Kueper 2004).

To avoid the computational cost of solving the NSE and improve the performance of the over-simplified CL and LCL, research has been focused on developing alternative models based on modifying the CL and LCL. Statistical parameters (e.g. relative roughness (Nazridoust et al. 2006), surface roughness parameters (Patir and Cheng 1978)) and empirical parameters e.g. joint roughness coefficient (Olsson and Barton 2001) (*JRC*) are incorporated to modify the CL by using data from flow experiments or values generated by the LCL to derive a relationship between the vertical aperture (also known as apparent aperture) and hydraulic aperture. As these models ignore flow behaviours at the local pore-scale, their performance varies significantly with the fracture void geometry. Ge (1997) derived an alternative flow governing equation based on aperture field modification, in which the aperture at each location is modified by considering the geometric properties of every local cell (see Figure 2.1). This approach is supported by Konzuk and Kueper (2004), who evaluated the modified aperture field with CL-based models and found that the CL, calculated with either the geometric mean aperture or incorporating surface roughness factors, predicted the flow rate within ±10% of the observed values for Reynolds number less than 1. Wang et al. (2015) developed an improved CL-based model by extending Ge's approach to account for the roughness effect of local cells as a means of aperture field modification. However, the validity of modifying the aperture field in terms of the geometric properties of each local cell may depend on the resolution of the aperture field data and variations of both aperture and surface

roughness (Berkowitz 2002; Dippenaar and Van Rooy 2016; Oron and Berkowitz 1998). Oron and Berkowitz (1998) conducted a leading-order approximation to the two-dimensional NSE and concluded that the CL assumption may be valid within certain segments as long as both the non-dimensional local roughness parameter and aspect ratio of the segments are significantly less than 1 (i.e. both walls are relatively smooth and the segment length is much longer than the segment half-aperture). However, in the absence of non-segmented area treatment and quantification of the local roughness effect, its application to fracture flow prediction is limited.

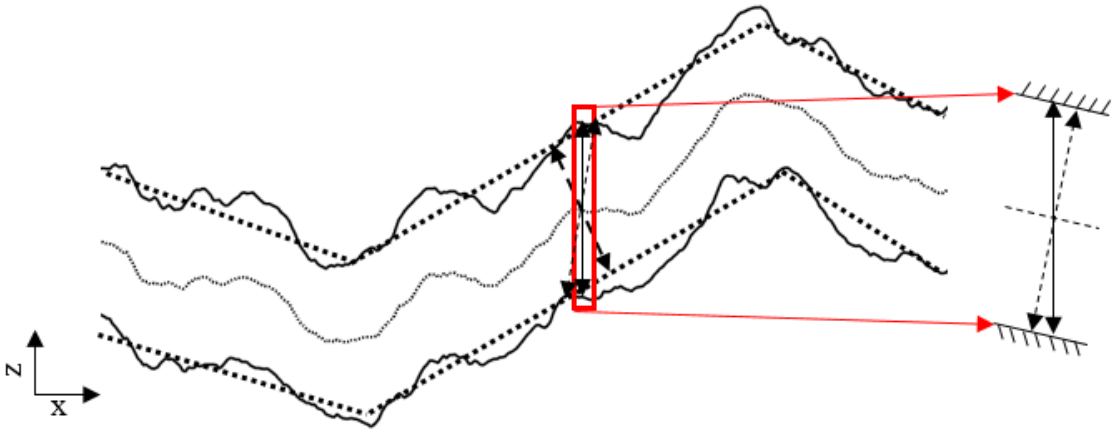

Figure 2.1 Different definitions of fracture aperture with black arrows representing the vertical aperture, dotted arrows for the aperture perpendicular to the local cell centreline (Ge 1997) and the bold dashed arrow for the segment aperture (Oron and Berkowitz 1998). The bold dashed lines are the segment walls and the dashed lines refer to the centrelines of the local cells. One typical local cell is illustrated as the area marked by the red block.

The purpose of this work is to present a modified cubic law (MCL) with improved performance in terms of predicting the volumetric flow rate in rough rock fractures. The aperture field was modified by considering the effects of flow tortuosity, aperture variation and local roughness. Numerical simulations of fracture flow were conducted in synthetic fractures with varying surface roughness and aperture by solving the NSE to assess the validity of the proposed MCL. Previous models were also used for comparisons to further test the robustness of the MCL presented here.

2.2 Model development

2.2.1 Assumptions for flow direction in segments

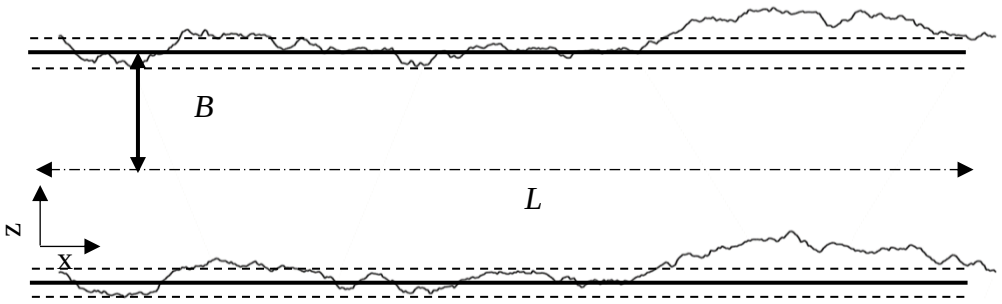

Figure 2.2 Illustration of one segment with B_s the half-aperture and L_s the segment length (Oron and Berkowitz 1998).

We begin by making assumptions for the flow direction field of a three-dimensional fracture with surface roughness. Take a cross-section of a fracture segment, as shown in Figure 2.2; B_s is the average half-aperture and L_s is the length of this fracture segment. It can be assumed that Poiseuille flow holds in the segment and the flow direction is governed by the segment geometry when B_s is much smaller than L_s and the roughness of both walls along the segment is limited (Oron and Berkowitz 1998). These two conditions require:

$$\delta = \frac{B_s}{L_s} \ll 1 \tag{2.5}$$

$$\varepsilon = \max\left(\frac{\sigma_u}{B_s}, \frac{\sigma_l}{B_s}\right) \ll 1 \tag{2.6}$$

where δ is the aspect ratio and ε is the non-dimensional local roughness parameter; σ_u and σ_l are the standard deviations of the roughness variations of upper and lower walls, respectively. Under both conditions, the representative flow direction follows the orientation of the geometric centreline of the segment (Ge 1997). The segments of each fracture can be determined by calculating δ and ε along each fracture cross-section using their assigned maximum values. We discuss the range and determination of δ and ε in Section 2.4.1.

2.2.2 Consideration of flow tortuosity

At the scale of a single fracture, flow tortuosity is defined as the ratio of the three-dimensional flow path length to straight-line distance of the fracture length (Walsh and Brace 1984). In this study, the tortuosity τ of each segment is defined as the ratio of flow path distance d_f to the straight-line distance d_s projected on the fracture plane:

$$\tau = d_f/d_s \tag{2.7}$$

The vertical aperture at each location within the approximated segment with walls of averaged straight lines (see Figure 2.2) can be determined according to the geometry of the approximated segment. As the aperture, defined in the CL, should be perpendicular to the flow direction, vertical apertures need to be translated into flow-oriented apertures defined as the segment aperture b_{sf}. We use the formula proposed by Ge (1997) to obtain the relation between the vertical aperture and b_{sf} within the segment:

$$b_{sf} = b_v \frac{2\cos\alpha_u \cos\alpha_l}{\cos\frac{\alpha_u-\alpha_l}{2}(\cos\alpha_u+\cos\alpha_l)} = b_v \cdot F_t \tag{2.8}$$

where b_v is the vertical aperture, α_u and α_l are the inclination angles of the upper and lower walls, respectively. Connective transmissivity (Brush and Thomson 2003; Nicholl et al. 1999) (T) between each local cell within the segment can be approximated using the harmonic mean of adjacent apertures:

$$T = \frac{2b(i)^3 b(i+1)^3}{b(i)^3+b(i+1)^3} \tag{2.9}$$

2.2.3 Quantification of local roughness effect

When equations (2.5) and (2.6) are satisfied (δ and ε are much smaller than 1), a fracture segment with complex roughness may be approximated, as shown in Figure 2.2, by two straight lines representing the average variability of the upper and lower walls. However, ε increases as the roughness of the segment increases, which increases the approximation errors of the average lines and the deviation needs to be included as a modifying factor. Since the majority of pressure drop is expected to take place in smaller apertures (Nazridoust et al. 2006), the effective aperture b_e is used to estimate the effect of smaller apertures and can be defined as:

$$b_e = b_{sf}\left(1 - \frac{\sigma_u+\sigma_l}{2B_s}\right) = b_{sf} \cdot F_{lr} \tag{2.10}$$

Note that the range of the local small-scale roughness considered here is from the grid spacing scale to the scale of the segment; roughness on scales less than the grid spacing is not included. The example shown in Figure 2.2 is solely for illustrative purposes and is not intended as a direct representation of our model.

2.2.4 Modified aperture field

Once the segments are determined, the set of apertures within each segment can be easily calculated and transferred into a modified aperture field $b_{modified}$ by combining equations (2.8), (2.9) and (2.10). For example, a set of apertures in the *x* direction can be described as:

$$b_{modified}(x) = {T_v}^{1/3} \cdot F_t \cdot F_{lr} \tag{2.11}$$

where $b_{modified}(x)$ is the modified aperture in the *x* direction, T_v is the connective transmissivity between adjacent vertical apertures, F_t is the tortuosity factor defined in equation (2.8) and F_{lr} is the local roughness modification factor defined in equation (2.10). As the fracture has been divided into a series of segments that satisfy the geometric conditions in equations (2.5) and (2.6), vertical apertures can be modified using equation (2.11). However, there may be some parts of the fracture area that do not satisfy the geometrical conditions. Following Ge's approach, to improve aperture estimation in these cases, the vertical aperture is modified by the geometric properties of each local cell. In these local cells, the walls are smooth, which means that F_{lr} is equal to 1 and equation (2.11) becomes:

$$b_{modified}(x) = {T_v}^{1/3} \cdot F_t \tag{2.12}$$

The entire aperture field is a combination of a series of modified apertures from equation (2.11) or (2.12) and can be described as:

$$b_{modified}(x, y) = [b_f(x, 1), b_f(x, 2), \dots\dots, b_f(x, y)] \tag{2.13}$$

2.2.5 Modified cubic law

As the aperture field has been modified to account for flow tortuosity, aperture variation and local roughness effects, we modify the fracture length *L* in the formulation of the standard CL for flow tortuosity. For each cross-section in the *x* direction, the flow path distance, D_f, is the sum of the flow path lengths of each segment and cell and thus D_f and the fracture length *L* are related by:

$$D_f = \sum d_f(x) = \sum \tau(x) d_s(x) = F_{length} \cdot L \tag{2.14}$$

Finally, given the discrepancy between the hydraulic aperture and geometric aperture, an extra factor (Renshaw 1995; Wang et al. 2015) is introduced to correct the calculated flow rate to give a more accurate flow prediction based on the modified aperture field. The proposed MCL is formulated as:

$$Q = \frac{\rho g <b_{modified}>^3}{12\mu F_{length}} W \frac{\Delta H}{L}\left[1 + (\frac{\sigma_{b_{modified}}}{<b_{modified}>})^2\right]^{-1.5} \quad (2.15)$$

where $<b_{modified}>$ is the arithmetic mean of the modified aperture field and $\sigma_{bmodfied}$ is the standard deviation of the modified aperture field.

2.3 Methodology

2.3.1 Synthetic three-dimensional rough fractures

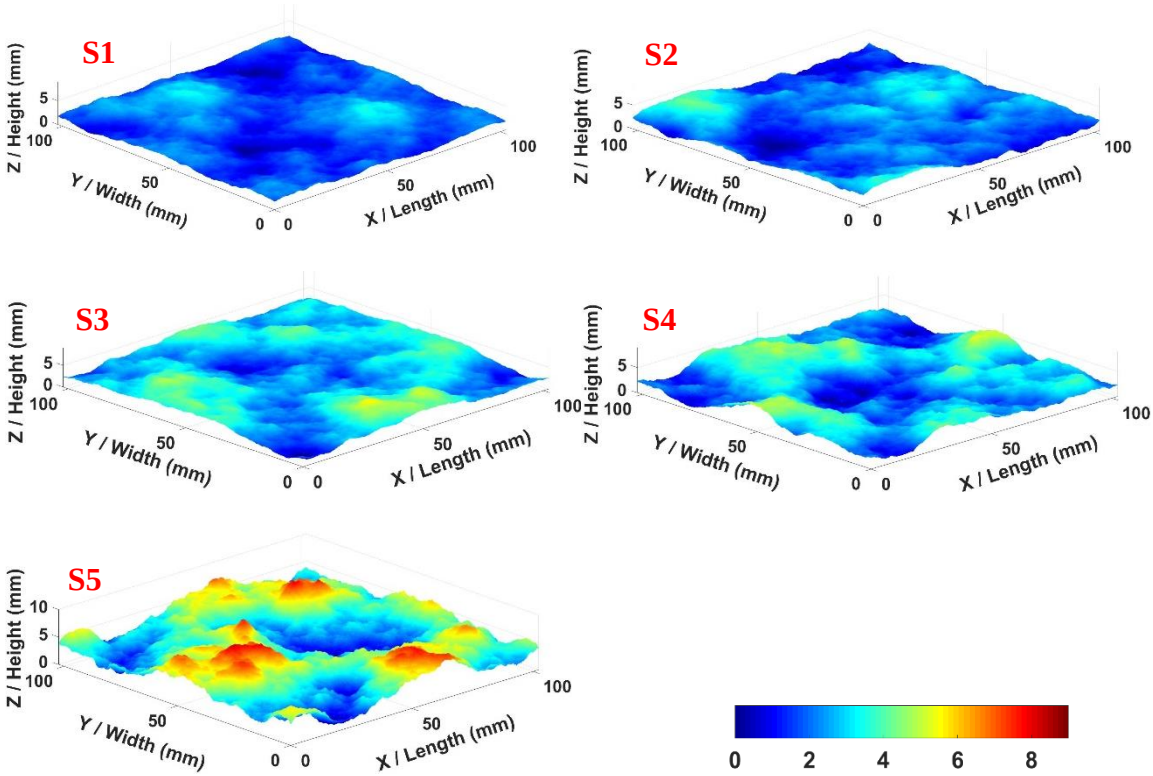

Figure 2.3 Height distribution of five rough surfaces generated with *JRC* of 7, 9, 11, 13 and 19 denoted as S1, S2, S3, S4 and S5, respectively.

Three-dimensional synthetic fracture surfaces were generated using the program SynFrac, which has been shown to reproduce the geometric properties of natural fractures and fracture surfaces (Ogilvie et al. 2006). Surface roughness was quantified using the root mean square first derivative value Z_2 (Myers 1962), and the joint roughness coefficient (*JRC*) (Barton 1973) of each surface was back-calculated using the formula proposed by Jang et al. (2014):

$$JRC = 54.57{Z_2}^{0.394} - 19.13 \qquad R^2 = 0.962 \quad (2.16)$$

Five fracture surfaces were selected with *JRC* values of 7, 9, 11, 13 and 19, as displayed in Figure 2.3. The range of *JRC* values was chosen because the purpose of this study is to derive

a modified CL for rough fractures; *JRC* values less than 7 were not included in the current research. The length and width of all surfaces were set to 102.3 mm. We used a grid spacing of 0.1 mm for surface generation, which corresponds to 1024×1024 points per surface. The statistical and geometric parameters of the generated surfaces are given in Table 2.1.

Table 2.1 Statistical and geometric parameters of five generated surfaces.

Parameters	S1	S2	S3	S4	S5
Length (mm)	102.3	102.3	102.3	102.3	102.3
Width (mm)	102.3	102.3	102.3	102.3	102.3
Resolution (mm^2)	0.01	0.01	0.01	0.01	0.01
Z_2 (-)	0.15	0.19	0.22	0.26	0.40
JRC (-)	7.02	9.05	11.01	12.98	19.07

The generated surfaces were duplicated and spaced vertically to form fractures with top and bottom surfaces. To introduce the effect of shear displacement, shifts from 1 to 25 mm were applied to the top surface along the *x* direction, which results in a mis-alignment of the two surfaces, hence a variable two-dimensional aperture field (with the mean vertical aperture from 0.46 to 6.21 mm and relative roughness from 0.10 to 1.84 mm). In total, forty-five fractures with different surface roughness and variable apertures were created and used for flow simulations.

2.3.2 Numerical simulation for solving the NSE in rough fractures

Fracture flow simulations were conducted by solving the NSE using the computational fluid dynamics (CFD) code implemented in the finite element software package COMSOL Multiphysics. Here, gravitational effects were ignored and we applied a pressure drop of 0.1 Pa/m between the flow inlet and outlet. A no-slip boundary was assigned to both surfaces and sides to assume no interaction with the rock matrix. We used standard property values for water: density ρ=1000 kg/m^3 and dynamic viscosity μ=0.001 Pa·s. The mesh was refined by increasing the number of mesh elements for each simulation until the difference between two successive simulation results was within 1%. Each fracture was discretised into approximately 11 million tetrahedral elements (see Figure 2.4) with larger elements away from the boundaries and smaller elements along them; the overall average element size is around 0.2 mm. A minimum aperture of 0.01 mm was assigned to maintain mesh quality and avoid difficulties in mesh generation. Due to the computational requirements, all the numerical experiments were conducted either on a remote server or the High Performance Computer (HPC) workstation at

the University of Adelaide. Each simulation took more than 12 hours on the remote server to reach a steady-state solution and about 2 hours on the HPC workstation.

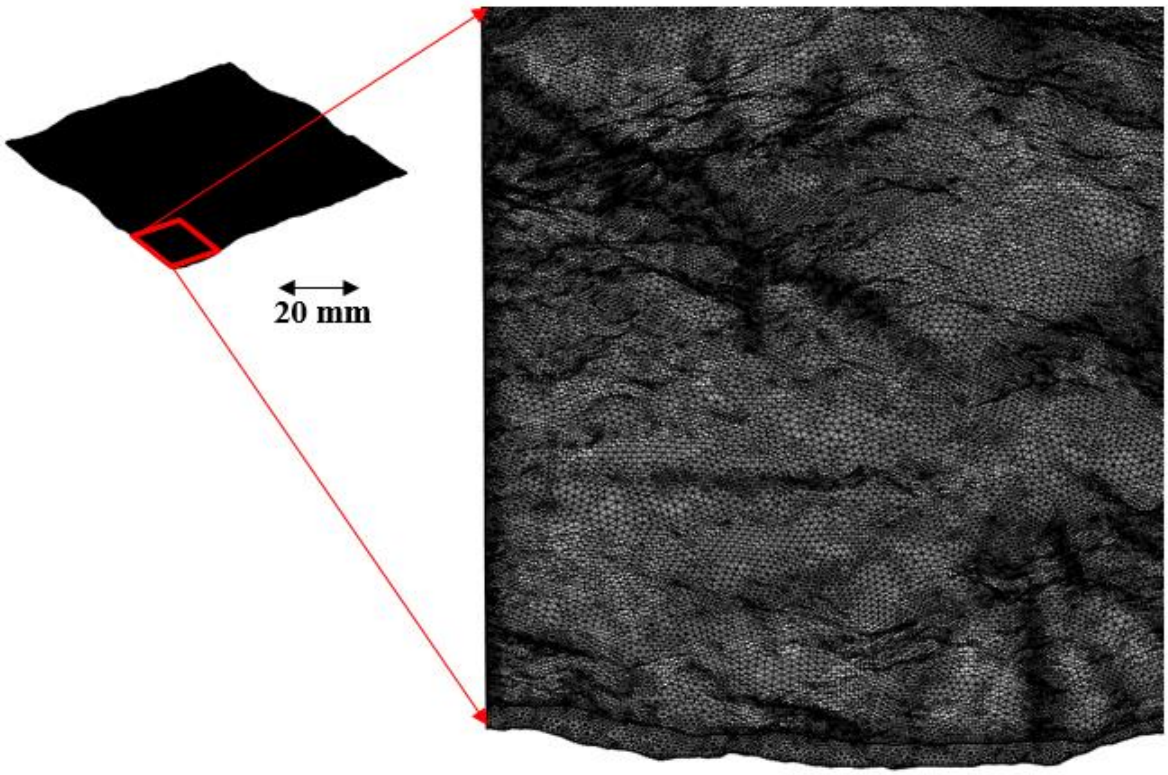

Figure 2.4 Example of mesh generation for fracture S2SH2 (with 2 mm shear displacement) with approximately 11 million tetrahedral elements.

2.3.3 Comparison with other models

To test the performance of our proposed MCL, we compared the volumetric flow rate calculated from the MCL to that from the CFD simulations; the deviation D_{MCL} is quantified as:

$$D_{MCL} = \frac{Q_{MCL} - Q_{NSE}}{Q_{MCL}} \times 100\% \tag{2.17}$$

in which Q_{MCL} is the volumetric flow rate calculated using the MCL and Q_{NSE} is the volumetric flow rate at the outlet boundary calculated from numerical simulations.

Results from the standard CL and two CL-based models proposed by Konzuk and Kueper (2004) and Wang et al. (2015), respectively, were used to assess the performance of MCL. The CL-based model proposed by Konzuk and Kueper (2004) uses the aperture modification that is based on the 'perpendicular aperture' concept from Ge (1997), and the geometric mean

approach to estimate the hydraulic aperture (denoted as b_{Konzuk}) from the vertical aperture field. The volumetric flow rate for this model is obtained by substituting b_{Konzuk} for the aperture b in the standard CL:

$$Q = \frac{\rho g {b_{Konzuk}}^3}{12\mu} W \frac{\Delta H}{L} \tag{2.18}$$

The modified CL proposed by Wang et al. (2015) also uses the concept of 'perpendicular aperture' to incorporate the flow tortuosity effect and addresses the roughness effect of local cells. A scale factor proposed by Renshaw (1995) is included to further modify the CL. Their model is expressed as:

$$Q = \frac{\rho g <b_{Wang}>^3}{12\mu} W \frac{\Delta H}{L} [1 + (\frac{\sigma_{b_{Wang}}}{<b_{Wang}>})^2]^{-1.5} \tag{2.19}$$

where b_{Wang} represents the modified aperture field and σ_{bWang} is the standard deviation of the modified aperture field.

The volumetric flow rates calculated using the standard CL and two CL-based models were compared with Q_{NSE} and the deviations, D_{CL}, D_{Konzuk} and D_{Wang} were calculated using equation (2.17) by replacing Q_{MCL} with the calculated volumetric flow rates Q_{CL}, Q_{Konzuk} and Q_{Wang}.

2.4 Results

2.4.1 Appropriate ranges for δ and ε

To determine appropriate values of δ and ε to use in the MCL, we first analysed the ranges of both parameters in the context of the physical meanings implicit in their definitions.

Take the middle segment S from a cross-section of one conceptual fracture, in which the segment has a half-aperture of B_1 and a segment length L_1. As shown in Figure 2.5a, the aspect ratio, δs, of S is less than 1 and it is obvious that the representative flow direction depends on the segment geometry that follows the orientation of its centreline. δ_S increases as B_1 increases and when δ_S is greater than 1 (Oron and Berkowitz 1998), as seen in Figure 2.5b, the flow direction no longer follows the centreline orientation of segment S but is more likely to depend on the geometrical properties of adjacent segments. Physically, the aspect ratio, δs, determines whether the flow in each segment is governed largely by its geometrical properties with negligible influence from adjacent segments.

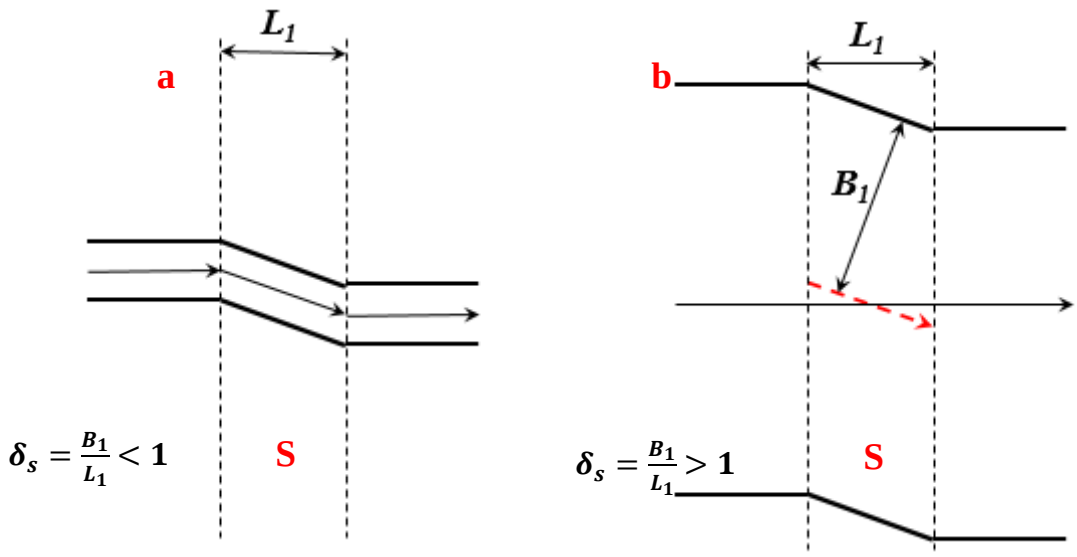

Figure 2.5 Flow direction in segment S for (a) δ_S<1, the arrow represents the flow direction that follows the orientation of the segment centreline, and (b) δ_S>1, the black arrows indicate flow direction and the red dashed-line arrow is the segment centreline orientation.

Although this assumption becomes more valid as δ becomes much less than 1, a smaller δ leads to a stricter criterion for forming segments. It is, therefore, necessary to find a suitable limit for δ so that the segments can be determined with acceptable errors. We set the maximum δ as 0.5, which is commonly used as the upper limit of the aspect ratio to derive perturbation solutions for the NSE (e.g. Basha and El-Asmar 2003), and the range of δ becomes:

$$0 < \delta \leq 0.5 \tag{2.20}$$

Similar to the aspect ratio, we determined an appropriate range for the local roughness parameter ε. As Poiseuille's law was assumed valid for flow in each segment, flow is predominantly in the central area within the fracture and only a small portion of flow takes place near both walls (Oron and Berkowitz 1998). As demonstrated in Figure 2.6, 10% of the fracture area near each wall (20% of the entire fracture area) accounts for only ~5% of total flow discharge through the fracture and only about 20% of total flow discharge through 20% of the fracture area close to the walls (40% of the entire fracture area). To prevent wall roughness from approaching the fracture centre, which would lead to significant disturbances, we set 0.25 as the maximum value for ε and its range is given as:

$$0 < \varepsilon \leq 0.25 \tag{2.21}$$

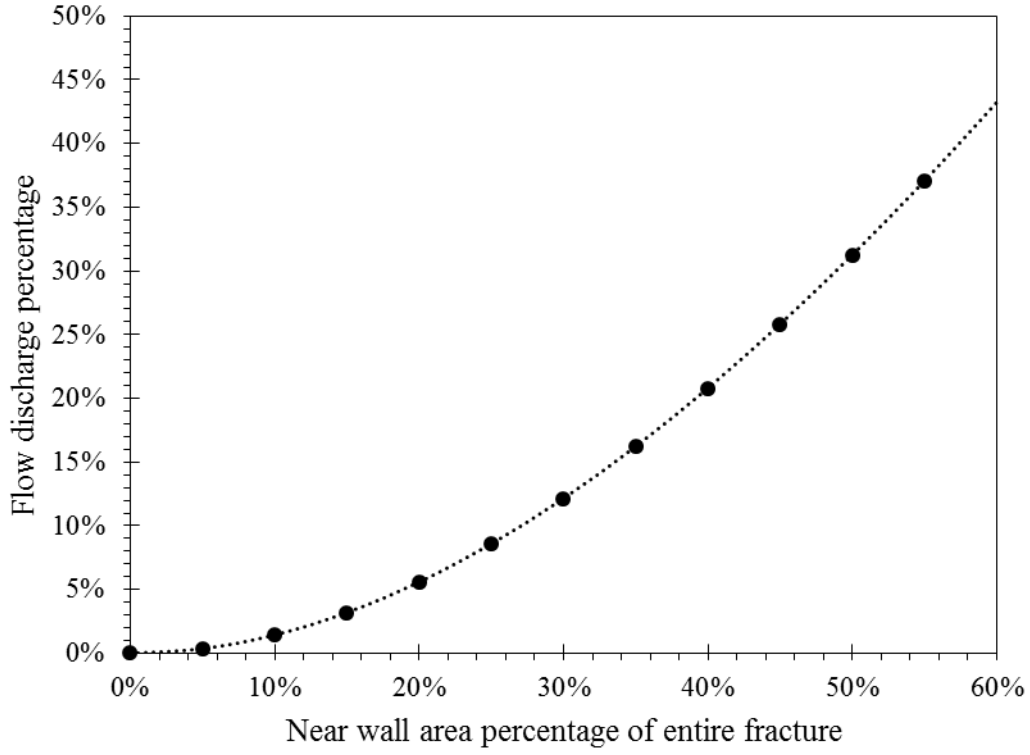

Figure 2.6 Relationship between the flow discharge percentage and near-wall area percentage for Poiseuille flow with parabolic velocity profile.

2.4.2 Segmented area and determination of δ and ε

The proportion of the area of identified segments in each fracture was evaluated for δ from 0.1 to 0.5 and ε from 0.15 to 0.25, respectively. As shown in Figure 2.7, when both δ and ε are at their minimum values (δ=0.1 and ε=0.15), the average proportion of segmented area identified out of the entire fracture area, $P_{average}$, is around 16%, while $P_{average}$ increases to over 98% as δ and ε both reach their maximum values (δ=0.5 and ε=0.25). This indicates that, as the criterion for forming segments is less strict, more segments can be identified, which is as expected.

As discussed in Section 2.2.4, equation (2.12) was applied to modify the vertical apertures of non-segmented areas based on the geometry of each local cell, which may lead to additional deviations. Therefore, to minimize the influence of non-segmented areas, we only expect the MCL to produce accurate results when the non-segmented area is less than 5% of the total fracture area, which means that the proportion of segmented area, P_s, of each fracture should be no less than 95%. For all 45 fractures to meet this requirement with the same δ and ε, four combinations of δ and ε were identified: δ=0.4 and ε=0.2 (denoted as C1, with only one case having P_s=89%), δ=0.5 and ε=0.2 (C2), δ=0.4 and ε=0.25 (C3) and δ=0.5 and ε=0.25 (C4), respectively.

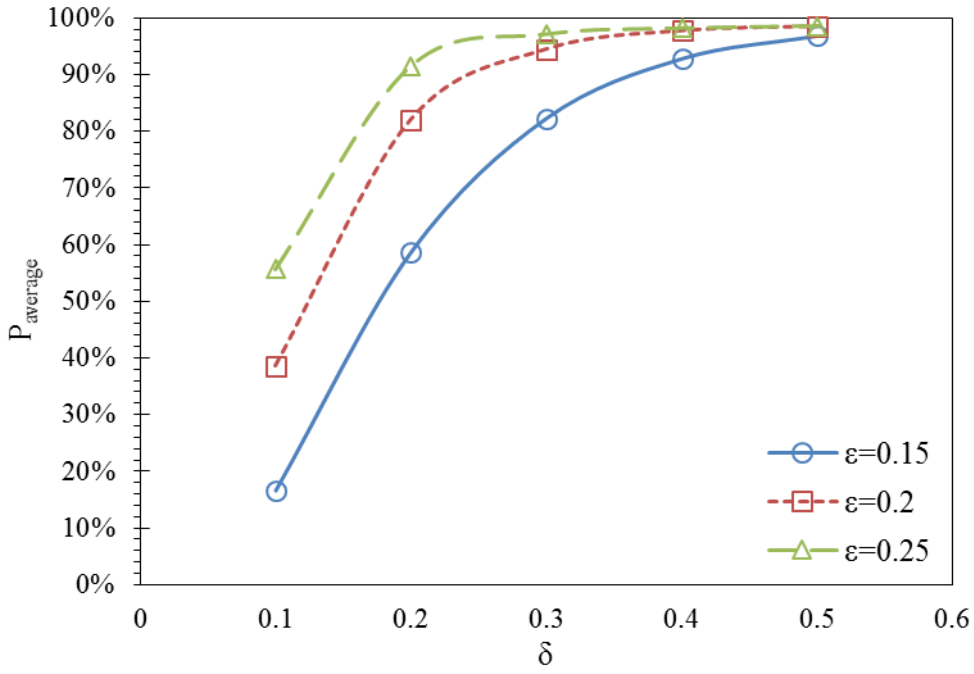

Figure 2.7 Average proportion of segmented area of all fractures ($P_{average}$) for δ from 0.1 to 0.5 and ε from 0.15 to 0.25.

2.4.3 Comparison with CFD results

The distributions of U/U_{max} in two sets of fractures with surface roughness of 7 and 19 and shifts of 1, 3, 5, 10 and 20 mm are plotted in Figure 2.8. When surfaces are smoother and both upper and lower surfaces are well matched (e.g., S1SH1), flow is evenly distributed with no apparent preferential path; as surfaces become rougher, or more misaligned during the shear displacement (e.g., S5SH3 and S5SH20), channelling effects are clearly apparent in more conductive regions. The phenomenon of preferential flow channels in fractures is widely reported in the literature (e.g. Pyrak-Nolte et al., 1988; Tsang and Tsang, 1989; Xiong et al., 2011).

The performance of the MCL was tested against numerical simulation results of fracture flow in terms of the volumetric flow rate. As shown in Figure 2.9, on average, deviations are within ±11% of the CFD results for all δ and ε combinations, with D_{C1}, D_{C2}, D_{C3} and D_{C4} ranging from -11.13% to 8.35%, -9.37% to 10.65%, -11.13% to 8.34% and -9.37% to 10.65%, respectively. The average effective deviation $\overline{|D|}$ of each combination is also shown in Figure 2.9, in which $\overline{|D|}_{C1}$= 4.72%, $\overline{|D|}_{C2}$= 6.14%, $\overline{|D|}_{C3}$= 4.66% and $\overline{|D|}_{C4}$ = 6.14%.

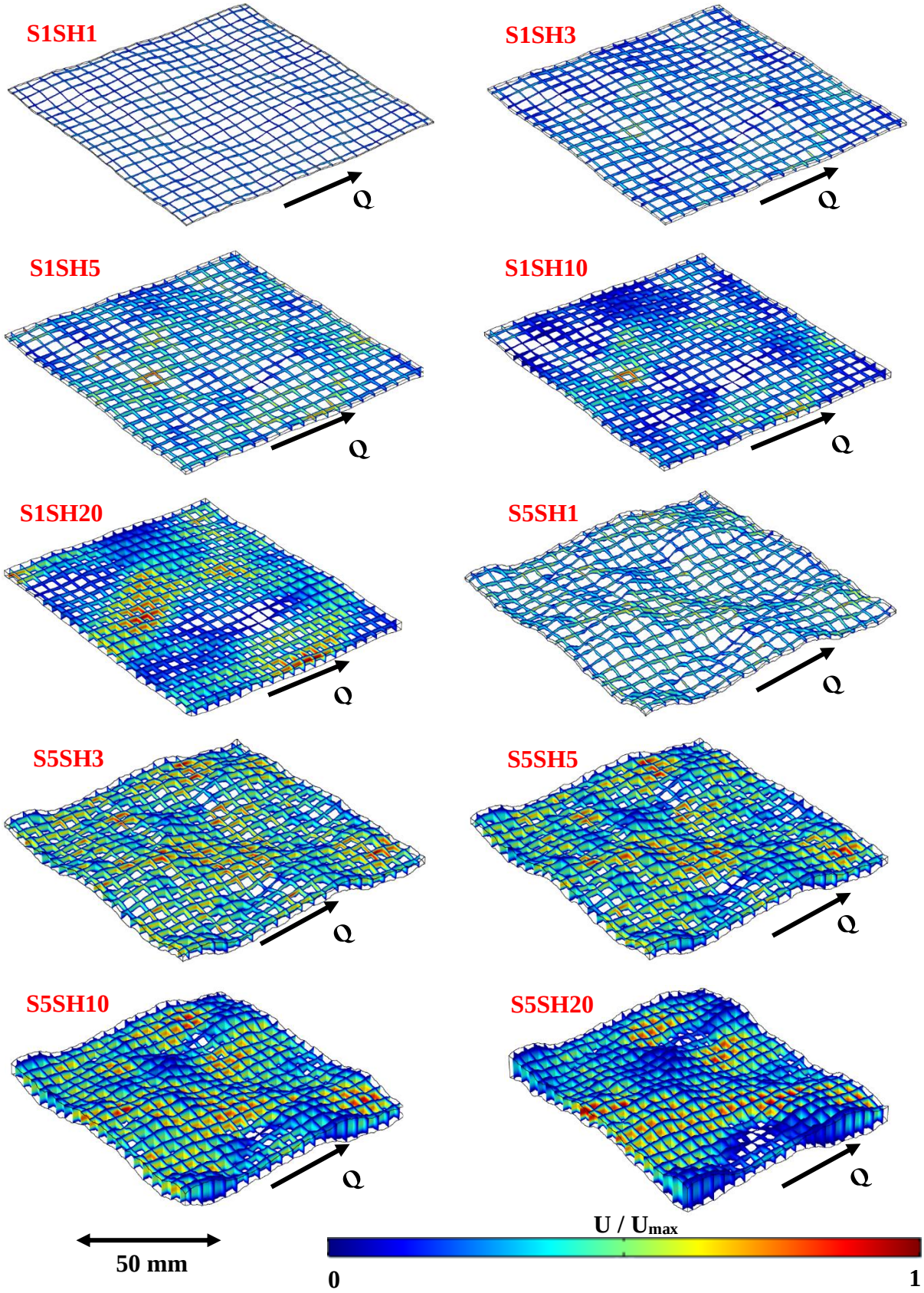

Figure 2.8 The ratio of velocity magnitude ***U*** to the maximum velocity U_{max} distributed within the fracture with *JRC* of 7 and 19 (i.e. S1 and S5) and with shifts of 1, 3, 5, 10 and 20 mm (denoted as SH1, SH3, SH5, SH10 and SH20).

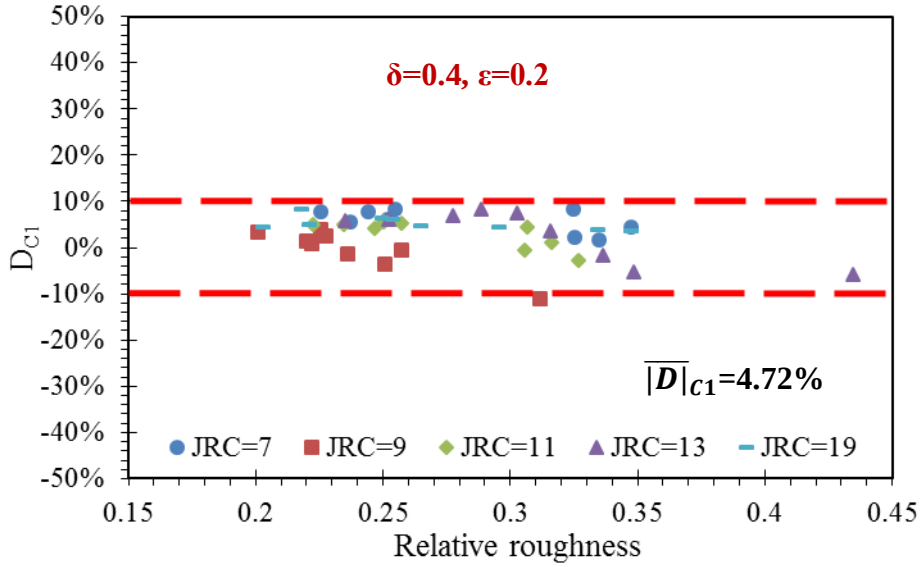
δ=0.4, ε=0.2
D_{C1}
$\overline{|D|}_{C1}$=4.72%
JRC=7 JRC=9 JRC=11 JRC=13 JRC=19
Relative roughness

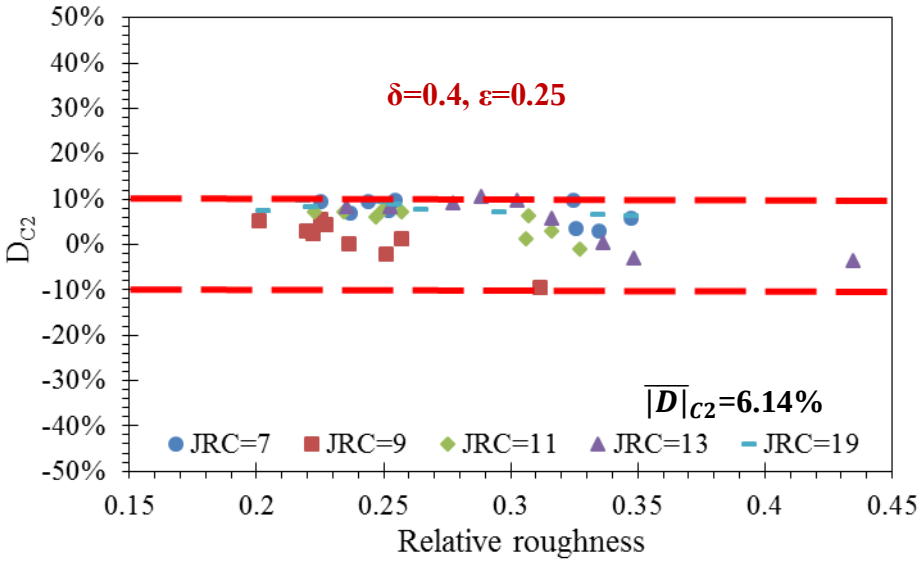
δ=0.4, ε=0.25
D_{C2}
$\overline{|D|}_{C2}$=6.14%
JRC=7 JRC=9 JRC=11 JRC=13 JRC=19
Relative roughness

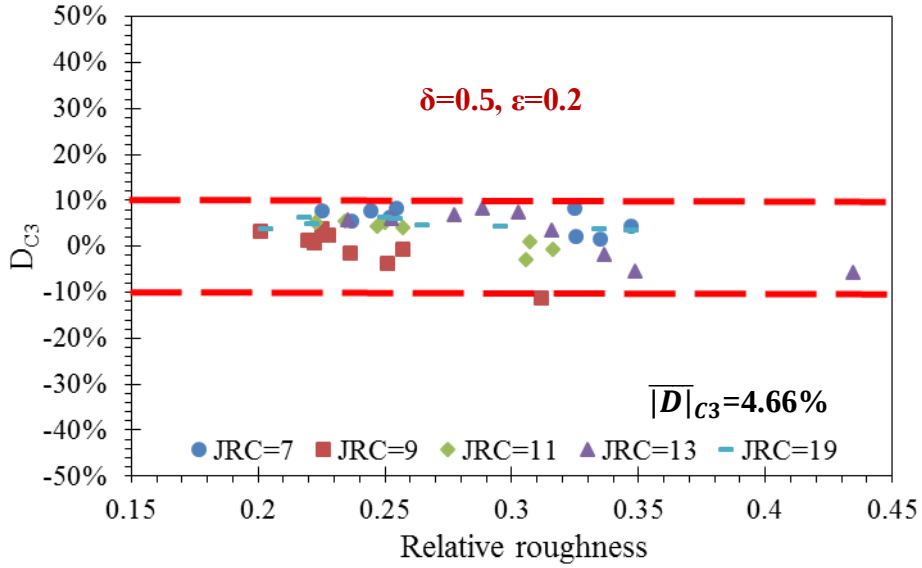
δ=0.5, ε=0.2
D_{C3}
$\overline{|D|}_{C3}$=4.66%
JRC=7 JRC=9 JRC=11 JRC=13 JRC=19
Relative roughness

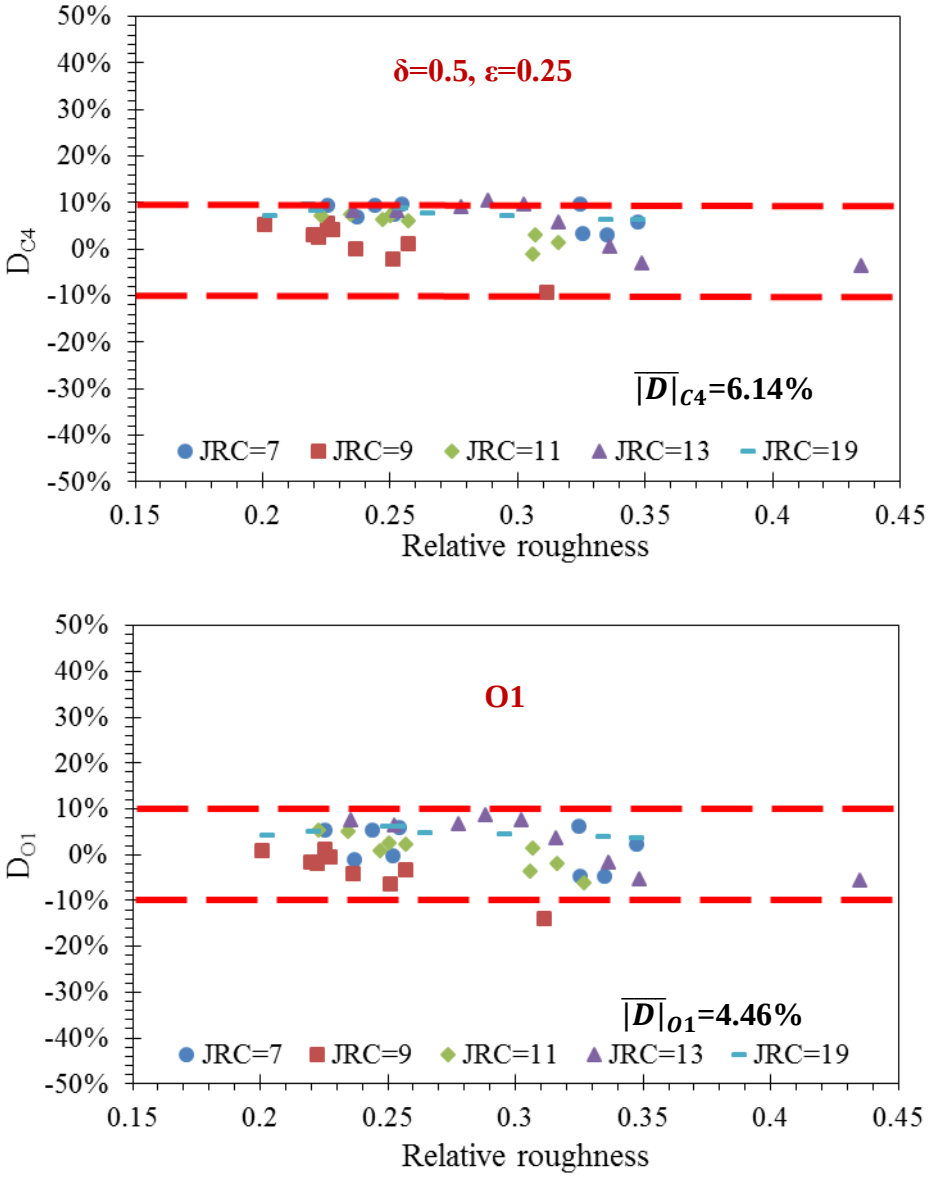

Figure 2.9 Deviation, *D*, of each fracture in terms of relative roughness. *D* is defined as the difference between the volumetric flow rate calculated from numerical simulation and that derived from the MCL with four combinations of δ and ε and the selected results O1, which are denoted as D_{C1}, D_{C2}, D_{C3}, D_{C4} and D_{O1}. Relative roughness is defined as the ratio of the vertical aperture standard deviation to mean aperture (Brush and Thomson 2003; Wang and Cardenas 2016).

As the same δ and ε were assigned in the MCL to predict the volumetric flow rate for all the fractures, we further examined the model performance by selecting the minimum δ and ε for each fracture while ensuring that P_s of every fracture was at least 95% (denoted as O1). As shown in Figure 2.9 and Table 2.2, the deviation of the results from O1, D_{O1}, ranges from -13.99% to 9.87% with the average effective deviation $\overline{|D|}_{O1}$ equalling 4.46%. $\overline{|D|}_{C1}$, $\overline{|D|}_{C2}$,

$\overline{|D|}_{C3}$, $\overline{|D|}_{C4}$and $\overline{|D|}_{O1}$ for each *JRC* case are also plotted. As seen in Figure 2.10, $\overline{|D|}_{C1}$ and $\overline{|D|}_{C3}$ are in good agreement for smaller *JRC*, $\overline{|D|}_{C2}$ and $\overline{|D|}_{C4}$ have nearly identical results except for *JRC*=13. In general, $\overline{|D|}_{C1}$, $\overline{|D|}_{C3}$ and $\overline{|D|}_{O1}$ are within 6.00% and $\overline{|D|}_{C2}$ and $\overline{|D|}_{C4}$ are within 8.00%, for all *JRC* cases.

Table 2.2 Average effective deviation of the standard CL ($\overline{|D|}_{CL}$), the model proposed by Konzuk and Kueper (2004) ($\overline{|D|}_{Konzuk}$), the formulation from Wang et al. (2015) ($\overline{|D|}_{Wang}$) and the MCL in the current study ($\overline{|D|}_{C1}$ and $\overline{|D|}_{O1}$).

Fractures set	$\overline{\lvert D\rvert}_{CL}$ (%)	$\overline{\lvert D\rvert}_{Konzuk}$ (%)	$\overline{\lvert D\rvert}_{Wang}$ (%)	$\overline{\lvert D\rvert}_{C1}$ (%)	$\overline{\lvert D\rvert}_{O1}$ (%)
JRC7	24.51	10.29	12.82	5.81	3.97
JRC9	18.08	7.31	8.21	3.15	3.70
JRC11	24.87	9.16	11.55	3.79	3.28
JRC13	29.04	10.63	12.01	5.66	5.98
JRC19	33.78	10.13	12.33	5.21	5.39
All fractures	26.06	9.50	11.38	4.72	4.46

Results from C1 and O1 were selected for comparison with other models. As shown in Figure 2.11 and Table 2.2, the proposed MCL outperforms the other three models not only in general results but also in each *JRC* case. The deviation (*D*) of flow prediction by the MCL (C1) ranges from -11.13% to 8.35% and the average effective deviation ($\overline{|D|}_{C1}$) is 4.72%. For the standard CL and formulations of Konzuk and Kueper (2004) and Wang et al. (2015), $\overline{|D|}_{CL}$, $\overline{|D|}_{Konzuk}$ and $\overline{|D|}_{Wang}$ are 26.06%, 9.50% and 11.38%, respectively. The average effective deviations of all the tested models in each *JRC* case are given in Table 2.2, from which it can be seen that the proposed MCL has the best performance with all average effective deviations less than 6%.

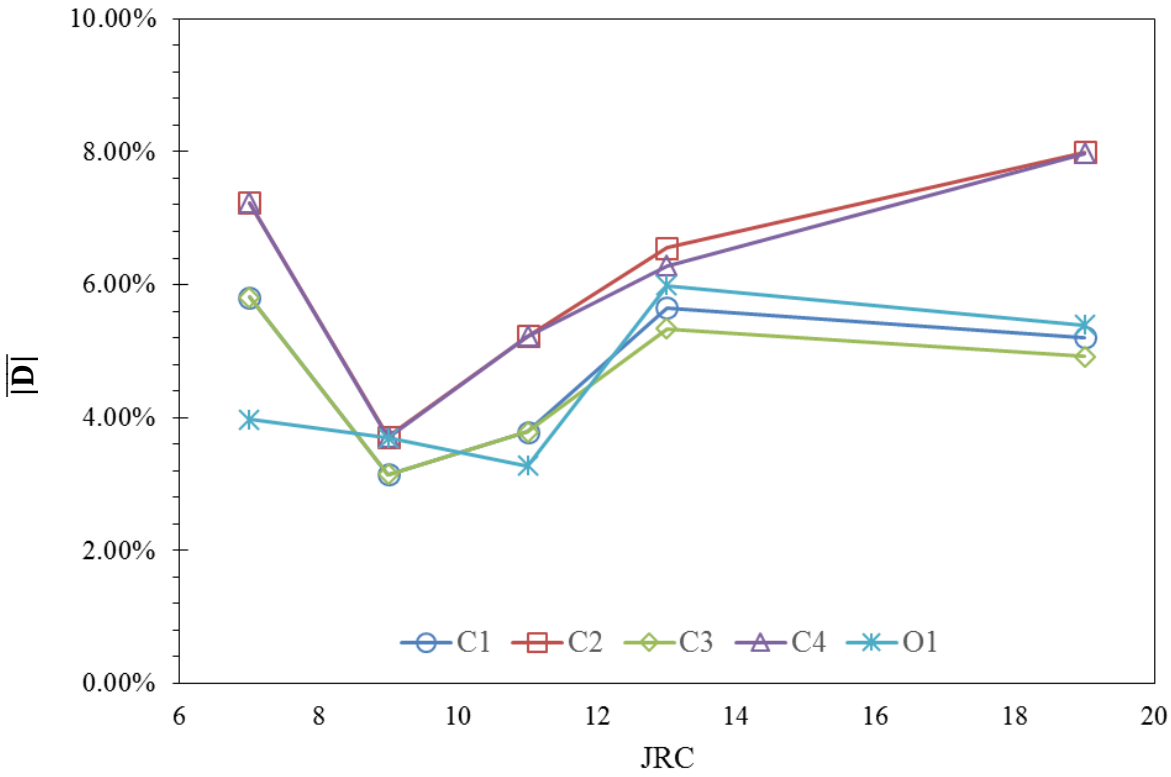

Figure 2.10. Average effective deviation $\overline{|D|}$ for fractures with different *JRC* using parameters from C1, C2, C3, C4, C5 and O1 in the MCL.

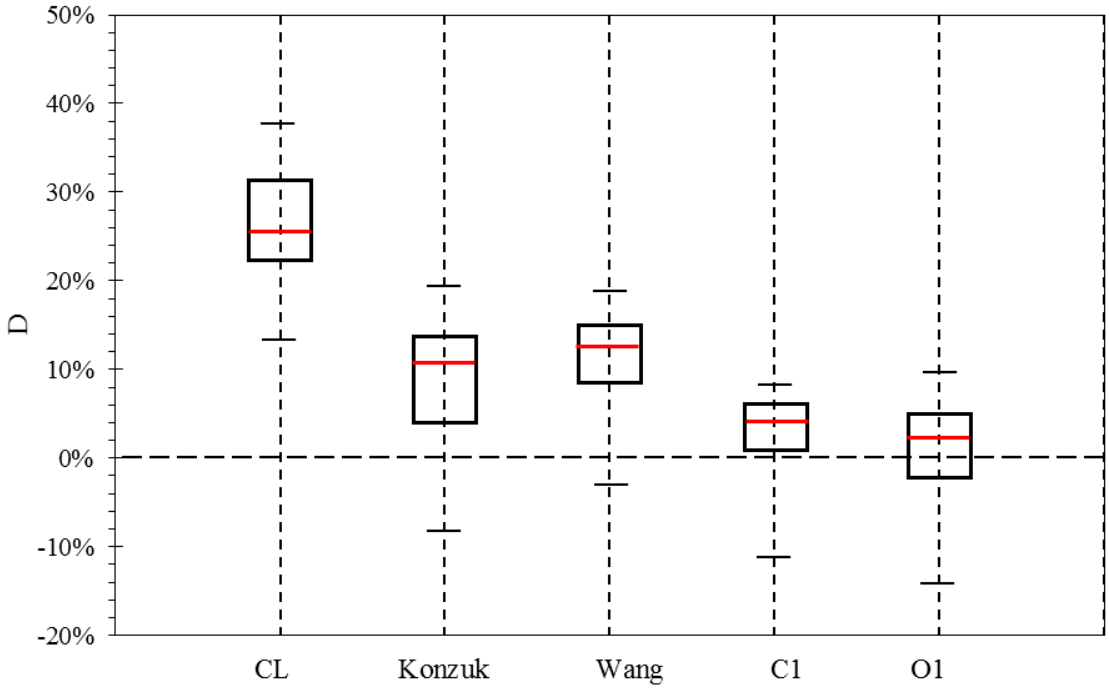

Figure 2.11 Box-Whisker plot showing the distributions of deviation *D* from the standard CL, the model proposed by Konzuk and Kueper (2004), the formulation in Wang et al. (2015) and the MCL in the current study (C1 and O1).

2.5 Discussion

2.5.1 Performance of the MCL

The proposed MCL performed well for the fractures used in this study with the deviations of predicted volumetric flow rate within ±11% of the CFD simulation results. The average effective deviation for the fractures used in this study is 5.4% (all four combinations, C1, C2, C3 and C4).

The performance of the proposed MCL depends largely on the combined effect of δ, ε and P_s. Theoretically, the MCL provides more accurate results when δ and ε are significantly less than 1 and P_s is close to 100% (i.e. segment aperture is much smaller than segment length, smooth segment walls and high proportion of segmented area). However, on one hand, smaller δ and ε lead to stricter criterion to form segments (i.e. more non-segmented area), which affects the performance of the MCL. On the other hand, maintaining high P_s requires increasing δ and ε so that more segments can be identified but increasing δ and ε will increase the deviation of the prediction. Nevertheless, from the range analysis of these parameters in our study, even the least strict geometric condition (C4) still provides a $\overline{|D|}$ of 6.14%.

Roughness parameters (e.g. *JRC*) may vary for different fracture sizes and scales. However, the scale effect has a negligible impact on the performance of the MCL since no scale-dependent parameters are included in the formulation. It is also worth noting that since the general hydraulic behaviours of entire segments are considered in the MCL instead of local individual cells, the influence of grid spacing on MCL may also be trivial as long as the grid spacing is sufficiently small to capture the essential roughness effects. The MCL accounts for the effect of small-scale roughness on scales from the grid spacing to segment scale; roughness on scales less than the grid spacing is not included in the construction of the fracture geometry. To check that the effect of roughness on scales less than the grid spacing is insignificant and the current grid spacing is capable of capturing the essential roughness, we calculated the correlation length of the aperture field in each fracture (ranging from 0.36 to 5.81 mm). The grid spacing in current study (0.1 mm) is less than one-third of the minimum correlation length (0.36 mm) of all fractures used in the study, which satisfies the requirement for grid spacing as discussed by Reimus et al. (1993) and Konzuk and Kueper (2004).

A sensitivity analysis has been conducted to examine the effect of different grid spacing on the general flow behaviour. As the three-dimensional fractures used in this study comprise a series of two-dimensional profiles, we extracted two-dimensional fracture profiles at y=0.05

m from all 45 fractures and reconstructed them using six different grid spacings from 0.1 to 1.0 mm. Flow simulations with the same settings (e.g. fluid properties and boundary conditions) were conducted in these reconstructed fractures (270 in total) and the volumetric flow rates of fractures with different grid spacings were compared (see Figure 2.12).

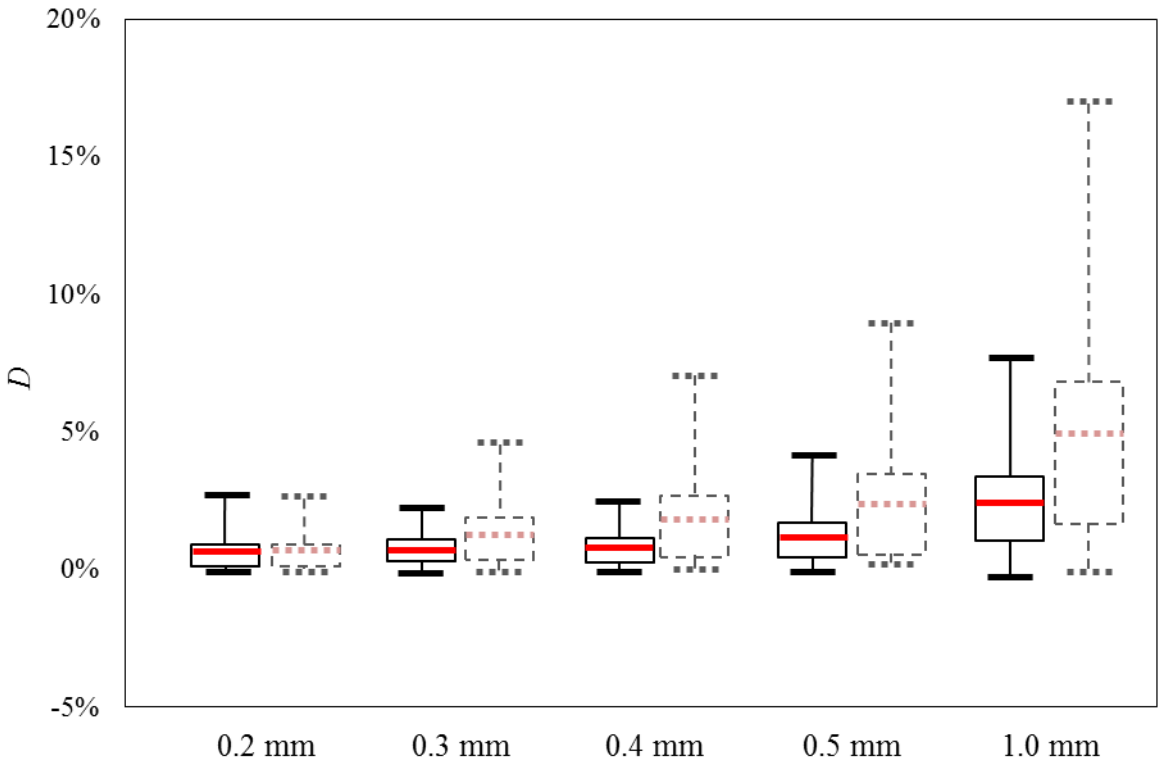

Figure 2.12. Box-Whisker plot showing the deviation D of the flow rate in fractures with grid spacings from 0.2 to 1.0 mm. For the results with solid boxes, D is defined as $(Q_{GS}-Q_{finer})/Q_{finer}\times100\%$ (denoted as D_2), where Q_{finer} is the flow rate of fractures with a finer grid spacing (e.g., for 0.3 mm grid spacing case, Q_{GS} is the result from 0.3 mm grid spacing and Q_{finer} is the result from 0.2 mm grid spacing). For the results with dashed boxes, D is defined as $(Q_{GS}-Q_{0.1})/Q_{0.1}\times100\%$ (denoted as D_2), where Q_{GS} is the flow rate of fractures with different grid spacing and $Q_{0.1}$ is the flow rate of fractures with 0.1 mm grid spacing. Note that the red bars represent the mean of deviation rather than the second quartile.

As can be seen from the solid boxes, the mean D_1 decreases from 2.44% to nearly 0.55% as the grid spacing reduces and tends to stabilize at 0.4 mm, which is slightly higher than the minimum correlation length. We also compared the results from different grid spacings with that of the 0.1 mm grid spacing, as shown with dashed boxes. For the 0.3 mm case, where the grid spacing is slightly smaller than the minimum correlation length, its deviation D_2 is, on average, 1.23%. When the grid spacing is 0.2 mm, the difference decreases, on average, to

0.55%. These results further indicate that the small-scale roughness, on scales less than the grid spacing, would have only a limited effect on the general flow behaviour as long as the grid spacing is less than the correlation length of the fracture aperture field.

2.5.2 Limitations of the current study

The main limitation of the current study is in the treatment of non-segmented areas, in which it is assumed that the flow direction is governed by each local fracture cell. The validity of such an assumption relies on both the aspect ratio of each cell and the alternation of the centreline orientation between adjacent cells. This assumption may be violated when either the aspect ratio is not small enough for the cell geometry to sufficiently constraint the flow or when the flow behaviour of nearby cells has a dominating impact on other cells. Thus, the non-segmented area should be limited to a small proportion of the total fracture area in order to provide accurate results. In extreme cases when no segment can be formed (P_s=0%), the aperture field will be modified by each local cell, which is effectively the same approach as Ge (1997) and Konzuk and Kueper (2004). Note that in-situ rock fractures are always in contact over a certain portion of the fracture area and hence, no segment will be formed in these contact areas where the apertures are zero. As our model is based on two-dimensional analyses, its performance may be affected in cases where strong flow channelling occurs due to fracture surfaces in contact. However, our aperture modification can still be applied in fractures with contacts and can improve the estimation of the aperture once the three-dimensional open channels are identified and transformed into two-dimensional ones. Further studies are currently in progress.

Another limitation is the assumption made for local roughness effect, where F_{lr} is used to estimate smaller apertures in each segment. Even when F_{lr} is the same for two segments, the local roughness effects may vary for different combinations of upper and lower wall geometry (i.e. wall alignment and roughness). For example, take two fracture segments with the same standard deviation of asperity height for both walls and the same mean aperture; one is perfectly matched and the other is mismatched. The local roughness will have different effects on the flow behaviours in these two segments but F_{lr} is the same. Although this variation has only a small impact on the general performance of the MCL when the geometrical and dynamical conditions are met, it would further improve the accuracy of the model if the local roughness effect is evaluated based on the various geometric combinations of segment walls with different roughness and alignment.

2.6 Summary

The modified cubic law (MCL) developed in this study has improved the performance (in terms of quantifying flow fields) of the standard cubic law (CL) by incorporating in the aperture field the modifying factors of flow tortuosity, aperture variation and local roughness effects. Flow simulations were conducted in 45 synthetic fractures with different surface roughness and aperture variations to test the performance of the proposed MCL.

In general, the proposed MCL provides improved flow predictions compared with those of the standard CL and previous versions of CL-based models. The deviation (*D*) of flow predictions from CFD simulations for synthetic fractures using the MCL (C1) ranges from -11.13% to 8.35% and the average effective deviation ($\overline{|D|}$) is 4.72%, while for the standard CL and the formulations of Konzuk and Kueper (2004) and Wang et al. (2015), the average effective deviations are 26.06%, 9.50% and 11.38% respectively. Moreover, the MCL (C1) performs the best under different surface roughness conditions with $\overline{|D|}$ less than 6% for all *JRC* cases used in this study. The proposed MCL provides a more accurate estimate of the hydraulic properties of the single fracture at low Reynolds number and it may be extended to study the hydraulic behaviours in fracture networks and other hydro-related problems in rough rock fractures.

Acknowledgements

This work is financially supported by a joint scholarship provided by the China Scholarship Council (CSC) and The University of Adelaide. We thank Murat Karakus and Hang Wang at The University of Adelaide and Lichun Wang from University of Texas at Austin for useful discussions.

References

Barton, N.: Review of a new shear-strength criterion for rock joints. Eng. Geol. 7, 287–332 (1973). doi:10.1016/0013-7952(73)90013-6

Basha, H.A., El-Asmar, W.: The fracture flow equation and its perturbation solution. Water Resour. Res. 39, 1365 (2003). doi:10.1029/2003WR002472

Berkowitz, B.: Characterizing flow and transport in fractured geological media: A review. Adv. Water Resour. 25, 861–884 (2002). doi:10.1016/S0309-1708(02)00042-8

Brown, S.R.: Fluid flow through rock joints: the effect of surface roughness. J. Geophys. Res. 92, 1337–1347 (1987). doi:10.1029/JB092iB02p01337

Brush, D.J., Thomson, N.R.: Fluid flow in synthetic rough-walled fractures: Navier-Stokes,

Stokes, and local cubic law simulations. Water Resour. Res. 39, 1085 (2003). doi:10.1029/2002WR001346

Dippenaar, M.A., Van Rooy, J.L.: On the cubic law and variably saturated flow through discrete open rough-walled discontinuities. Int. J. Rock Mech. Min. Sci. 89, 200–211 (2016). doi:10.1016/j.ijrmms.2016.09.011

Ge, S.: A governing equation for fluid flow in rough fractures. Water Resour. Res. 33, 53–61 (1997). doi:10.1029/96WR02588

Jang, H.S., Kang, S.S., Jang, B.A.: Determination of Joint Roughness Coefficients Using Roughness Parameters. Rock Mech. Rock Eng. 47, 2061–2073 (2014). doi:10.1007/s00603-013-0535-z

Konzuk, J.S., Kueper, B.H.: Evaluation of cubic law based models describing single-phase flow through a rough-walled fracture. Water Resour. Res. 40, 1–17 (2004). doi:10.1029/2003WR002356

Myers, N.O.: Characterization of surface roughness. Wear. 5, 182–189 (1962). doi:10.1016/0043-1648(62)90002-9

Nazridoust, K., Ahmadi, G., Smith, D.H.: A new friction factor correlation for laminar, single-phase flows through rock fractures. J. Hydrol. 329, 315–328 (2006). doi:10.1016/j.jhydrol.2006.02.032

Nicholl, M.J., Rajaram, H., Glass, R.J., Detwiler, R.: Saturated flow in a single fracture: Evaluation of the Reynolds equation in measured aperture fields. Water Resour. Res. 35, 3361–3373 (1999). doi:10.1029/1999WR900241

Ogilvie, S.R., Isakov, E., Glover, P.W.J.: Fluid flow through rough fractures in rocks. II: A new matching model for rough rock fractures. Earth Planet. Sci. Lett. 241, 454–465 (2006). doi:10.1016/j.epsl.2005.11.041

Olsson, R., Barton, N.: An improved model for hydromechanical coupling during shearing of rock joints. Int. J. Rock Mech. Min. Sci. 38, 317–329 (2001). doi:10.1016/S1365-1609(00)00079-4

Oron, A.P., Berkowitz, B.: Flow in rock fractures: The local cubic law assumption reexamined. Water Resour. Res. 34, 2811–2825 (1998). doi:10.1029/98WR02285

Patir, N., Cheng, H.S.: An Average Flow Model for Determining Effects of Three-Dimensional Roughness on Partial Hydrodynamic Lubrication. J. Lubr. Technol. 100, 12–17 (1978). doi:10.1115/1.3453103

Pyrak-Nolte, L.J., Cook, N.G.W., Nolte, D.D.: Fluid percolation through single fractures. Geophys. Res. Lett. 15, 1247–1250 (1988). doi:doi:10.1029/GL015i011p01247

Reimus, P.W., Robinson, B.A., Glass, R.J.: Aperture characteristics, saturated fluid flow, and tracer transport calculations for a natural fracture.pdf. In: In Proceedings of the 4th Annual International Conference on High Level Radioactive Waste. pp. 2009–2016. , Las Vegas, NV, USA (1993)

Renshaw, C.E.: On the relationship between mechanical and hydraulic apertures in rough-walled fractures. J. Geophys. Res. 100, 24629–24636 (1995). doi:10.1029/95JB02159

Snow, D.T.: Anisotropie Permeability of Fractured Media. Water Resour. Res. 5, 1273–1289

(1969). doi:10.1029/WR005i006p01273

Tsang, Y.W.: The Effect of Tortuosity on Fluid Flow Through a Single Fracture. Water Resour. Res. 20, 1209–1215 (1984). doi:10.1029/WR020i009p01209

Tsang, Y.W., Tsang, C.F.: Flow channeling in a single fracture as a two-dimensional strongly heterogeneous permeable medium. Water Resour. Res. 25, 2076–2080 (1989). doi:10.1029/WR025i009p02076

Walsh, J.B., Brace, W.F.: The effect of pressure on porosity and the transport properties of rock. J. Geophys. Res. 89, 9425–9431 (1984). doi:10.1029/JB089iB11p09425

Wang, L., Cardenas, M.B.: Development of an empirical model relating permeability and specific stiffness for rough fractures from numerical deformation experiments. J. Geophys. Res. Solid Earth. 121, 4977–4989 (2016). doi:10.1002/2016JB013004

Wang, L., Cardenas, M.B., Slottke, D.T., Ketcham, R.A., Sharp, J.M.: Modification of the Local Cubic Law of fracture flow for weak inertia, tortuosity, and roughness. Water Resour. Res. 51, 2064–2080 (2015). doi:10.1002/2014WR015815

Witherspoon, P.A., Wang, J.S.Y., Iwai, K., Gale, J.E.: Validity of Cubic Law for fluid flow in a deformable rock fracture. Water Resour. Res. 16, 1016–1024 (1980). doi:10.1029/WR016i006p01016

Xiong, X., Li, B., Jiang, Y., Koyama, T., Zhang, C.: Experimental and numerical study of the geometrical and hydraulic characteristics of a single rock fracture during shear. Int. J. Rock Mech. Min. Sci. 48, 1292–1302 (2011). doi:10.1016/j.ijrmms.2011.09.009

Xu, C., Dowd, P.A., Tian, Z.F.: A simplified coupled hydro-thermal model for enhanced geothermal systems. Appl. Energy. 140, 135–145 (2015). doi:10.1016/j.apenergy.2014.11.050

Yeo, I.W., de Freitas, M.H., Zimmerman, R.W.: Effect of shear displacement on the aperture and permeability of a rock fracture. Int. J. Rock Mech. Min. Sci. 35, 1051–1070 (1998). doi:10.1016/S0148-9062(98)00165-X

Zimmerman, R., Bodvarsson, G.: Hydraulic conductivity of rock fractures. Transp. Porous Media. 23, 1–30 (1996). doi:10.1007/BF00145263

Zimmerman, R., Yeo, I.: Fluid Flow in Rock Fractures: From the Navier-Stokes Equations to the Cubic Law. Dyn. fluids Fract. rock. 213–224 (2000). doi:10.1029/GM122p0213

Zimmerman, R.W.: Fluid Flow in Rock Fractures. In: Proc. 11th Int. Conf. on Computer Methods and Advances in Geomechanics. pp. 89–107. , Turin, Italy (2005)

Zimmerman, R.W., Kumar, S., Bodvarsson, G.S.: Lubrication theory analysis of the permeability of rough-walled fractures. Int. J. Rock Mech. Min. Sci. 28, 325–331 (1991). doi:10.1016/0148-9062(91)90597-F

Zou, L., Jing, L., Cvetkovic, V.: Roughness decomposition and nonlinear fluid flow in a single rock fracture. Int. J. Rock Mech. Min. Sci. 75, 102–118 (2015). doi:10.1016/j.ijrmms.2015.01.016

Chapter 3: Perturbation Solutions for Flow in a Slowly Varying Fracture and the Estimation of Its Transmissivity

Statement of Authorship

Title of Paper	Perturbation solutions for flow in a slowly varying fracture and the estimation of its transmissivity
Publication Status	☑ Published ☐ Accepted for Publication ☐ Submitted for Publication ☐ Unpublished and Unsubmitted work written in manuscript style
Publication Details	Wang, Z., C. Xu, and P. Dowd (2019), Perturbation solutions for flow in a slowly varying fracture and the estimation of its transmissivity, Transport in Porous Media, 128(1), 97–121.

Principal Author

Name of Principal Author (Candidate)	Zhihe Wang
Contribution to the Paper	Development of the methods, conduct of the analysis, validation and drafting the manuscript.
Overall percentage (%)	70%
Certification:	This paper reports on original research I conducted during the period of my Higher Degree by Research candidature and is not subject to any obligations or contractual agreements with a third party that would constrain its inclusion in this thesis. I am the primary author of this paper.
Signature	Date 22/08/2019

Co-Author Contributions

By signing the Statement of Authorship, each author certifies that:

i. the candidate's stated contribution to the publication is accurate (as detailed above);

ii. permission is granted for the candidate in include the publication in the thesis; and

iii. the sum of all co-author contributions is equal to 100% less the candidate's stated contribution.

Name of Co-Author	Chaoshui Xu
Contribution to the Paper	Supervision, design of the work and reviewing the manuscript.
Signature	Date 22/08/2019

Name of Co-Author	Peter Dowd
Contribution to the Paper	Supervision, design of the work and reviewing the manuscript.
Signature	Date 21/8/2019

Please cut and paste additional co-author panels here as required.

Abstract

Flow in fractures or channels is of interest in many environmental and geotechnical applications. Most previously published perturbation analyses for fracture flow assume that the ratio of the flow in the fracture aperture direction to flow in the fracture length direction is of the same order as the ratio of the mean fracture aperture to fracture length and hence the dominant flow is in the fracture length direction. This assumption may impose an overly-strict requirement for flow in the fracture length direction to be dominant, which limits the applicability of the solutions. This study uses the ratio of the aperture variation to fracture length as the perturbation parameter to derive perturbation solutions for flow in two-dimensional fractures under both the pressure boundary condition (PBC) and flow rate boundary condition (FBC). The solutions are cross-validated with direct numerical solutions of the Navier-Stokes equations and solutions from published perturbation analyses using the geometry of two-dimensional symmetric wedges and fractures with sinusoidal varying walls. The study shows that, compared with the PBC solution, the FBC solution is in a closer agreement with simulation results and provides a better estimate of the fracture transmissivity especially when inertial effects are more than moderate. The improvement is due mainly to the FBC solution providing a more accurate quantification of inertial effects. The solutions developed in this study provide improved means of analysing the hydraulic properties of fractures/channels and can be applied to complex flow conditions and fracture geometries.

3.1 Introduction

Fluid flow through fractured geological media is a vital process in a variety of environmental and geotechnical applications including underground water systems, petroleum and geothermal reservoirs, underground rock excavations and hazardous waste disposal (e.g., Hunt and Sahimi 2017; Pyrak-Nolte and Nolte 2016; Xu et al. 2015; Zimmerman and Bodvarsson 1996). Although most problems that arise in these engineering applications are at large-scale, a sound knowledge of the controlling mechanism of fluid flow at pore-scale is essential to providing important insights and directions for solving problems at larger scales (Berkowitz 2002; Kitanidis and Dykaar 1997).

Flow in fractures or channels is normally treated as a steady-state incompressible fluid flowing within two parallel planar plates separated by a constant aperture so that the flow behaviours can be described by the cubic law (CL), where the flow rate is related to the cube of the fracture aperture for a given pressure or hydraulic gradient (e.g., Lomize 1951; Witherspoon et al. 1980). Fractures and channels, occurring naturally or as the result of human disturbance, commonly have a complex void geometry and hence, have a varying aperture field (e.g., Brown 1987; Zou et al. 2017). To account for the spatial variability of fracture aperture, the Reynolds equation, also known as the local cubic law (LCL), is widely used to improve the flow estimation in rough-walled fractures by assuming that the CL applies at each explicit location throughout the fracture (Zimmerman et al. 1991). However, the validity of using the LCL to describe the fracture flow has frequently been questioned in previous experimental and numerical studies. For example, Yeo et al. (1998) observed that, on average, the LCL over-estimates the flow rate measured from experiments by a factor of 1.85. Brush and Thomson (2003) conducted a numerical analysis and found that the LCL over-estimates the flow rate by a factor up to 1.25, even when inertial effects are not considered. Numerous studies have since focused on developing alternative models by modifying the CL and LCL. Some studies (e.g., Nazridoust et al. 2006; Olsson and Barton 2001; Patir and Cheng 1978) attempted to incorporate statistical and empirical parameters into the CL using data from experiments or numerical simulations to estimate the equivalent hydraulic aperture (Brown 1987). Other approaches included modifications to the aperture field by considering the effects of aperture variation and flow tortuosity at the local scale (Ge 1997; Konzuk and Kueper 2004) or fracture segment scale (Oron and Berkowitz 1998; Wang et al. 2018). Although these approaches may have improved the prediction of flow, the fundamental CL assumption remains, in which flow is always one-dimensional with negligible inertial effects, either globally or locally. This

assumption limits the ability of previous CL-based models to accommodate more complex flow conditions and fracture geometries that are widely encountered in realistic problems.

Physically, the complexity of the flow behaviours in a fracture with complex void geometry can be well-described by the three-dimensional Navier-Stokes equations (Zimmerman 2005). However, solving the three-dimensional Navier-Stokes equations numerically in this case is expensive in terms of computational time and memory requirements (Brush and Thomson 2003; Wang et al. 2018). In this context, many approximate solutions to the two-dimensional Navier-Stokes equations are derived through perturbation expansion; conceptual models can then be developed based on these approximate solutions to provide better estimates of flow in fractured rocks (Basha and El-Asmar 2003). Wang (1978) derived a perturbation expansion to Stokes flow in a two-dimensional periodic fracture by assigning a pressure difference between the inflow and outflow boundaries using the ratio of the mean aperture to fracture length as the perturbation parameter. Kitanidis and Dykaar (1997) derived a similar perturbation solution to Stokes flow in a fracture bounded by two sinusoidal walls. Basha and El-Asmar (2003) conducted and evaluated the perturbation analysis for fracture flow in various fracture wall configurations with the same perturbation parameter. In these studies, inertial effects are either neglected or the Reynolds number is defined by the discharge of flow through parallel plates separated by the mean aperture over the kinematic viscosity, which may lead to deviations in the quantification of inertial effects. In addition, using the ratio of the mean aperture to fracture length as the perturbation parameter may impose an overly-strict requirement for the domination of flow in the fracture length direction over flow in the fracture aperture direction, which limits the application scope of the solutions (Zimmerman 2005). Sisavath et al. (2003) derived a perturbation solution to the problem of two-dimensional flow in a fracture with two sinusoidal walls by prescribing a discharge at the flow inlet boundary with the ratio of the amplitude to fracture length as the perturbation parameter, but the inertial effects are not incorporated in their study. Throughout these analyses, the solutions are in different forms for the pressure boundary condition (PBC), obtaining the flow rate with a given pressure difference, and the flow rate boundary condition (FBC), obtaining the pressure difference with a given flow rate. However, to the best of our knowledge, there is no published study with a detailed evaluation or comparison of the PBC and FBC solutions and thus the ability of both solutions to describe flow through fractures is not clear.

The purpose of this study is to improve the analysis of the hydraulic properties of fractures for complex flow conditions and varying fracture geometries by conducting perturbation

analysis. The derived solutions can provide a theoretical basis for the analysis of, for example, fracture transmissivity (e.g., Basha and El-Asmar 2003; Hasegawa and Fukuoka 1980; Nicholl et al. 1999) and eddy formation at local positions (e.g., Hasegawa and Izuchi 1983; Kitanidis and Dykaar 1997). In this work, perturbation solutions to the two-dimensional Navier-Stokes equations were derived for both the PBC and FBC. The stream function under the PBC was derived using an approach similar to the method proposed by Kitanidis and Dykaar (1997) but with an additional consideration of inertial effects, the stream function for the FBC was obtained largely by following the approach discussed by Van Dyke (1987). With the auxiliary condition, the perturbation solutions were derived to the second-order. The derived solutions were tested with two-dimensional symmetric wedges using the ratio of the aperture variation to fracture length as the perturbation parameter. The solutions based on two different boundary conditions were then compared with numerical simulation results in terms of different wedge geometries and different Reynolds number in the range of 0.1 to 20, which covers three main flow regimes. Fractures with sinusoidal varying walls were also used for additional validations. In general, the FBC solution was found to be in a closer agreement with the simulation results especially when inertial effects are more than moderate. Perturbation solutions from previous studies were also used in a comparative study of fracture transmissivity to examine further the performance of the FBC perturbation solution presented in this study. Compared with previously published perturbation solutions, the FBC solution improves the accuracy of the estimated transmissivity and can be applied to a wider range of fracture geometries (i.e., no constraint on the ratio of the mean aperture to fracture length).

3.2 Problem formulation

3.2.1 Governing equations

Consider a steady-state flow in a two-dimensional fracture (normal to the mean plane of a generic fracture in three-dimensions) with a slowly varying aperture (Van Dyke 1987; Kitanidis and Dykaar 1997) as shown in Figure 3.1, in which the fluid is incompressible and the walls are impermeable. The fracture length and width are in the x and y directions, respectively. For flow in subsurface fractures, the governing equations are given by the Navier-Stokes equations (NSE), assuming that the gravity forms the only body force and with the condition for mass continuity (e.g., Crandall et al. 2010; Zimmerman and Bodvarsson 1996):

$$u\frac{\partial u}{\partial x} + w\frac{\partial u}{\partial y} = -\frac{1}{\rho}\frac{\partial P}{\partial x} + \nu\left(\frac{\partial^2 u}{\partial x^2} + \frac{\partial^2 u}{\partial y^2}\right) \tag{3.1}$$

$$u\frac{\partial w}{\partial x} + w\frac{\partial w}{\partial y} = -\frac{1}{\rho}\frac{\partial P}{\partial y} + \nu\left(\frac{\partial^2 w}{\partial x^2} + \frac{\partial^2 w}{\partial y^2}\right) \tag{3.2}$$

$$\frac{\partial u}{\partial x} + \frac{\partial w}{\partial y} = 0 \tag{3.3}$$

where u and w are velocities in the x and y directions, respectively, ρ is the fluid density, P is the reduced pressure and v is the kinematic viscosity of the fluid. The first two equations are effectively momentum continuity equations and the third describes mass conservation. The first two terms on the left-hand sides of equations (3.1) and (3.2) are the advective terms that account for inertial forces, the third term represents the pressure gradient and the last two terms are for viscous forces. Equations (3.1) and (3.2) become Stokes equations when inertial terms are negligibly small compared to viscous terms (i.e., Reynolds number Re=0) and become Euler equations when viscous effects are neglected (Kundu and Cohen 2008).

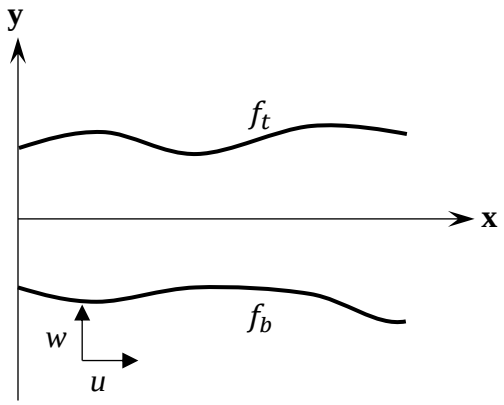

Figure 3.1 Illustration of a two-dimensional fracture with a slowly varying aperture.

3.2.2 Boundary conditions

Non-slip boundary and impermeable wall (no flux across the fracture walls) conditions are assumed for both the top and bottom walls, leading to:

$$u|_{y=f_t(x)} = 0,\ w|_{y=f_t(x)} = 0 \tag{3.4}$$

$$u|_{y=f_b(x)} = 0,\ w|_{y=f_b(x)} = 0 \tag{3.5}$$

where $f_t(x)$ and $f_b(x)$ are functions that describe the geometry of the top and bottom walls as shown in Figure 3.1. The fracture aperture H is then given by $f_t(x)$-$f_b(x)$ that varies along the horizontal axis x to provide a varying aperture in the fracture length direction.

A non-zero pressure difference between the inflow and outflow boundaries produces a flow Q through the fracture, resulting in the following boundary conditions:

$$P|_{x=x_1} = P(x_1) \tag{3.6}$$

$$P|_{x=x_2} = P(x_2) \tag{3.7}$$

Where x_1 and x_2 are the locations of the fracture inflow and outflow boundaries and hence the length of fracture considered is $l=x_1-x_2$ and the pressure difference is $\Delta P=P(x_1)-P(x_2)$.

3.2.3 The stream function

The stream function Ψ is defined by

$$u = \frac{\partial \Psi}{\partial y},\ w = -\frac{\partial \Psi}{\partial x} \tag{3.8}$$

Substituting the stream function into the governing equations and cancelling out the pressure terms after differentiating equations (3.1) and (3.2) over y and x, respectively, we find that the defined stream function must satisfy:

$$\frac{\partial}{\partial y}\left(\frac{\partial \Psi}{\partial y}\frac{\partial^2 \Psi}{\partial x \partial y} - \frac{\partial \Psi}{\partial x}\frac{\partial^2 \Psi}{\partial y^2}\right) - \frac{\partial}{\partial x}\left(-\frac{\partial \Psi}{\partial y}\frac{\partial^2 \Psi}{\partial x^2} + \frac{\partial \Psi}{\partial x}\frac{\partial^2 \Psi}{\partial x \partial y}\right) = \nu\left(\frac{\partial^4 \Psi}{\partial x^4} + 2\frac{\partial^4 \Psi}{\partial x^2 \partial y^2} + \frac{\partial^4 \Psi}{\partial y^4}\right) \tag{3.9}$$

Equation (3.9) becomes the bi-harmonic equation under the Stokes flow condition, where the terms on the left-hand side of the equation become zero (Kitanidis and Dykaar 1997; Wang 1978).

3.2.4 The auxiliary condition

As the pressure terms are eliminated in equation (3.9), an auxiliary relationship needs to be derived to relate the pressure term to the stream function. Since a steady-state flow is prescribed under a given pressure difference, the mean pressure difference over the fracture aperture in the length direction can be assumed to equal a constant mean pressure difference (Hasegawa and Izuchi 1983), leading to:

$$\Delta P = \int_{x_1}^{x_2} \frac{1}{H(x)}\left(\int_{f_b(x)}^{f_t(x)} \frac{\partial P}{\partial x} dy\right) dx \tag{3.10}$$

The pressure derivative $\partial p/\partial x$ can easily be obtained from equation (3.1) and, after inserting the stream function, it becomes:

$$\frac{\partial P}{\partial x} = \mu\left(\frac{\partial^3 \Psi}{\partial x^2 \partial y} + \frac{\partial^3 \Psi}{\partial y^3}\right) + \rho\left(\frac{\partial \Psi}{\partial x}\frac{\partial^2 \Psi}{\partial y^2} - \frac{\partial \Psi}{\partial y}\frac{\partial^2 \Psi}{\partial x \partial y}\right) \tag{3.11}$$

in which μ is the dynamic viscosity. Equation (3.10), together with equation (3.11), provides the auxiliary condition that gives the relationship between the mean pressure difference and stream function. The final solution is obtained by solving equation (3.9), using associated boundary conditions, together with equation (3.10).

3.3 Solutions

3.3.1 Solution for the pressure boundary condition

Under the pressure boundary condition, a known pressure difference is assigned between the inflow and outflow boundaries, hence we are seeking to derive the amount of discharge through the fracture at the given pressure difference. First, all distance terms are made dimensionless by dividing them by the mean fracture aperture H_m. Then the discharge per unit width, Q, and the stream function are divided by Q_m to become dimensionless. Q_m is the discharge per unit width in a fracture with a uniform aperture H_m, and can be given by the CL as:

$$Q_m = -\frac{H_m^3}{12\mu}\frac{\Delta P}{l} \tag{3.12}$$

The following additional non-dimensional variables are also used in the derivation:

$$X = \epsilon x, \quad Y = \frac{y}{h(X)} = \frac{y}{h(\epsilon x)}, \quad R_p = \frac{Q_m}{\nu}. \tag{3.13}$$

where ϵ is a small dimensionless parameter that describes the gradual change of aperture along the fracture length i.e. the ratio of the aperture variation to length, ω/l (Van Dyke 1987; Sisavath et al. 2003), which is the perturbation parameter used in this study; h is half the fracture aperture; and R_p is the Reynolds number defined under the PBC. Note that, for simplicity, we keep the same symbols in the derivation below, but these symbols are now the dimensionless counterparts of their original definitions. With these dimensionless variables, equation (3.9) becomes

$$R_p\left[\frac{\epsilon}{h}\frac{\partial\Psi}{\partial Y}\frac{\partial}{\partial X}\left(\frac{1}{h^2}\frac{\partial^2\Psi}{\partial Y^2}\right)+\frac{\epsilon^3}{h}\frac{\partial\Psi}{\partial Y}\frac{\partial^3\Psi}{\partial X^3}-\epsilon^3\frac{\partial\Psi}{\partial X}\frac{\partial^2}{\partial X^2}\left(\frac{1}{h}\frac{\partial\Psi}{\partial Y}\right)-\frac{\epsilon}{h^3}\frac{\partial\Psi}{\partial X}\frac{\partial^3\Psi}{\partial Y^3}\right]=\epsilon^4\frac{\partial^4\Psi}{\partial X^4}+ 2\epsilon^2\frac{\partial^2}{\partial X^2}\left(\frac{1}{h^2}\frac{\partial^2\Psi}{\partial Y^2}\right)+\frac{1}{h^4}\frac{\partial^4\Psi}{\partial Y^4} \tag{3.14}$$

Consider a symmetric fracture for which x varies from 0 to l and y varies from -h to h. The dimensionless auxiliary condition is given by

$$1=-\frac{1}{12\omega}\int_0^{\omega}\int_0^1\epsilon^2\left[\frac{2h_X{}^2}{h^3}\frac{\partial\Psi}{\partial Y}-\frac{h_{XX}}{h^2}\frac{\partial\Psi}{\partial Y}-\frac{h_X}{h^2}\frac{\partial}{\partial X}\left(\frac{\partial\Psi}{\partial Y}\right)-\frac{h_X}{h^2}\frac{\partial}{\partial X}\left(\frac{\partial\Psi}{\partial Y}\right)+\frac{1}{h}\frac{\partial^2}{\partial X^2}\left(\frac{\partial\Psi}{\partial Y}\right)\right]+\frac{1}{h^3}\frac{\partial^3\Psi}{\partial Y^3}+ R_p\left\{\frac{\epsilon}{h^2}\frac{\partial\Psi}{\partial X}\frac{\partial^2\Psi}{\partial Y^2}-\frac{\epsilon}{h}\frac{\partial\Psi}{\partial Y}\left[-\frac{h_X}{h^2}\frac{\partial\Psi}{\partial Y}+\frac{1}{h}\frac{\partial}{\partial X}\left(\frac{\partial\Psi}{\partial Y}\right)\right]\right\}dY\,dX \tag{3.15}$$

The associated boundary conditions are

$$\left.\frac{\partial\Psi}{\partial Y}\right|_{Y=\pm1}=0, \quad \Psi|_{Y=\pm1}=\pm\frac{Q}{2}. \tag{3.16}$$

Using the perturbation parameter, ϵ, the stream function and discharge can be expressed as the sum of different order terms:

$$\Psi = \Psi_0 + \epsilon\Psi_1 + \epsilon^2\Psi_2 + \cdots \tag{3.17}$$

$$Q = Q_0 + \epsilon Q_1 + \epsilon^2 Q_2 + \cdots \tag{3.18}$$

The terms up to the second-order are obtained by substituting equations (3.17) and (3.18) into (3.14) to (3.16). Retaining the terms at different orders after derivation, the stream function up to the second-order terms can be found as:

$$\Psi_0 = Q_0\left(\frac{3}{4}Y - \frac{1}{4}Y^3\right) \tag{3.19}$$

$$\Psi_1 = \frac{3R_p{Q_0}^2 h_X}{1120}(5Y - 11Y^3 + 7Y^5 - Y^7) + \frac{1}{4}Q_1(3Y - Y^3) \tag{3.20}$$

$$\Psi_2 = \frac{{R_p}^2 Q_0}{3449600}\left[{h_X}^2(2875Y - 8222Y^3 + 8778Y^5 - 4488Y^7 + 1155Y^9 - 98Y^{11}) - hh_{XX}(1213Y - 3279Y^3 + 3234Y^5 - 1518Y^7 + 385Y^9 - 35Y^{11})\right] + \frac{3Q_0}{40}(4h_X^2 - hh_{XX})(Y - 2Y^3 + Y^5) + \frac{9R_pQ_1h_X}{560}(5Y - 11Y^3 + 7Y^5 - Y^7) + \frac{1}{4}Q_2(3Y - Y^3) \tag{3.21}$$

where h_X and h_{XX} are the first and second derivative of h with respect to X, respectively. Equations (3.19) to (3.21) become identical to the stream function obtained in Kitanidis and Dykaar (1997) when R_p is 0. The associated discharge up to the second-order terms can be given as:

$$Q_0 = \left(\int_0^\omega \frac{1}{8\omega h^3}\,dX\right)^{-1} \tag{3.22}$$

$$Q_1 = \int_0^\omega \frac{9R_p{Q_0}^3 h_X}{280\omega h^3}\,dX \tag{3.23}$$

$$Q_2 = \int_0^\omega \frac{3{Q_0}^2{h_X}^2}{40\omega h^3} - \frac{{Q_0}^2 hh_{XX}}{20\omega h^3} + \frac{9R_p{Q_0}^2 Q_1 h_X}{140\omega h^3} + \frac{13{R_p}^2{Q_0}^4}{26950\omega h^3}({h_X}^2 - \frac{3}{4}hh_{XX})dX \tag{3.24}$$

The detailed derivation is given in Appendix A1.

3.3.2 Solution under the flow rate boundary condition

For the flow rate boundary condition, a given flow rate Q is initially assigned and the solution that we are seeking is for the pressure difference between the flow boundaries. All distance terms within the fracture are made dimensionless by dividing them by the mean fracture aperture H_m and the stream function is made dimensionless by dividing it by half the discharge $Q/2$. Then the mean pressure difference ΔP is divided by the mean pressure difference per unit width of a fracture with a uniform aperture, ΔP_m, given by the CL as:

$$\Delta P_m = -\frac{12\mu lQ}{{H_m}^3} \tag{3.25}$$

The same symbol is used for the mean pressure difference, ΔP, but it is now dimensionless. Now introduce the following non-dimensional variables:

$$X = \epsilon x, \quad Y = \frac{y}{h(X)} = \frac{y}{h(\epsilon x)}, \quad R_q = \frac{Q/2}{\nu} \tag{3.26}$$

Note that the first two variables are the same as those defined earlier but the Reynolds number R_q defined here differs from that in the previous section. Using these non-dimensional variables, equation (3.9) becomes

$$R_q\left[\frac{\epsilon}{h}\frac{\partial\Psi}{\partial Y}\frac{\partial}{\partial X}\left(\frac{1}{h^2}\frac{\partial^2\Psi}{\partial Y^2}\right) + \frac{\epsilon^3}{h}\frac{\partial\Psi}{\partial Y}\frac{\partial^3\Psi}{\partial X^3} - \epsilon^3\frac{\partial\Psi}{\partial X}\frac{\partial^2}{\partial X^2}\left(\frac{1}{h}\frac{\partial\Psi}{\partial Y}\right) - \frac{\epsilon}{h^3}\frac{\partial\Psi}{\partial X}\frac{\partial^3\Psi}{\partial Y^3}\right] = \epsilon^4\frac{\partial^4\Psi}{\partial X^4} + 2\epsilon^2\frac{\partial^2}{\partial X^2}\left(\frac{1}{h^2}\frac{\partial^2\Psi}{\partial Y^2}\right) + \frac{1}{h^4}\frac{\partial^4\Psi}{\partial Y^4} \tag{3.27}$$

Given the fracture symmetry, the dimensionless auxiliary condition is given by

$$\Delta P = -\int_0^\omega \int_0^1 \frac{1}{24\omega}\left[\epsilon^2\frac{\partial^2}{\partial X^2}\left(\frac{1}{h}\frac{\partial\Psi}{\partial Y}\right) + \frac{1}{h^3}\frac{\partial^3\Psi}{\partial Y^3}\right] + \frac{R_q}{24\omega}\left[\frac{\epsilon}{h^2}\frac{\partial\Psi}{\partial X}\frac{\partial^2\Psi}{\partial Y^2} - \frac{\epsilon}{h}\frac{\partial\Psi}{\partial Y}\frac{\partial}{\partial X}\left(\frac{1}{h}\frac{\partial\Psi}{\partial Y}\right)\right] dY\, dX \tag{3.28}$$

and the associated boundary conditions are given by (Van Dyke 1987):

$$\left.\frac{\partial\Psi}{\partial Y}\right|_{Y=\pm1} = 0, \quad \Psi|_{Y=\pm1} = \pm1 \tag{3.29}$$

The stream function and mean pressure difference can be written as a sum of different order terms:

$$\Psi = \Psi_0 + \epsilon\Psi_1 + \epsilon^2\Psi_2 + \cdots \tag{3.30}$$

$$\Delta P = \Delta P_0 + \epsilon\Delta P_1 + \epsilon^2\Delta P_2 + \cdots \tag{3.31}$$

The solution of the stream function up to the second-order terms is obtained by substituting equations (3.30) and (3.31) into (3.27) and (3.29), and has the form as:

$$\Psi_0 = \frac{1}{2}(3Y - Y^3) \tag{3.32}$$

$$\Psi_1 = \frac{3R_q h_X}{280}(5Y - 11Y^3 + 7Y^5 - Y^7) \tag{3.33}$$

$$\Psi_2 = \frac{{R_q}^2}{431200}\left[{h_X}^2(2875Y - 8222Y^3 + 8778Y^5 - 4488Y^7 + 1155Y^9 - 98Y^{11}) - hh_{XX}(1213Y - 3279Y^3 + 3234Y^5 - 1518Y^7 + 385Y^9 - 35Y^{11})\right] + \frac{3}{20}(4h_X^2 - hh_{XX})(Y - 2Y^3 + Y^5) \tag{3.34}$$

The stream function under the FBC, equations (3.32) to (3.34), are in agreement with the stream function obtained in Van Dyke (1987). The associated mean pressure difference for the first three order terms are obtained by inserting the stream function into equation (3.28):

$$\Delta P_0 = \int_0^\omega \frac{1}{8\omega h^3} dX \tag{3.35}$$

$$\Delta P_1 = -\int_0^\omega \frac{9R_q h_X}{140\omega h^3} dX \tag{3.36}$$

$$\Delta P_2 = -\int_0^{\omega} \frac{3h_X^2 - 2hh_{XX}}{40\omega h^3} + \frac{13{R_q}^2}{13475\omega h^3}\left(2{h_X}^2 - \frac{3}{2}hh_{XX}\right) dX \tag{3.37}$$

The detailed derivation process is given in Appendix A2.

3.4 Flow in two-dimensional wedges

3.4.1 Perturbation solutions

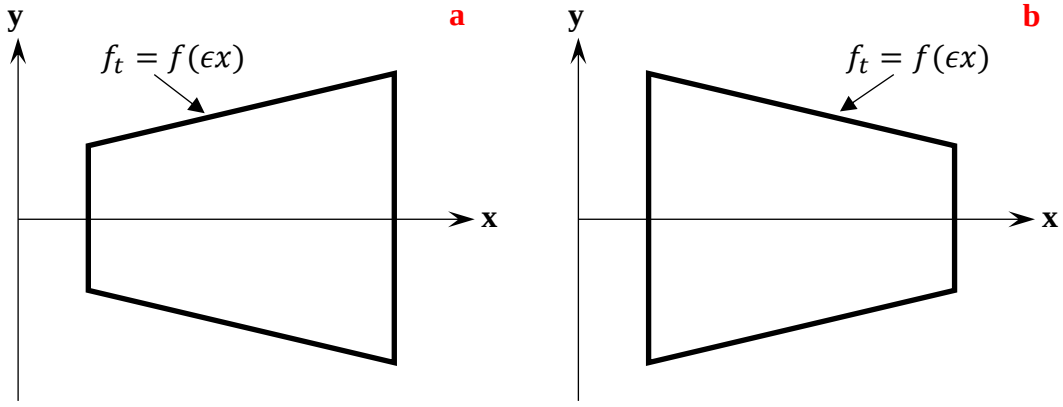

Figure 3.2 Two symmetric wedges with (a) one diverging wedge and (b) one converging wedge.

Flow in various fracture geometries has been studied by considering fracture walls as parallel plates, saw-tooth shaped walls and sinusoidally-varying walls (e.g., Crandall et al. 2010; Nicholl et al. 1999; Sisavath et al. 2003). Among these approximations, fracture is found to be well described by a series of connected wedges (e.g., Brush and Thomson 2003; Nicholl et al. 1999; Wang et al. 2018) and we use a wedge-shaped fracture to obtain the final solutions in this section. Consider a two-dimensional symmetric wedge as shown in Figure 3.2, the upper wall can be described as:

$$f_t(x) = h(x_1) + \frac{h(x_2) - h(x_1)}{l} x \tag{3.38}$$

The aperture along the wedge length can be obtained as

$$H(x) = f_t(x) - f_b(x) = H(x_1) \pm \frac{\omega}{l} x \tag{3.39}$$

where $\omega = |H(x_2) - H(x_1)|$; $H(x_2) - H(x_1)$ is positive (+) when the wedge is diverging and negative (-) when it is converging. An appropriate choice of the perturbation parameter ϵ would be ω/l, which describes the relative aperture variation along the wedge length (Van Dyke 1987). Substituting equation (3.39), in dimensionless form, into equations (3.22) to (3.24) and (3.18), the discharge to the second-order can be obtained, in dimensional form, as follows:

$$Q = -\frac{{H_m}^3}{12\mu}\frac{\Delta P}{l}\left\{\left(1-\frac{\omega^2}{4{H_m}^2}\right)^2 \pm \epsilon\frac{9Rp}{70}\left(1-\frac{\omega^2}{4{H_m}^2}\right)^4 + \epsilon^2\left[\frac{3}{20}\left(1-\frac{\omega^2}{4{H_m}^2}\right)^2 + \frac{131Rp^2}{3850}\left(1-\frac{\omega^2}{4{H_m}^2}\right)^6\right]\right\} \tag{3.40}$$

Substituting equation (3.39), in dimensionless form, into equations (3.35) to (3.37) and (3.31), the pressure difference to the second-order can be obtained, in dimensional form, as:

$$\Delta P = -\frac{12\mu lQ}{{H_m}^3}\left(1-\frac{\omega^2}{4{H_m}^2}\right)^{-2}\left[1 \mp \epsilon\frac{9R_q}{35} - \epsilon^2\left(\frac{3}{20}+\frac{52{R_q}^2}{13475}\right)\right] \tag{3.41}$$

Note that the perturbation parameter physically represents the extent of aperture variation relative to length, although the derived perturbation solutions, i.e., equations (3.24) and (3.37), were tested in wedges with linear profile walls in this section, both solutions can easily be applied to other wall geometries, e.g., sinusoidal or parabolic profiles. In fact, as long as the wall profile functions $f_t(x)$ and $f_b(x)$ are defined, h_X and h_{XX} can be evaluated to obtain perturbation solutions. In addition, we derived and tested the solutions for fractures with sinusoidal walls in Appendix B. As a gradual change of aperture is assumed to maintain the dominant flow along the length direction in the present study, abrupt changes of aperture can negate this assumption and hence the derived solutions are not applicable in these cases. However, gradual aperture variation is normally considered and reported in practice (e.g. Kitanidis and Dykaar 1997; Zimmerman 2005), which ensures the dominant flow in one main direction (i.e., the influence of flow in *y* direction on the flow dominant feature is not significant).

3.4.2 Comparison with simulation results

To examine the validity of the perturbation solutions derived in this study, flow simulations in two-dimensional wedges were conducted by solving the NSE directly using COMSOL MultiPhysics. Two geometrical parameters, the ratio of the aperture variation to mean aperture (ω/H_m) and the ratio of the aperture variation to fracture length (ϵ), were used to determine the wedge geometry. Mean aperture H_m was fixed to 1 mm while ϵ was given varying values to demonstrate different extents of aperture variation. Inertial effects were quantified by the Reynolds number as defined by (Zimmerman et al. 2004):

$$Re = \frac{Q}{v} \tag{3.42}$$

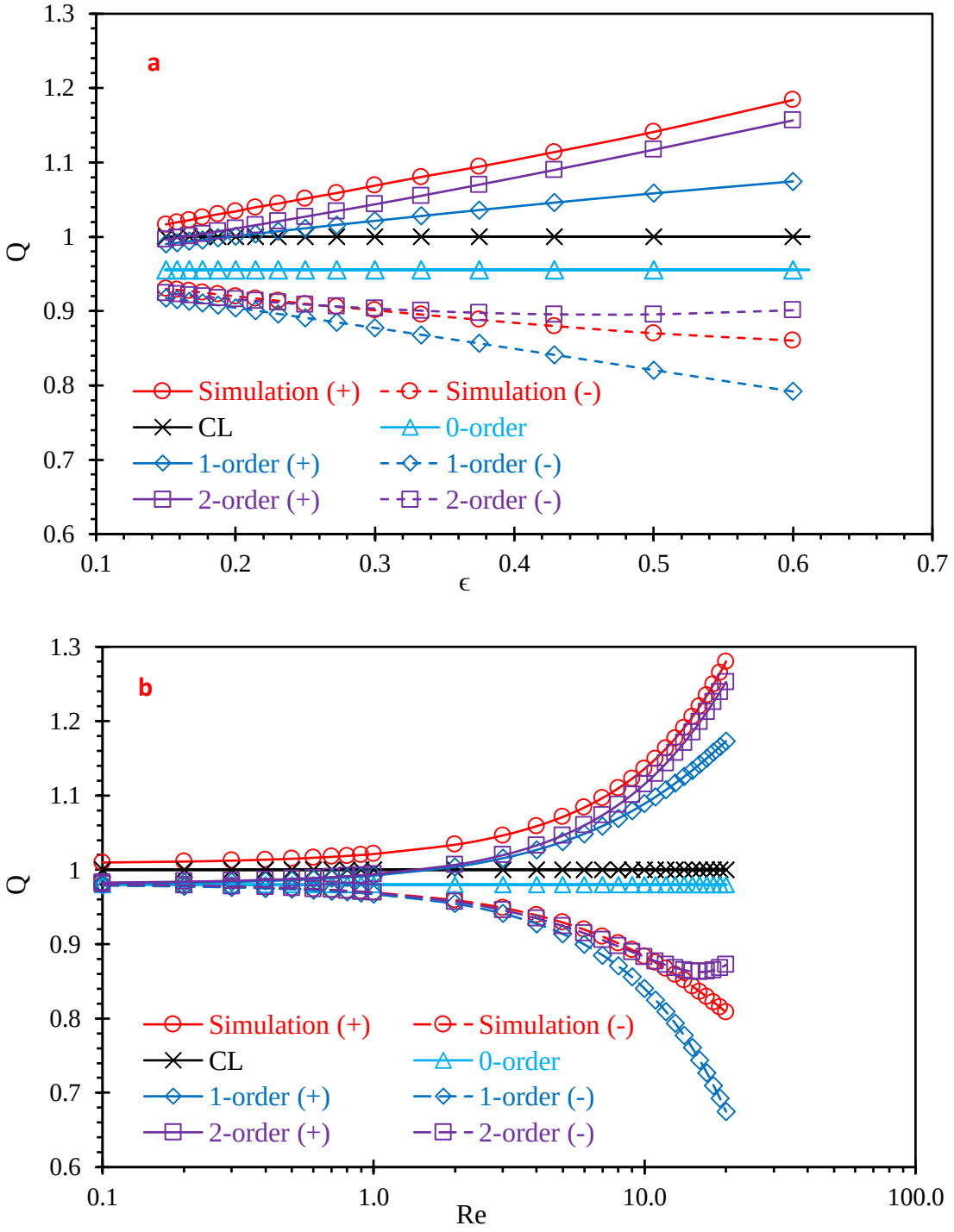

Figure 3.3. Comparison of the discharge obtained from the PBC solution and simulation results. The plots show the effects of the perturbation parameter ϵ and the Reynolds number *Re*; (a) Q at different ϵ, where Q is the volumetric flow rate from different solutions normalized by Q_m; (b) Q at different *Re*. D_q is defined as $(Q_{solution}-Q_{simulation})/Q_{simulation}\times 100\%$; $Q_{solution}$ is the volumetric flow rate obtained from the CL, 0-order solution, 1-order solution and 2-order solution; and $Q_{simulation}$ is the volumetric flow rate obtained from the simulations; (+) refers to the case of a diverging wedge and (-) a converging wedge.

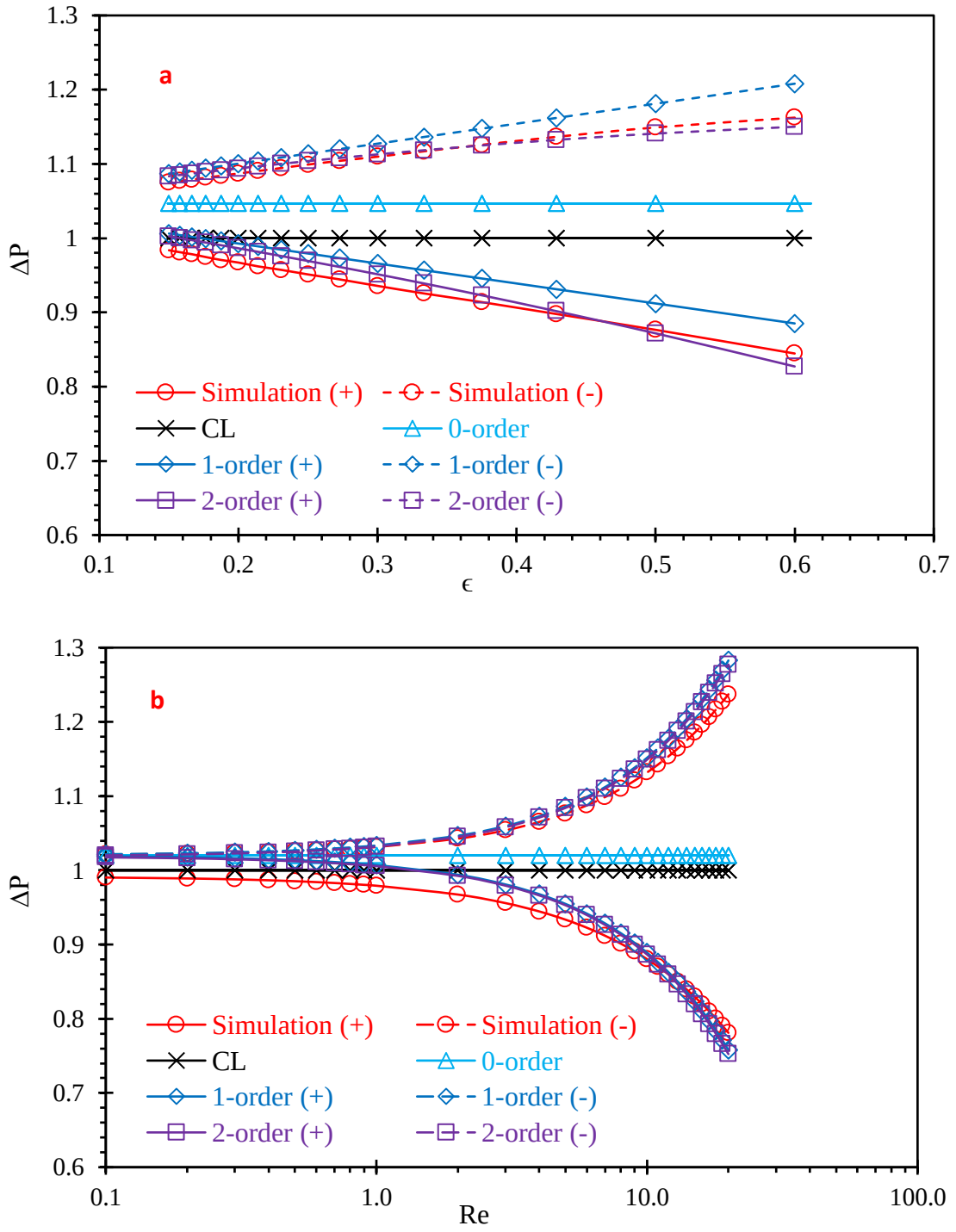

Figure 3.4. Comparison of the pressure difference obtained from the FBC solution and simulation results showing the effects of the perturbation parameter ϵ and Reynolds number *Re*; (a) ΔP at different ϵ, ΔP is the pressure difference from different solutions normalized by ΔP_m; (b) ΔP at different *Re*. D_p is defined as $(\Delta P_{solution}-\Delta P_{simulation})/\Delta P_{simulation}\times 100\%$; $\Delta P_{solution}$ is the pressure difference obtained from the CL, 0-order solution, 1-order solution and 2-order solution; and $\Delta P_{simulation}$ is the pressure difference obtained from simulations; (+) refers to the case of a diverging wedge and (-) a converging wedge.

Water was used as the fluid in the simulations with density ρ=1000 kg·m^{-3} and dynamic viscosity μ=0.001 Pa·s. The boundary conditions used in the simulation were exactly the same as those used in the derivation of the perturbation solutions, i.e., non-slip boundary and impermeable wall as given in equations (3.4) and (3.5). Mesh was refined until there was a negligible difference between two successive refinements. Both diverging and converging wedges were included in the current study. The volumetric flow rate at the inflow boundary and the pressure difference between inflow and outflow boundaries can be obtained directly from simulations. The derived solution, equation (3.40), was assessed against the simulation results in terms of the effects of wedge geometry and *Re*. In Figure 3.3a, results from the CL (using the arithmetic mean of the aperture) and perturbation solutions at different orders are compared with the simulation results with ϵ ranging from 0.15 to 0.60 and ω/H_m fixed at 0.3. *Re* is set to 2 so that inertial effects are insignificant (Wang et al. 2018; Zimmerman et al. 2004). In general, the second-order (referred as 2-order hereafter) solution provides results that are the closest to the simulation results with deviation D_q ranging from -2.4% to 4.5% and mean effective deviation $\overline{|D_q|}$ of 1.6%. The successive improvement as more terms are included is clearly demonstrated. As ϵ increases, the degree of violation of the assumption of slow aperture variation along the fracture length increases and, therefore, all results deviate increasingly from the simulation results as ϵ increases.

Inertial effects were studied by fixing ϵ at 0.1 and ω/H_m at 0.2 with *Re* ranging from 0.1 to 20, which covers three main flow regimes including the Darcy-flow regime (*Re*<1), weak inertial regime (1<*Re*<10) and strong inertial regime (*Re*>10) (Zimmerman et al. 2004). For the weak inertial regime, Darcy-type flow can still be considered valid for engineering applications, but this assumption loses its validity and leads to increasingly greater deviation as the Reynolds number passes its critical value (Oron and Berkowitz 1998; Xiong et al. 2018; Zimmerman et al. 2004). As can be seen in Figure 3.3b, simulation results show that the assumption of Darcy-type flow can be considered valid when *Re*<10 with about ±10% of deviation at *Re*=10. The flow rates obtained from simulation, $Q_{simulation}$, are mostly axisymmetric for diverging and converging cases, whereas the results from the 2-order perturbation solution show a strong non-axisymmetric behaviour as *Re* surpasses the critical value, due to the asymmetry in the formulation for the two cases, see equation (3.40). Similar non-axisymmetric behaviours for the 2-order solution can also be observed in Figure 3.3a. Generally, good agreement is observed between the results from the 2-order perturbation solution and simulation results, with D_q ranging from -2.7% to 7.9% and mean effective

deviation $\overline{|D_q|}$ of 1.7% for 0.1<*Re*<20. In the strong inertial regime, $\overline{|D_q|}$ increases to 2.5% while $\overline{|D_q|}$ is 1.3% when *Re*<10.

The perturbation solution under the FBC, equation (3.41), was also tested using the same set of simulation results as shown in Figure 3.4. From Figure 3.4a and 3.4b, the 2-order pressure difference obtained from the FBC solution agrees even better with the simulation results with D_q ranging from -2.1% to 2.0% for ϵ from 0.15 to 0.60 when inertial effects are weak (*Re*=2) and the mean effective deviation $\overline{|D_p|}$ is 1.1%. Similar to the PBC, results from the FBC increasingly deviate from simulation results when *Re*>10. Overall, D_q ranges from -3.2% to 3.7% and the mean effective deviation $\overline{|D_p|}$ is 1.6% when *Re* is in the range of 0.1 to 20. When *Re* is greater than 10, $\overline{|D_p|}$ increases to 2.0% whereas $\overline{|D_p|}$ is less than 1.4% under the flow regime with weak inertial effects.

3.4.3 Comparison with previous perturbation solutions

A wide range of definitions were used in previous studies to describe the ability of a fracture to pass fluid, these include the fracture permeability *k*, friction factor *f*, resistance *R* and transmissivity *T* (e.g., Nazridoust et al. 2006; Nicholl et al. 1999; Yang et al. 1995; Zimmerman and Bodvarsson 1996). The definitions are based mostly on the incorporation of the equivalent hydraulic aperture in their formulations. In this section, we further assess the performance of our derived perturbation solution by comparing the obtained results with previously published studies. The FBC solution, equation (3.41), is compared with the perturbation solutions (up to 2-order) proposed by Kitanidis and Dykaar (1997) and Basha and El-Asmar (2003) in terms of estimating the fracture transmissivity *T* and equivalent hydraulic aperture H_e. In both studies, the same boundary condition is adopted by imposing a pressure difference between inflow and outflow boundaries, which results in solutions for discharge in a similar form to equation (3.40).

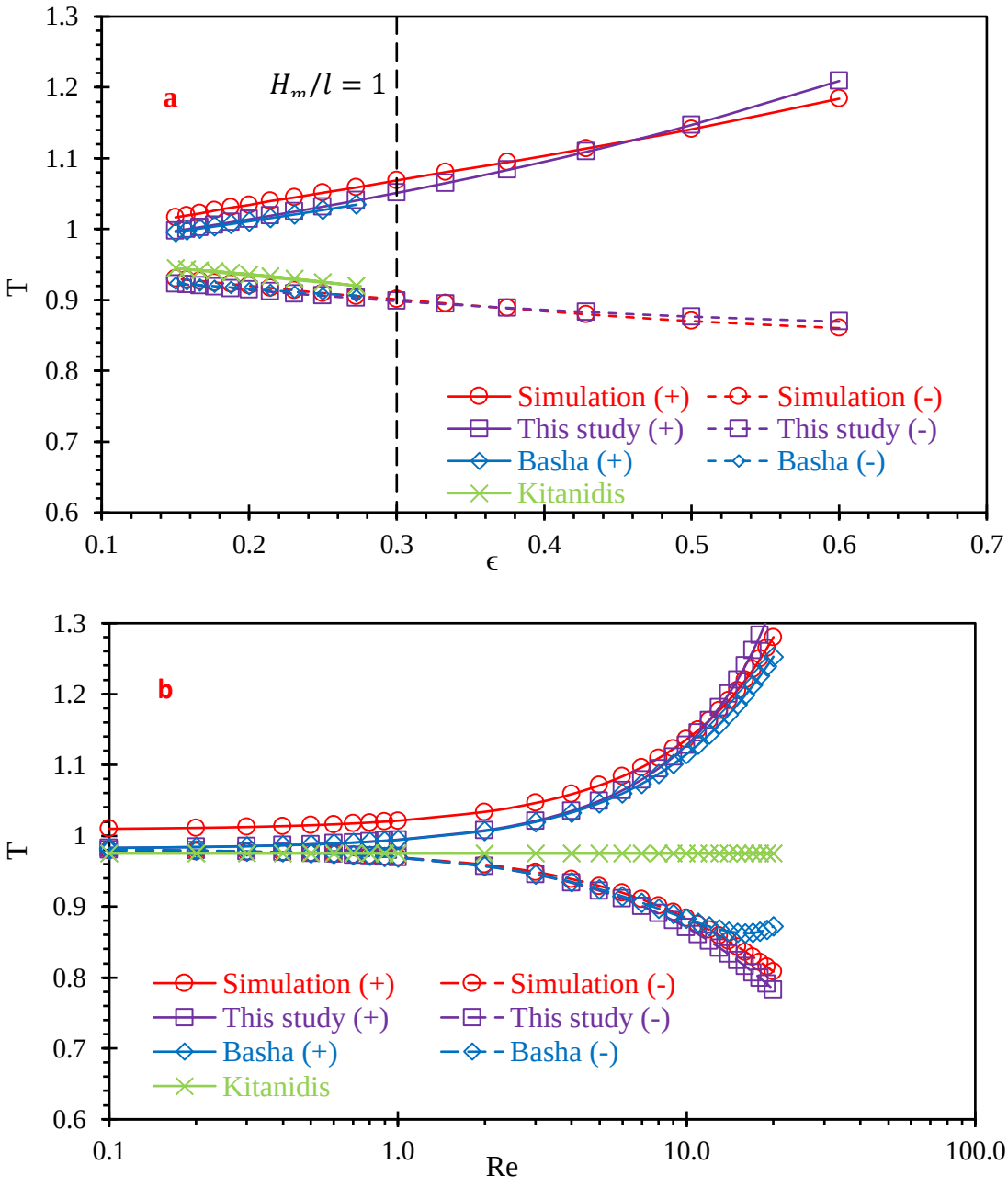

Figure 3.5. Results of comparing the FBC perturbation solution derived in the current study with perturbation solutions from Kitanidis and Dykaar (1997) and Basha and El-Asmar (2003) at different perturbation parameter ϵ (a); and different Reynolds number *Re* (b). Transmissivity *T* is defined as $T=H_e^3$, where H_e is the equivalent hydraulic aperture obtained from flow simulations, perturbation solutions in the current study and previous studies of Kitanidis and Dykaar (1997) and Basha and El-Asmar (2003), normalized by H_m. Deviation D_H is defined as $(H_e-H_{eS})/H_{eS}\times100\%$, which quantifies the accuracy in terms of estimating H_e, in which H_{eS} is the equivalent hydraulic aperture obtained from flow simulations.

Kitanidis and Dykaar (1997) ignored inertial effects by setting *Re*=0 and, therefore, the 1-order term vanishes and the solution leads to identical results for both the diverging and converging cases (see Figure 3.5). Basha and El-Asmar (2003) considered inertial effects and defined the Reynolds number the same as R_p in equation (3.13). Since the ratio of the mean aperture to fracture length, H_m/l, is used as the perturbation parameter for series expansion in both Kitanidis and Dykaar (1997) and Basha and El-Asmar (2003), their solutions are not applicable in conditions where $H_m/l \geq 1$. However, results in Figure 3.5a indicate that equation (3.41) still provides an accurate estimate of *T* even when H_m/l is greater than 1, with $\overline{|D_H|}$, the mean effective deviation in terms of equivalent hydraulic aperture, equal to 0.4% (H_m/l ranging from 1 to 2). To compare our results with previously reported solutions at varying *Re*, as seen in Figure 3.5b, H_m/l is fixed to 0.5. As shown by the plotted crosses, results from Kitanidis and Dykaar (1997) are constant throughout the entire range of *Re* regardless of whether wedges are converging or diverging because inertial effects are ignored. Results from Basha and El-Asmar (2003), plotted as diamond shapes, are in good agreement with the simulation results at low *Re* but start to deviate at *Re*=10 especially for the converging case. Equation (3.41) agrees well with the simulation results over the entire range of *Re* for both diverging and converging wedges with the smallest mean effective deviation $\overline{|D_H|}$ of 0.5%, in terms of the estimated value of H_e.

3.5 Discussion

3.5.1 Validity of the cubic law and Reynolds approximation

The CL is widely used to estimate flow in fractures in a variety of engineering applications by using the constant mean aperture as the equivalent hydraulic aperture. If we accept that a deviation of ±10% or less validate the use of the CL for fracture flow prediction, the criteria for applying the CL can be derived from equations (3.40) and (3.41):

$$\left|\left(1-\frac{\omega^2}{4{H_m}^2}\right)^2\left\{1 \pm \epsilon\frac{9R_p}{70}\left(1-\frac{\omega^2}{4{H_m}^2}\right)^2+\epsilon^2\left[\frac{3}{20}+\frac{131{R_p}^2}{3850}\left(1-\frac{\omega^2}{4{H_m}^2}\right)^4\right]\right\}-1\right| \leq 10\% \tag{3.43}$$

$$\left|\left(1-\frac{\omega^2}{4{H_m}^2}\right)^{-2}\left[1 \mp \epsilon\frac{9R_q}{35}-\epsilon^2\left(\frac{3}{20}+\frac{52{R_q}^2}{13475}\right)\right]-1\right| \leq 10\% \tag{3.44}$$

The validity of the CL depends on small ω over both the mean aperture and fracture length with small *Re*. The former represents the geometrical condition in which the fracture wall geometry approaches parallel plates as ω decreases. The latter accounts for the dynamical condition in which inertial effects are negligibly small compared with viscous effects (Oron

and Berkowitz 1998). These two conditions combined determine the validity of applying the CL to flow predictions for rock fractures.

Under both the pressure and flow rate boundary conditions, the 0-order terms effectively represent the Reynolds approximation to fracture flow. Similar criteria can be derived from the perturbation solutions by assuming that a deviation of ±10% or less is acceptable for the Reynolds equation to hold valid:

$$\left|\pm\epsilon\frac{9R_p}{70}\left(1-\frac{\omega^2}{4{H_m}^2}\right)^2+\epsilon^2\left[\frac{3}{20}+\frac{131{R_p}^2}{3850}\left(1-\frac{\omega^2}{4{H_m}^2}\right)^4\right]\right|\leq 10\% \tag{3.45}$$

$$\left|\mp\epsilon\frac{9R_q}{35}-\epsilon^2\left(\frac{3}{20}+\frac{52{R_q}^2}{13475}\right)\right|\leq 10\% \tag{3.46}$$

The Reynolds approximation is valid when ω is small over the fracture length and small *Re*, suggesting a slow variation of fracture aperture with negligible inertial effects, which are two fundamental assumptions for deriving the Reynolds equation from the NSE (Zimmerman et al. 1991). Figure 3.6 shows the curves of ϵ and *Re* thresholds, below which the combined contribution from higher-order terms (i.e., 1-order and 2-order) is within ±10% of the 0-order terms for the diverging wedge case based on equations (3.45) and (3.46). The curves can therefore be considered as the limits in pairs of ϵ and *Re* values where below the curves the Reynolds approximation can provide a reasonable estimate of flow.

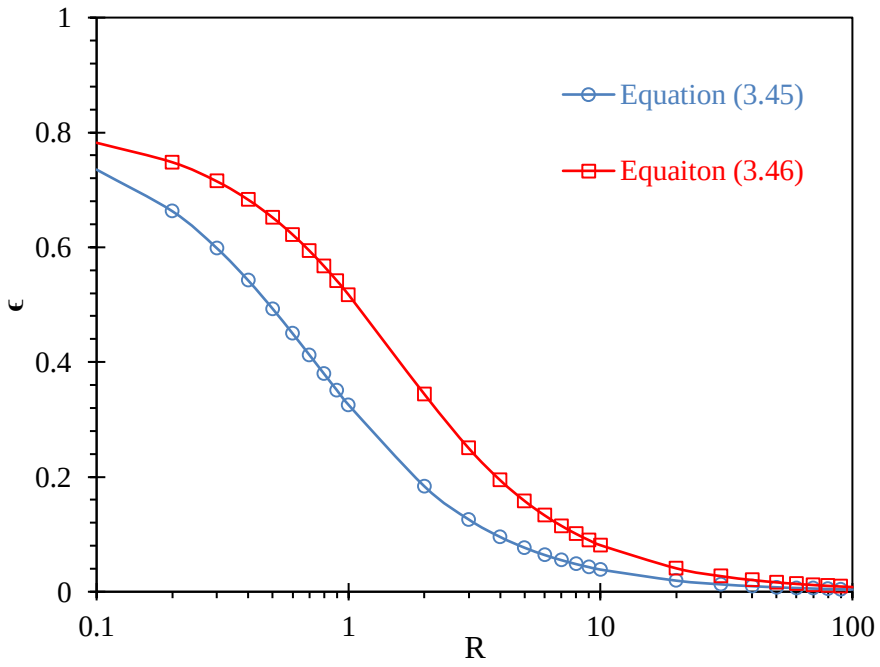

Figure 3.6 Combinations of ϵ and *R* where below the curves, higher-order terms are within ±10% of the 0-order terms for diverging cases. *R* represents R_p for the PBC and R_q for the FBC as defined in Section 3.3, where ω/H_m is set to 0.9.

3.5.2 Effect of aperture variation

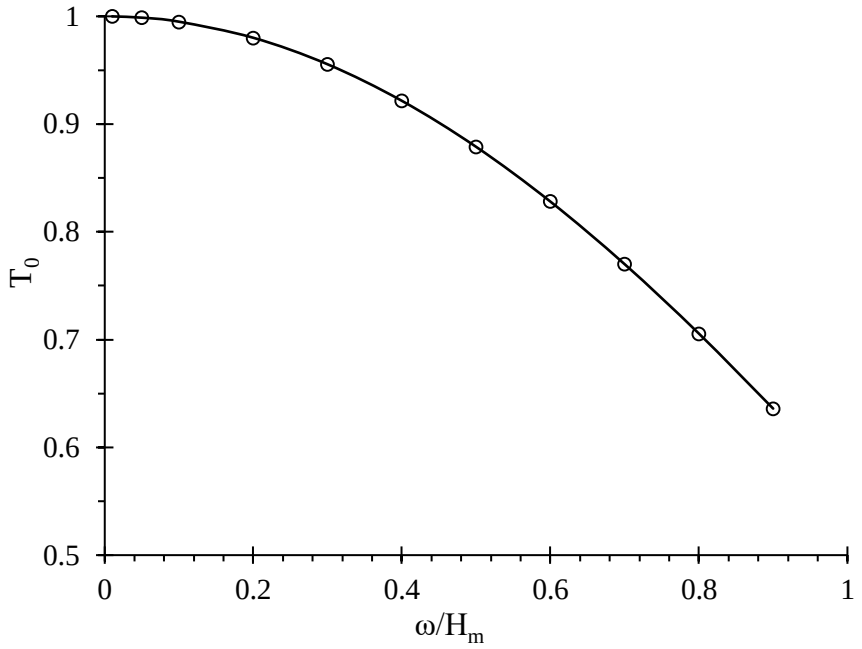

Figure 3.7. Effect of ω/H_m on the 0-order solution (Reynolds approximation). 0-order transmissivity $T_0=H_0^3$ and H_0 is the equivalent hydraulic aperture from the 0-order solution normalized by the mean aperture H_m.

From the dimensional solutions in Section 3.4.1, the aperture variation ω along the fracture length contributes to the deviation of results from the CL through both the perturbation parameter ϵ and ω/H_m. It can be seen from equations (3.40) and (3.41) that higher-order terms approach 0 (i.e., perturbation solutions approach the Reynolds approximation) and the solutions become dominated mainly by 0-order terms when ω is much smaller than the fracture length. 0-order terms approach 1 (i.e., Reynolds equation approaches the CL) when ω is much smaller than the mean aperture. The effect of ϵ has been discussed in previous sections and we now look at the effect of ω/H_m. Figure 3.7 illustrates the effect of ω/H_m on the 0-order solution, in which T_0 increases from 0.64, when ω/H_m is 0.9, to 0.98 when ω/H_m=0.2. The contribution of the Reynolds approximation to the solutions, which depends solely on the value of ω/H_m, decreases as the values of ϵ and *Re* increase (see Figures 3.3 and 3.4). Therefore, higher-order terms need to be included to provide a better estimate when either the aperture variation along the fracture length becomes significant or the inertial terms have greater effects.

3.5.3 Inertial effects

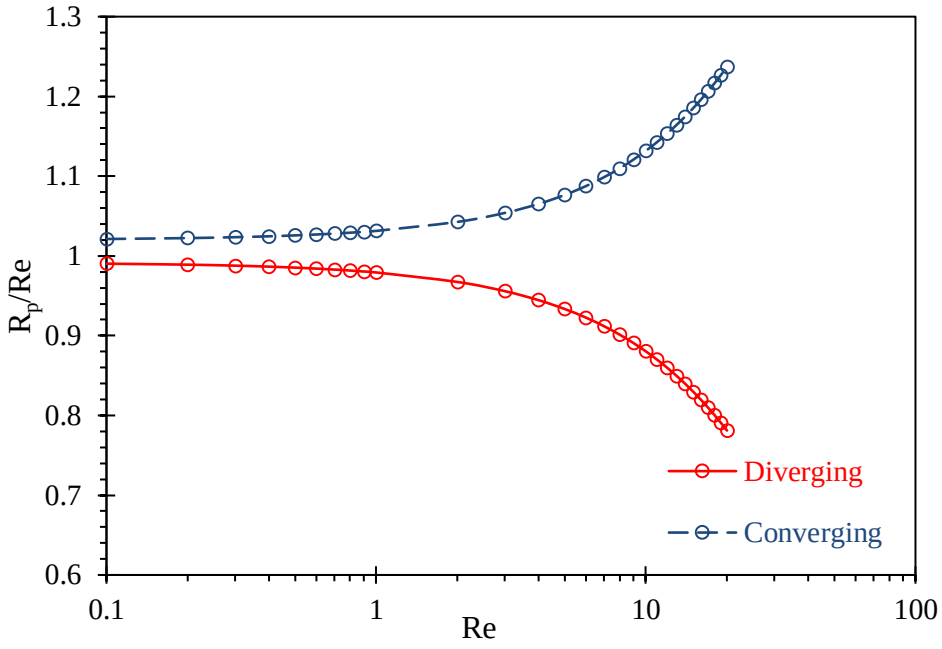

Figure 3.8. R_p normalized by *Re* at different *Re* for diverging and converging cases.

Inertial effects are commonly quantified by the Reynolds number, which describes the ratio of inertia to viscous forces. Our results indicate that perturbation solutions start to deviate from the numerical simulation results when entering the strong inertial regime (see Figure 3.3 and 3.4). This is due to the fact that as *Re* surpasses its critical value, higher-order terms (e.g., the 2-order in this study) begin to show more contribution than lower order terms (e.g., the 0-order term in this study), therefore, more higher-order terms (e.g., 3-order) need to be incorporated to provide more accurate results. However, from Figure 3.4b, our 2-order FBC solution is still a good match with simulation results even when *Re* is greater than 10. Another reason for the relatively sharp increase in the deviation of equation (3.40) from the numerical simulation results in the converging case (in Figure 3.3b) is a result of over-estimating the Reynolds number using R_p. As can be seen in Figure 3.8, the over-estimation of the Reynolds number for converging cases increases to more than 10% when *Re*=8 and over 20% at *Re*=16. This over-estimation of inertial effects leads to a further increase in the proportion of contributions from higher-order terms, resulting in a greater over-prediction of the discharge for the converging wedge case. This does not happen with the FBC cases since the known discharge *Q* is in the definition of R_q. In addition, the mismatch between R_p and *Re* increases as *Re* increases, which leads to more deviation for terms higher than 0-order when *Re* is above moderate values.

3.6 Conclusions

In this study, two sets of perturbation solutions have been derived under both the pressure boundary condition (PBC) and flow rate boundary condition (FBC) for flow in two-dimensional fractures with slowly varying apertures. The stream function, up to the second-order, is derived for both boundary conditions. Solutions are then obtained by incorporating the auxiliary condition, which defines a mean pressure difference along the fracture length. To demonstrate the application, the solutions have been applied to two-dimensional symmetric wedges and fractures with sinusoidal varying walls using the ratio of aperture variation to fracture length, ω/l, as the perturbation parameter. The results from our perturbation solutions are then compared with numerical simulation results by solving directly the Navier-Stokes equations and results from published perturbation solutions. In general, our solutions for both boundary conditions agree well with the numerical simulation results. For flow in wedge-shaped fractures, the PBC solution has an effective deviation $\overline{|D_q|}$ of 1.6% for ϵ ranging from 0.15 to 0.6 at Re=2; and an effective deviation $\overline{|D_q|}$ of 1.7% for Re ranging from 0.1 to 20 when ϵ=0.1. The solution for the FBC has a slightly better performance with an effective deviation, $\overline{|D_p|}$, of 1.1% and 1.6% for the same combinations of ϵ and Re. Closer agreement can be found for the FBC solution over the PBC solution for higher Re, mainly due to the mismatch between Re and R_p, where Q_m is used instead of the exact discharge, Q, to describe the inertial effects in the PBC. It is, therefore, concluded that the FBC solution provides a more accurate estimate of the fracture transmissivity and equivalent hydraulic aperture.

Criteria for the validity of applying the cubic law and Reynolds approximation have also been derived based on the second-order perturbation solutions. In addition to the required geometrical conditions, both the cubic law assumption and Reynolds approximation are only valid for weak or negligible inertial effects. In this sense, the perturbation solutions derived in this study provide better alternatives for analysing the hydraulic properties of fractures and channels for more complex flow conditions and a wider range of geometries. The present work does not solve directly the problem of flow in a fracture network (Jiang et al. 2014; Jiang et al. 2013; Xu et al. 2018b). However, as in a few existing studies (e.g., Huang et al. 2018; Richeng et al. 2018) where the complex discrete fracture geometric properties (e.g., surface roughness and contacts) are incorporated in the fracture network for flow modelling, the solutions presented in this work may be extended to study such problems once the fracture network geometrical information is provided, although further work may be needed.

Appendix A: Derivation of perturbation solutions

In this appendix, we summarise the derivation process of the stream function and perturbation solutions (to the second-order) under both the pressure and flow rate boundary conditions.

A1 Perturbation solution under the pressure boundary condition

Equation (3.14) can be expanded in terms of the perturbation parameter ϵ using equation (3.17) with terms of different orders. For the 0-order:

$$\frac{\partial^4 \Psi_0}{\partial Y^4} = 0 \tag{3.47}$$

Integrating equation (3.47) over *Y* and making use of the 0-order boundary condition:

$$\left.\frac{\partial \Psi_0}{\partial Y}\right|_{Y=\pm 1} = 0,\ \Psi_0|_{Y=\pm 1} = \pm\frac{Q_0}{2} \tag{3.48}$$

the stream function at the 0-order can be obtained:

$$\Psi_0 = Q_0\left(\frac{3}{4}Y - \frac{1}{4}Y^3\right) \tag{3.49}$$

Substituting the 0-order stream function into the auxiliary condition i.e., equation (3.15) and, after integration, the 0-order discharge is derived as:

$$Q_0 = \left(\int_0^{\omega} \frac{1}{8\omega h^3}\, dX\right)^{-1} \tag{3.50}$$

Following the same procedure, using the 1-order terms and equation (3.14):

$$\frac{\partial^4 \Psi_1}{\partial Y^4} = -2R_p h_X \frac{\partial \Psi_0}{\partial Y}\frac{\partial^2 \Psi_0}{\partial Y^2} - R_p h_X Y \frac{\partial \Psi_0}{\partial Y}\frac{\partial^3 \Psi_0}{\partial Y^3} - R_p h \frac{\partial \Psi_0}{\partial X}\frac{\partial^3 \Psi_0}{\partial Y^3} \tag{3.51}$$

Integrating equation (3.51) over *Y* and making use of the 1-order boundary condition:

$$\left.\frac{\partial \Psi_1}{\partial Y}\right|_{Y=\pm 1} = 0,\ \Psi_1|_{Y=\pm 1} = \pm\frac{Q_1}{2} \tag{3.52}$$

the stream function at the 1-order is obtained:

$$\Psi_1 = \frac{3R_p {Q_0}^2 h_X}{1120}(5Y - 11Y^3 + 7Y^5 - Y^7) + \frac{1}{4}Q_1(3Y - Y^3) \tag{3.53}$$

Substituting the 1-order stream function into the auxiliary condition and, after integration, the 1-order discharge is derived:

$$Q_1 = \int_0^{\omega} \frac{9R_p Q_0^3 h_X}{280\omega h^3}\, dX \tag{3.54}$$

Similarly, for the 2-order:

$$\frac{\partial^4\Psi_2}{\partial Y^4} = R_p\left[h^3\frac{\partial\Psi_0}{\partial Y}\frac{\partial}{\partial X}\left(\frac{1}{h^2}\frac{\partial^2\Psi_1}{\partial Y^2}\right) - 2h_X\frac{\partial\Psi_1}{\partial Y}\frac{\partial^2\Psi_0}{\partial Y^2} - h_X Y\frac{\partial\Psi_1}{\partial Y}\frac{\partial^3\Psi_0}{\partial Y^3} - h\frac{\partial\Psi_0}{\partial X}\frac{\partial^3\Psi_1}{\partial Y^3} - h\frac{\partial\Psi_1}{\partial X}\frac{\partial^3\Psi_0}{\partial Y^3}\right] - 2\left[(6h_X^2 - 2hh_{XX})\frac{\partial^2\Psi_0}{\partial Y^2} + (6h_X^2 - hh_{XX})Y\frac{\partial^3\Psi_0}{\partial Y^3}\right] \quad (3.55)$$

Using the same approach, the solution of the 2-order stream function is:

$$\Psi_2 = \frac{{R_p}^2 Q_0}{3449600}\left[{h_X}^2(2875Y - 8222Y^3 + 8778Y^5 - 4488Y^7 + 1155Y^9 - 98Y^{11}) - hh_{XX}(1213Y - 3279Y^3 + 3234Y^5 - 1518Y^7 + 385Y^9 - 35Y^{11})\right] + \frac{3Q_0}{40}(4h_X^2 - hh_{XX})(Y - 2Y^3 + Y^5) + \frac{9R_pQ_1h_X}{560}(5Y - 11Y^3 + 7Y^5 - Y^7) + \frac{1}{4}Q_2(3Y - Y^3) \quad (3.56)$$

Substituting the 2-order stream function into the auxiliary condition to give the solution of the 2-order discharge:

$$Q_2 = \int_0^\omega \frac{3{Q_0}^2{h_X}^2}{40\omega h^3} - \frac{{Q_0}^2 hh_{XX}}{20\omega h^3}dX + \int_0^\omega \frac{9R_p{Q_0}^2Q_1h_X}{140\omega h^3}dX + \int_0^\omega \frac{13{R_p}^2{Q_0}^4}{26950\omega h^3}\left[{h_X}^2 - \frac{3}{4}hh_{XX}\right]dX \quad (3.57)$$

Note that the Reynolds number R_p here is defined as the discharge of a fracture with a constant aperture, divided by the kinematic viscosity.

A2 Perturbation solution under the flow rate boundary condition

The stream function at each order under the flow rate boundary condition can be derived using a similar approach to that discussed in the previous section but with a different form of boundary condition, i.e., equation (3.29). Following the same procedure, the stream function up to the 2-order can be obtained as shown in equations (3.32) to (3.34). Expanding the auxiliary condition by substituting equation (3.30) into equation (3.28) and retaining up to the 2-order:

$$\Delta P = -\int_0^\omega\int_0^1 \frac{1}{24\omega}\left[\epsilon^2\frac{\partial^2}{\partial X^2}\left(\frac{1}{h}\frac{\partial\Psi_0}{\partial Y}\right) + \frac{1}{h^3}\frac{\partial^3\Psi_0}{\partial Y^3} + \frac{\epsilon}{h^3}\frac{\partial^3\Psi_1}{\partial Y^3} + \frac{\epsilon^2}{h^3}\frac{\partial^3\Psi_2}{\partial Y^3}\right] + \frac{R_q}{24\omega}\left[\frac{\epsilon}{h^2}\frac{\partial\Psi_0}{\partial X}\frac{\partial^2\Psi_0}{\partial Y^2} - \frac{\epsilon}{h}\frac{\partial\Psi_0}{\partial Y}\frac{\partial}{\partial X}\left(\frac{1}{h}\frac{\partial\Psi_0}{\partial Y}\right) + \frac{\epsilon^2}{h^2}\frac{\partial\Psi_0}{\partial X}\frac{\partial^2\Psi_1}{\partial Y^2} - \frac{\epsilon^2}{h}\frac{\partial\Psi_0}{\partial Y}\frac{\partial}{\partial X}\left(\frac{1}{h}\frac{\partial\Psi_1}{\partial Y}\right) + \frac{\epsilon^2}{h^2}\frac{\partial\Psi_1}{\partial X}\frac{\partial^2\Psi_0}{\partial Y^2} - \frac{\epsilon^2}{h}\frac{\partial\Psi_1}{\partial Y}\frac{\partial}{\partial X}\left(\frac{1}{h}\frac{\partial\Psi_0}{\partial Y}\right)\right]dY\,dX \quad (3.58)$$

Substituting the stream function solutions (equations (3.32) to (3.34)) into equation (3.58) and, after integration and rearrangement, the pressure difference up to the 2-order is:

$$\Delta P = \int_0^\omega \frac{1}{8\omega h^3} - \epsilon\frac{9R_qh_X}{140\omega h^3} - \epsilon^2\left[\frac{3h_X^2 - 2hh_{XX}}{40\omega h^3} + \frac{13{R_q}^2}{13475\omega h^3}\left(2{h_X}^2 - \frac{3}{2}hh_{XX}\right)\right]dX \quad (3.59)$$

Note that the Reynolds number R_q here is defined as half of the given fracture discharge divided by the kinematic viscosity.

Appendix B: Flow in a two-dimensional fracture with periodic aperture variations

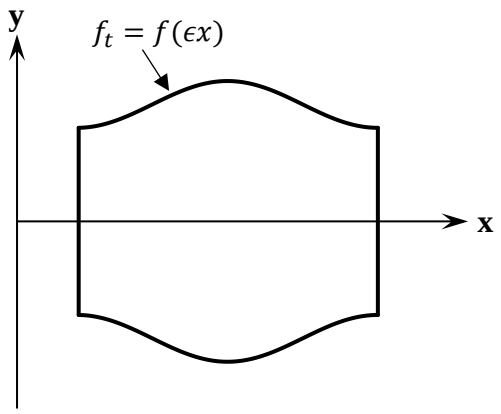

Figure B1. An example of a periodically varying fracture with sinusoidal wall profiles

The proposed perturbation solutions were tested further for the fracture case with sinusoidal wall profiles, as shown in Figure B1. The dimensionless half aperture is given by (Basha and El-Asmar 2003; Hasegawa and Izuchi 1983):

$$h(x) = h_m[1 - a\cos(\frac{2\pi x}{l})] \tag{3.60}$$

where h_m is the mean half aperture and α is the magnitude of wall roughness (Zimmerman et al. 1991), the perturbation parameter here is given by $\epsilon=\omega/l$ ($\omega=4a$). Substituting equation (3.60), together with equation (3.26), into the derived dimensionless PBC perturbation solution, one can obtain the dimensional solution up to 2-order (Gradshteyn and Ryzhik 2014) as:

$$Q = -\frac{{H_m}^3}{12\mu}\frac{\Delta p}{l}Q_0\left[1 - \epsilon^2\pi^2\frac{1-a^2}{16(2+a^2)}(\frac{1}{5} + \frac{26{R_p}^2{Q_0}^2}{13475})\right] \tag{3.61}$$

$$Q_0 = \frac{2(1-a^2)^{5/2}}{2+a^2} \tag{3.62}$$

where the Reynolds approximation, equation (3.62), can also be found in e.g., Basha and El-Asmar (2003); Zimmerman et al. (1991). Using the same procedure for the FBC condition, one can obtain:

$$\Delta p = -\frac{12\mu lQ}{{H_m}^3}\frac{2+a^2}{2(1-a^2)^{5/2}}\left[1 + \epsilon^2\pi^2\frac{1}{32(1-a^2)^{3/2}}\left(\frac{1}{5} + \frac{104{R_q}^2}{13475}\right)\right] \tag{3.63}$$

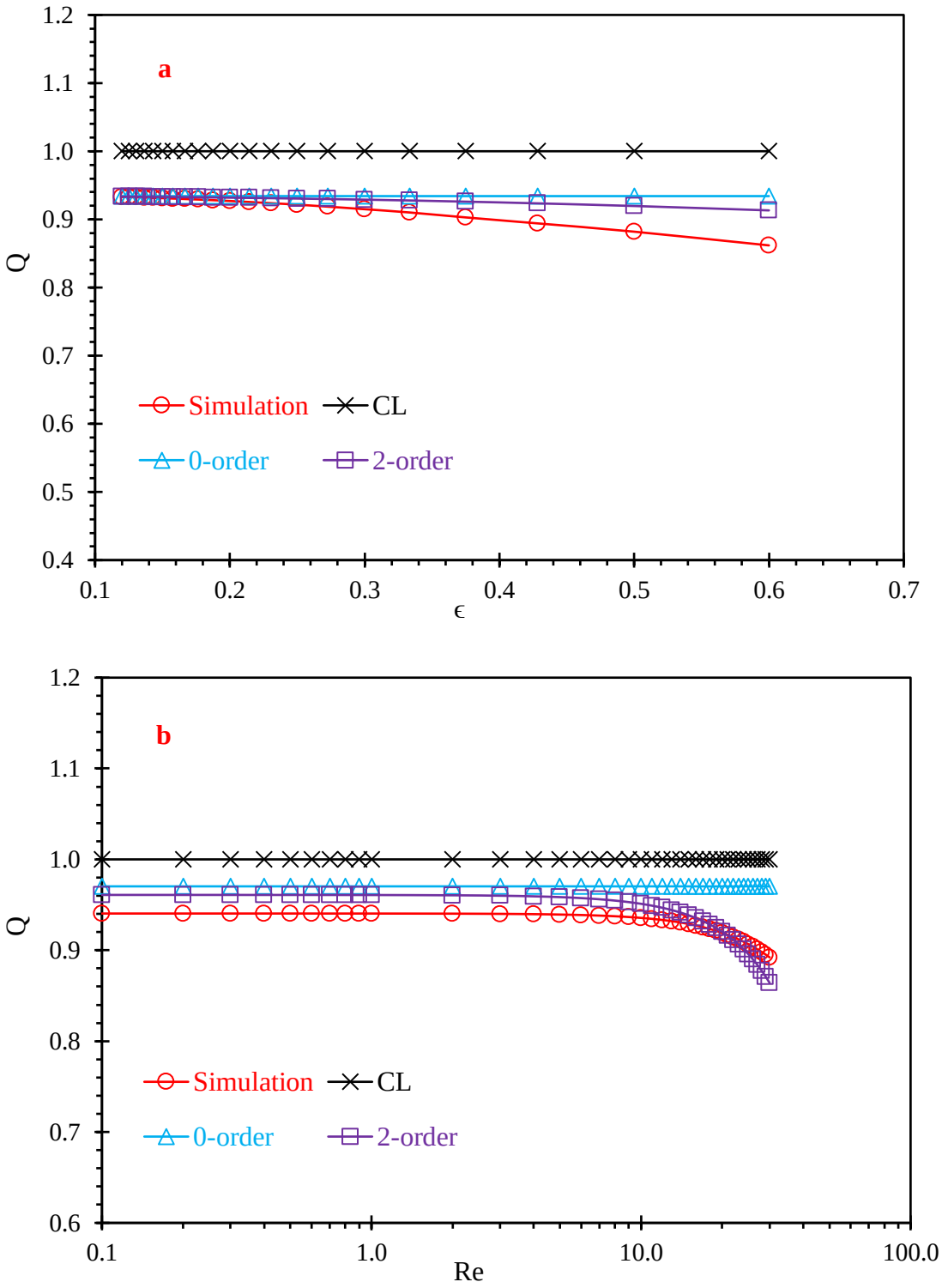

Figure B2. Comparison of the discharge obtained from the PBC solution and simulation results. The plots show the effects of the perturbation parameter ϵ and Reynolds number *Re*. (a) Q at different ϵ, and (b) Q at different *Re*, where Q is the volumetric flow rate from different solutions normalized by Q_m.

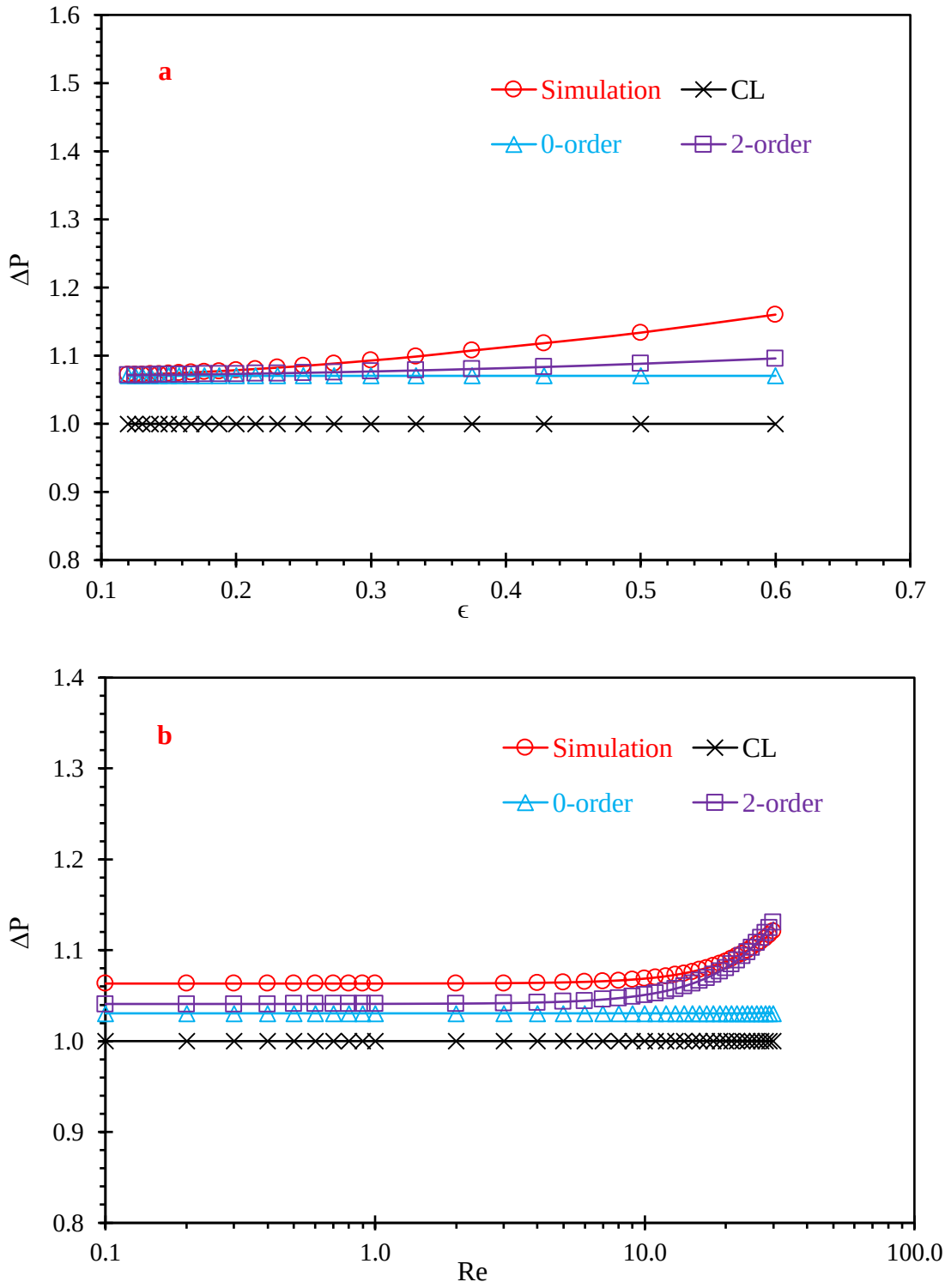

Figure B3. Comparison of the pressure difference obtained from the FBC solution and simulation results showing the effects of the perturbation parameter ϵ and Reynolds number *Re*. (a) ΔP at different ϵ, and (b) ΔP at different *Re*. ΔP is the pressure difference from different solutions normalized by ΔP_m.

Similar to Section 3.4.2, equations (3.61) and (3.63) were compared with simulation results. In general, both solutions agree well with simulation results as shown in Figures B2a and B3a, for different ϵ in the range of 0.12-0.60, where *Re* and α/h_m are set at 2 and 0.3. The mean effective deviation of PBC and FBC solutions from the numerical solution are generally identical at 1.2%. For different *Re* in the range of 0.1-30, the results are shown in Figures B2b and B3b, where ϵ and α/h_m are set at 0.4 and 0.2, respectively. The mean effective deviation of the PBC solution from the numerical solution is 1.6%, while the FBC solution has more accurate results with a mean effective deviation of 1.4%.

Acknowledgments

This work received financial support from a joint scholarship provided by the China Scholarship Council (CSC) and The University of Adelaide (No. 201506430003).

References

Basha, H.A., El-Asmar, W.: The fracture flow equation and its perturbation solution. Water Resour. Res. 39, 1365 (2003). doi:10.1029/2003WR002472

Berkowitz, B.: Characterizing flow and transport in fractured geological media: A review. Adv. Water Resour. 25, 861–884 (2002). doi:10.1016/S0309-1708(02)00042-8

Brown, S.R.: Fluid flow through rock joints: the effect of surface roughness. J. Geophys. Res. 92, 1337–1347 (1987). doi:10.1029/JB092iB02p01337

Brush, D.J., Thomson, N.R.: Fluid flow in synthetic rough-walled fractures: Navier-Stokes, Stokes, and local cubic law simulations. Water Resour. Res. 39, 1085 (2003). doi:10.1029/2002WR001346

Crandall, D., Ahmadi, G., Smith, D.H.: Computational Modeling of Fluid Flow through a Fracture in Permeable Rock. Transp. Porous Media. 84, 493–510 (2010). doi:10.1007/s11242-009-9516-9

Van Dyke, M.: Slow Variations in Continuum Mechanics. Adv. Appl. Mech. 25, 1–45 (1987). doi:10.1016/S0065-2156(08)70276-X

Ge, S.: A governing equation for fluid flow in rough fractures. Water Resour. Res. 33, 53–61 (1997). doi:10.1029/96WR02588

Gradshteyn, I.S., Ryzhik, I.M.: Table of Integrals, Series, and Products. Academic Press (2014)

Hasegawa, E., Fukuoka, N.: Leakage of a Fluid through a Narrow Channel with a Wavy Wall. Bull. JSME. 23, 2042–2046 (1980). doi:10.1248/cpb.37.3229

Hasegawa, E., Izuchi, H.: On Steady Flow through a Channel Consisting of an Uneven Wall and a Plane Wall Part 1. Case of No Relative Motion in Two Walls. Bull. JSME. 26, 532–542 (1983). doi:10.1248/cpb.37.3229

Huang, N., Liu, R., Jiang, Y., Li, B., Yu, L.: Advances in Water Resources E ff ects of fracture

surface roughness and shear displacement on geometrical and hydraulic properties of three-dimensional crossed rock fracture models. 113, 30–41 (2018). doi:10.1016/j.advwatres.2018.01.005

Hunt, A.G., Sahimi, M.: Transport and Reaction in Porous Media: Percolation Scaling, Critical-Path Analysis, and Effective-Medium Approximation. Rev. Geophys. (2017). doi:10.1002/2017RG000558

Jiang, Q., Yao, C., Ye, Z., Zhou, C.: Seepage flow with free surface in fracture networks. Water Resour. Res. 49, 176–186 (2013). doi:10.1029/2012WR011991

Jiang, Q., Ye, Z., Zhou, C.: A numerical procedure for transient free surface seepage through fracture networks. J. Hydrol. 519, 881–891 (2014). doi:10.1016/j.jhydrol.2014.07.066

Kitanidis, P.K., Dykaar, B.B.: Stokes flow in a slowly varying two-dimensional periodic pore. Transp. Porous Media. 26, 89–98 (1997). doi:10.1023/A:1006575028391

Konzuk, J.S., Kueper, B.H.: Evaluation of cubic law based models describing single-phase flow through a rough-walled fracture. Water Resour. Res. 40, 1–17 (2004). doi:10.1029/2003WR002356

Kundu, P.K., Cohen, I.M.: Fluid mechanics. Academic Press (2008)

Lomize, G.M.: Filtratsiia v Treshchinovatykh Porod (Water Flow in Jointed Rock) (in Russian), (1951)

Nazridoust, K., Ahmadi, G., Smith, D.H.: A new friction factor correlation for laminar, single-phase flows through rock fractures. J. Hydrol. 329, 315–328 (2006). doi:10.1016/j.jhydrol.2006.02.032

Nicholl, M.J., Rajaram, H., Glass, R.J., Detwiler, R.: Saturated flow in a single fracture: Evaluation of the Reynolds equation in measured aperture fields. Water Resour. Res. 35, 3361–3373 (1999). doi:10.1029/1999WR900241

Olsson, R., Barton, N.: An improved model for hydromechanical coupling during shearing of rock joints. Int. J. Rock Mech. Min. Sci. 38, 317–329 (2001). doi:10.1016/S1365-1609(00)00079-4

Oron, A.P., Berkowitz, B.: Flow in rock fractures: The local cubic law assumption reexamined. Water Resour. Res. 34, 2811–2825 (1998). doi:10.1029/98WR02285

Patir, N., Cheng, H.S.: An Average Flow Model for Determining Effects of Three-Dimensional Roughness on Partial Hydrodynamic Lubrication. J. Lubr. Technol. 100, 12–17 (1978). doi:10.1115/1.3453103

Pyrak-Nolte, L.J., Nolte, D.D.: Approaching a universal scaling relationship between fracture stiffness and fluid flow. Nat. Commun. 7, 10663 (2016). doi:10.1038/ncomms10663

Richeng, L., Bo, L., Yujing, J., Liyuan, Y.: Advances in Water Resources A numerical approach for assessing e ff ects of shear on equivalent permeability and nonlinear fl ow characteristics of 2-D fracture networks. 111, 289–300 (2018). doi:10.1016/j.advwatres.2017.11.022

Sisavath, S., Al-Yaaruby, a., Pain, C.C., Zimmerman, R.W.: A Simple Model for Deviations from the Cubic Law for a Fracture Undergoing Dilation or Closure. Pure Appl. Geophys. 160, 1009–1022 (2003). doi:10.1007/PL00012558

Wang, C.-Y.: Drag due to a striated boundary in slow Couette flow. Phys. Fluids. 21, 697 (1978). doi:10.1063/1.862279

Wang, Z., Xu, C., Dowd, P.: A Modified Cubic Law for single-phase saturated laminar flow in rough rock fractures. Int. J. Rock Mech. Min. Sci. 103, 107–115 (2018). doi:10.1016/j.ijrmms.2017.12.002

Witherspoon, P.A., Wang, J.S.Y., Iwai, K., Gale, J.E.: Validity of Cubic Law for fluid flow in a deformable rock fracture. Water Resour. Res. 16, 1016–1024 (1980). doi:10.1029/WR016i006p01016

Xiong, F., Jiang, Q., Ye, Z., Zhang, X.: Nonlinear flow behavior through rough-walled rock fractures: The effect of contact area. Comput. Geotech. 102, 179–195 (2018). doi:10.1016/j.compgeo.2018.06.006

Xu, C., Dowd, P.A., Tian, Z.F.: A simplified coupled hydro-thermal model for enhanced geothermal systems. Appl. Energy. 140, 135–145 (2015). doi:10.1016/j.apenergy.2014.11.050

Xu, C., Fidelibusk, C., Wang, Z., Dowd, P.: A simplified equivalent pipe network approach to model flow in poro-fractured rock masses. (2018)

Yang, G., Myer, L.R., Brown, R., Cook, G.W.: Microscopic analysis of macroscopic transport properties of single natural fractures using graph theory alogrithms. Geophys. Res. Lett. 22, 1429–1432 (1995)

Yeo, I.W., de Freitas, M.H., Zimmerman, R.W.: Effect of shear displacement on the aperture and permeability of a rock fracture. Int. J. Rock Mech. Min. Sci. 35, 1051–1070 (1998). doi:10.1016/S0148-9062(98)00165-X

Zimmerman, R., Bodvarsson, G.: Hydraulic conductivity of rock fractures. Transp. Porous Media. 23, 1–30 (1996). doi:10.1007/BF00145263

Zimmerman, R.W.: Fluid Flow in Rock Fractures. In: Proc. 11th Int. Conf. on Computer Methods and Advances in Geomechanics. pp. 89–107. , Turin, Italy (2005)

Zimmerman, R.W., Al-Yaarubi, A., Pain, C.C., Grattoni, C.A.: Non-linear regimes of fluid flow in rock fractures. Int. J. Rock Mech. Min. Sci. 41, 1–7 (2004). doi:10.1016/j.ijrmms.2004.03.036

Zimmerman, R.W., Kumar, S., Bodvarsson, G.S.: Lubrication theory analysis of the permeability of rough-walled fractures. Int. J. Rock Mech. Min. Sci. 28, 325–331 (1991). doi:10.1016/0148-9062(91)90597-F

Zou, L., Jing, L., Cvetkovic, V.: Modeling of Solute Transport in a 3D Rough-Walled Fracture–Matrix System. Transp. Porous Media. 116, 1005–1029 (2017). doi:10.1007/s11242-016-0810-z

Chapter 4: A Non-Linear Version of the Reynolds Equation for Flow in Rock Fractures with Complex Void Geometry

Statement of Authorship

Title of Paper	A non-linear version of the Reynolds equation for flow in rock fractures with complex void geometries
Publication Status	☐ Published ☐ Accepted for Publication ☑ Submitted for Publication ☐ Unpublished and Unsubmitted work written in manuscript style
Publication Details	Wang, Z., C. Xu, P. Dowd, F. Xiong, and H. Wang (2019), A non-linear version of the Reynolds equation for flow in rock fractures with complex void geometries, Water Resources Research.

Principal Author

Name of Principal Author (Candidate)	Zhihe Wang
Contribution to the Paper	Development of the methods, conduct of the analysis, validation and drafting the manuscript.
Overall percentage (%)	70%
Certification:	This paper reports on original research I conducted during the period of my Higher Degree by Research candidature and is not subject to any obligations or contractual agreements with a third party that would constrain its inclusion in this thesis. I am the primary author of this paper.
Signature	Date: 22/08/2019

Co-Author Contributions

By signing the Statement of Authorship, each author certifies that:

i. the candidate's stated contribution to the publication is accurate (as detailed above);

ii. permission is granted for the candidate in include the publication in the thesis; and

iii. the sum of all co-author contributions is equal to 100% less the candidate's stated contribution.

Name of Co-Author	Chaoshui Xu
Contribution to the Paper	Supervision, design of the work and reviewing the manuscript.
Signature	Date: 22/08/2019

Name of Co-Author	Peter Dowd
Contribution to the Paper	Supervision, design of the work and reviewing the manuscript.
Signature	Date: 21/8/2019

Name of Co-Author	Feng Xiong
Contribution to the Paper	Validation and reviewing the manuscript.
Signature	Date: 8.22/2019

Name of Co-Author	Hang Wang
Contribution to the Paper	Validation and reviewing the manuscript.
Signature	Date: 22/Aug/2019

Abstract

This study presents a non-linear Reynolds equation (NRE) for single-phase flow through a rock fracture. The fracture void geometry is considered formed by connected wedge-shaped cells at pore-scale, based on the measured aperture field. An approximate analytical solution to the two-dimensional Navier-Stokes equations is derived using the perturbation method to account for flow non-linearity in wedge-shaped geometries. The derived perturbation solution shows that the main contributors to the general flow behaviours in local wedges are the degree of aperture variation relative to mean aperture, the ratio of the aperture variation to length, the Reynolds number and the degree of wedge asymmetry. The transmissivity of the entire fracture is then solved with a field of varying local cell transmissivity along both longitude and latitude directions on the fracture plane. The performance of the proposed NRE is tested against flow experiments and flow simulations by solving numerically the three-dimensional Navier-Stokes equations for three cases of rock fractures with different void geometries. Results from the proposed model are in close agreement with those obtained from simulations and experiments. The pressure difference obtained from the NRE demonstrates the same non-linear behaviour as that obtained from the simulations in the strong inertial regime. Overall, the mean discrepancy between the proposed model and flow simulations is 5.7% for Reynolds number ranging from 0.1 to 20, indicating that the proposed NRE captures well the flow non-linearity in rock fractures.

4.1 Introduction

Flow often passes preferentially through fractures in sub-surface rocks with low permeability in a wide range of engineering applications including oil/gas recovery from fractured reservoirs, heat extraction from deep enhanced geothermal systems and hazardous waste disposal in underground repositories (Brown 1987; Hunt and Sahimi 2017; Mallikamas and Rajaram 2010; Tsang and Tsang 1987; Xu et al. 2015; Zimmerman and Bodvarsson 1996). As a basic element of understanding a complex fracture system, knowledge of flow behaviours in a single fracture is fundamental to addressing flow-related problems in fractured rock masses (Pyrak-Nolte et al. 1988; Zou et al. 2017). Rock fractures can normally extend to metres or greater in length and width while the apertures are mostly on the scale of millimetres or microns (Brown et al. 1998; Konzuk and Kueper 2004; Xu et al. 2018). An initial simplifying approach to modelling flow through a rock fracture is to assume that the fracture is bounded by two parallel planar walls with a constant aperture (Lomize 1951; Snow 1951; Witherspoon et al. 1980). This approximation yields the cubic law, which relates linearly the flow rate to the cube of the fracture aperture at a given pressure gradient (Renshaw 1995; Tsang and Witherspoon 1981). The cubic law has since been widely used to study flow-related problems in rock fractures. However, from experiments and numerical simulations, the applicability of the cubic law approximation to modelling fluid flow in realistic rock fractures is problematic as fracture surface roughness can generate a variable aperture within the fracture plane and this effect is not considered in the cubic law (Konzuk and Kueper 2004; Neuzil and Tracy 1981; Witherspoon et al. 1980). To account for the spatially varying feature of fracture apertures, the Reynolds equation has been adopted to include the aperture variation of local cells at pore-scale (Brown 1987; Walsh 1981). The Reynolds equation assumes that the cubic law holds at each local aperture position under the geometrical and kinematical conditions of gradual aperture change and negligible inertial effects (Brush and Thomson 2003; Oron and Berkowitz 1998). Although the Reynolds approximation is consistent with the laboratory observation that the variable aperture field and the extent of the fracture surface contact both play essential roles in determining fracture hydraulic properties, flow is found over-estimated by up to 47% when compared with experimental results (Nicholl et al. 1999; Yeo et al. 1998). This discrepancy may largely be due to the inaccurate quantification of the effect of aperture variability and not considering the spatial undulation of fracture mid-surface, which can lead to tortuous flow paths (Brush and Thomson 2003; Lee et al. 2014; Mallikamas and Rajaram 2010).

To improve the performance of the classic models (i.e. the cubic law and Reynolds equation), modifications have been incorporated to quantify the effect of fracture surface roughness on flow behaviours. For example, Ge (1997) proposed a modified version of the Reynolds equation by considering the effect of local tortuosity and later evolved into the concept of perpendicular aperture, where the originally measured local vertical apertures were adjusted to be perpendicular to the assumed local flow directions. Oron and Berkowitz (1998) conducted a leading-order approximation to the two-dimensional (2D) Navier-Stokes equations (NSE) and argued that the fracture aperture should be determined by the geometry of each identified fracture segment. Nicholl et al. (1999) obtained the transmissivity of a local wedge-shaped cell from the analytical solution under the creeping flow condition and also evaluated different approximate formulations for the local transmissivity, e.g., using arithmetic and harmonic average schemes. Others attempted to improve directly the cubic law by introducing modifying factors from surface roughness indices (e.g. Olsson and Barton, 2001) and statistical quantifications of surface roughness effects (e.g. Nazridoust et al., 2006). In general, a number of the modified cubic law based models have been found to improve the flow prediction of the classic models (Konzuk and Kueper 2004). However, most of the pore-scale modifications are based on subjective choices of aperture definition for local cells or applying direct average schemes to adjacent apertures. As a result, their robustness can be affected by the resolution of the aperture field (Berkowitz 2002). For modifications at the scale of a single fracture, the validity of these approaches may vary from case to case and the applied modifications are often less successful when strong channelling effects are present. In addition, inertial effects are either totally neglected in previously published cubic law based models or the flow dynamical condition is restricted to the Darcy flow regime where the Reynolds number (R) is less than one.

The three-dimensional (3D) Navier-Stokes equations (NSE) can provide an accurate description of flow through rock fractures with complex and irregular void geometry (Zimmerman and Bodvarsson 1996). The exact analytical solution to the NSE is only available for limited cases e.g. fractures with parallel planar walls. Solving numerically the NSE for 3D rock fractures with fine representation of the void geometry is computationally demanding, which has restricted its application to mostly small-scale problems (Brush and Thomson 2003; Wang et al. 2018; Zou et al. 2017). In this context, a further extension to the cubic law assumption was made by deriving approximate analytical solutions to the NSE using the perturbation method for 2D fractures with sinusoidally, linearly and quadratically varying

apertures (Basha and El-Asmar 2003; Hasegawa and Izuchi 1983; Kitanidis and Dykaar 1997). Previous studies have shown that the results from perturbation solutions are consistent with numerical simulation results (Sisavath et al. 2003; Wang et al. 2019). However, the application of these solutions to realistic rock fractures is rather limited. One problem associated with the 2D perturbation solutions is that the aperture can only vary in one direction, but in realistic 3D rock fractures, the variation of apertures should be in both longitude and latitude directions (Zimmerman 2005). In two-dimensional fractures, flow is blocked and the overall fracture transmissivity becomes zero when the two fracture walls are in contact. However, in realistic 3D rock fractures, fluid flows around the contact area through available close channels and the overall fracture transmissivity is not determined by a series of parallel 2D channels but rather, a complex 3D tortuous channel network (Tsang and Tsang 1987; Zimmerman et al. 1992).

The purpose of this study is to propose a non-linear flow model that accounts for the effects of fracture void geometry and inertia on the hydraulic properties of rock fractures. The proposed non-linear version of the Reynolds equation is based on representing the measured fracture void geometry with a series of connecting wedges formed using adjacent apertures in both longitude and latitude directions along the fracture plane, which is a common approximation approach for the fracture void geometry (Brush and Thomson 2003; Ge 1997). The perturbation solution to the NSE is derived to the second-order for two-dimensional wedge-shaped fractures using the ratio of the aperture variation to length as the perturbation parameter. This study differs from previous perturbation analyses in that the derived perturbation solution is used to describe the flow behaviours in wedge-shaped local cells rather than obtaining the transmissivity of the entire fracture. Pressure and flow fields are then solved in a varying pore-scale transmissivity field along both directions of the fracture plane with a constant pressure difference between inflow and outflow boundaries to obtain the overall fracture transmissivity. The performance of the proposed non-linear version of the Reynolds equation is assessed by comparing the predictions with experimental measurements and results from solving numerically the 3D NSE in three rock fractures. These fractures have different relative surface roughness and contact ratios and the assessment is done for the range of R from 0.1 to 20, which covers the Darcy flow regime (R<1), weak inertial regime (1<R<10) and strong inertial regime (R>10) (Zimmerman et al. 2004).

4.2 Material and method

4.2.1 Problem formulation

Without loss of generality, a fracture is assumed to be horizontal with longitudinal (*x*) and latitudinal (*y*) extents. When estimating or simulating flow in a single rock fracture, the fracture void geometry is widely approximated by simply connecting the measured adjacent elevation points of the top and bottom surfaces (Brown 1987; Brush and Thomson 2003; Konzuk and Kueper 2004). As a result, this approximation discretises the fracture void geometry into a series of two-dimensional (2D) connected wedges in both longitude and latitude directions, as shown in Figure 4.1. Finding the solution for the transmissivity of each 2D wedge and then solve the flow/pressure field of the 3D fracture is used in the original and modified versions of the Reynolds equation (e.g. Ge, 1997; Nicholl et al., 1999; Brush and Thomson, 2003).

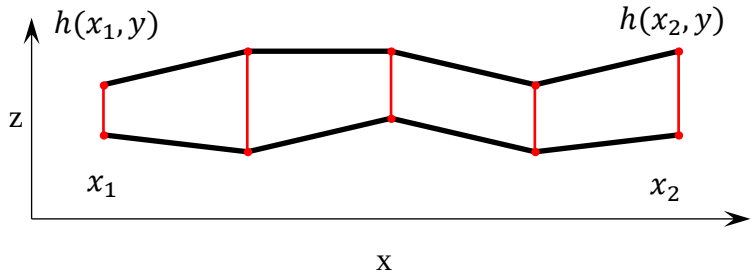

Figure 4.1 Illustration of a series of two-dimensional connected local wedges along the longitude direction *x*; a similar set of connected wedges can also be formed along the latitude direction *y*.

Considering a single 2D wedge as shown in Figure 4.2, the top and bottom wall functions can be defined as:

$$b_t(x) = \frac{h(x_1)}{2} + \frac{h(x_2)-h(x_1)}{2l}x + \frac{b_t(x_2)+b_b(x_2)}{2l}x = \frac{h_m}{2} - \frac{a}{4} - \frac{a-c}{2l}x \quad (4.1)$$

$$b_b(x) = -\frac{h(x_1)}{2} - \frac{h(x_2)-h(x_1)}{2l}x + \frac{b_t(x_2)+b_b(x_2)}{2l}x = -\frac{h_m}{2} + \frac{a}{4} - \frac{a-c}{2l}x \quad (4.2)$$

where b_t and b_b are, respectively, the top and bottom wall functions in the *x* direction; *h* is the aperture given by $h=b_t-b_b$; x_1 and x_2 are the locations of the two wedge edges, the length *l* is thus defined by $l=x_2-x_1$; h_m is the mean aperture given by $h_m=h(x_2)/2+h(x_1)/2$; *a* is defined as the difference between the two wedge edges i.e., $a=h(x_2)–h(x_1)$; *c* describes the wedge asymmetry defined by $c=b_t(x_2)-b_t(x_1)+b_b(x_2)-b_b(x_1)$, where *c/2* is equal to the elevation difference between the two mid-points at both ends of the wedge.

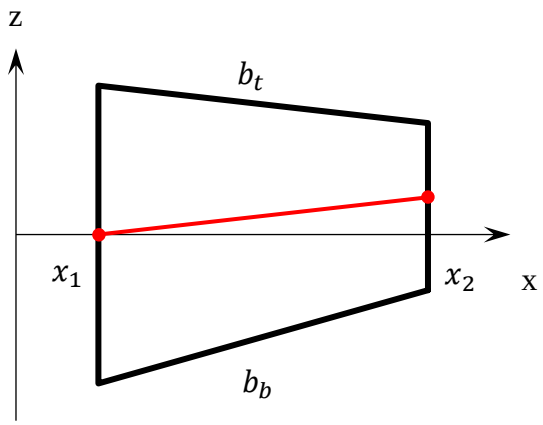

Figure 4.2 Illustration of a local wedge along the *x* direction, the red solid line connects the mid-points at both edges of the wedge.

The governing equations for the incompressible steady-state flow within the wedge-shaped representation of local cell are given by the Navier-Stokes equations (NSE) together with the condition for mass continuity (Basha and El-Asmar 2003; Zimmerman and Bodvarsson 1996):

$$\rho\left(u\frac{\partial u}{\partial x}+w\frac{\partial u}{\partial z}\right)=-\frac{\partial p}{\partial x}+\mu\left(\frac{\partial^2 u}{\partial x^2}+\frac{\partial^2 u}{\partial z^2}\right) \tag{4.3}$$

$$\rho\left(u\frac{\partial w}{\partial x}+w\frac{\partial w}{\partial z}\right)=-\frac{\partial p}{\partial z}+\mu\left(\frac{\partial^2 w}{\partial x^2}+\frac{\partial^2 w}{\partial z^2}\right) \tag{4.4}$$

$$\frac{\partial u}{\partial x}+\frac{\partial w}{\partial z}=0 \tag{4.5}$$

where u and w are velocities in the x and z directions, respectively; ρ is the fluid density; p is the reduced pressure; and μ is the dynamic viscosity of the fluid.

For the boundary conditions, a flow rate q per unit width of the fracture (in y) is produced with a pressure difference Δp between the inflow and outflow boundaries; both the top and bottom walls are considered having non-slip and impermeable wall features (no flux across the walls).

4.2.2 Perturbation solution

Exact analytical solution to the NSE is currently only available for limited cases e.g. fractures with parallel planar walls, which leads to the cubic law (CL). In this study, perturbation expansion is used to find the approximate analytical solution for more complex wall geometries. The derivation of the perturbation solution follows mostly the work by Wang et al. (2019) with an additional extension to consider geometric asymmetry. This section provides a brief description of the approach and one can refer to the previous study for the detailed derivation process.

The stream function ψ is defined by

$$u = \frac{\partial \psi}{\partial z},\ w = -\frac{\partial \psi}{\partial x}. \tag{4.6}$$

Substituting the stream function into the NSE in section 4.2.1, the stream function is found to satisfy the following relation:

$$\rho\left[\frac{\partial}{\partial z}\left(\frac{\partial \psi}{\partial z}\frac{\partial^2 \psi}{\partial x \partial z} - \frac{\partial \psi}{\partial x}\frac{\partial^2 \psi}{\partial z^2}\right) - \frac{\partial}{\partial x}\left(-\frac{\partial \psi}{\partial z}\frac{\partial^2 \psi}{\partial x^2} + \frac{\partial \psi}{\partial x}\frac{\partial^2 \psi}{\partial x \partial z}\right)\right] = \mu\left(\frac{\partial^4 \psi}{\partial x^4} + 2\frac{\partial^4 \psi}{\partial x^2 \partial z^2} + \frac{\partial^4 \psi}{\partial z^4}\right) \tag{4.7}$$

For the auxiliary condition, the mean pressure difference over the fracture width and length can be assumed to equal a given constant mean pressure difference (Hasegawa and Izuchi 1983), leading to:

$$\Delta p = \int_{x_1}^{x_2} \frac{1}{h}\left(\int_{b_b}^{b_t} \frac{\partial p}{\partial x} dz\right) dx \tag{4.8}$$

where the pressure derivative $\partial p/\partial x$ can be obtained from equation (4.3) using the stream function:

$$\frac{\partial p}{\partial x} = \mu\left(\frac{\partial^3 \psi}{\partial x^2 \partial z} + \frac{\partial^3 \psi}{\partial z^3}\right) + \rho\left(\frac{\partial \psi}{\partial x}\frac{\partial^2 \psi}{\partial z^2} - \frac{\partial \psi}{\partial z}\frac{\partial^2 \psi}{\partial x \partial z}\right) \tag{4.9}$$

Equation (4.8) provides the auxiliary condition that establishes the relationship between the mean pressure difference and stream function. The final solution is obtained by solving equation (4.8) with the stream function under associated boundary conditions.

The stream function and pressure difference can be made dimensionless and expressed as expanded series with a small parameter ϵ:

$$\Psi = \Psi_0 + \epsilon\Psi_1 + \epsilon^2\Psi_2 + O(\epsilon^3) \tag{4.10}$$

$$\Delta P = \Delta P_0 + \epsilon\Delta P_1 + \epsilon^2\Delta P_2 + O(\epsilon^3) \tag{4.11}$$

where ϵ in this study is defined as $\epsilon=\omega/L$, and L is the dimensionless length given by $L=l/h_m$; ω is the dimensionless absolute aperture variation defined as $\omega=|a|/h_m$; Ψ is the dimensionless stream function defined as $\Psi=\psi/q$; ΔP is the dimensionless pressure difference given as $\Delta P=\Delta p/\Delta p_m$ and Δp_m is the pressure difference of flow through a fracture with a uniform aperture defined from the CL as:

$$\Delta p_m = \frac{12\mu l Q}{{h_m}^3} \tag{4.12}$$

The solution of the stream function up to the second-order can be derived by substituting equation (4.10) into the dimensionless version of equation (4.7) with the associated boundary conditions. The dimensionless pressure difference for the first three terms can then be obtained from equation (4.8) as

$$\Delta P_0 = \frac{1}{\omega}\int_0^{\omega}\frac{1}{H^3}dX \tag{4.13}$$

$$\Delta P_1 = -\frac{1}{\omega}\int_0^{\omega}\frac{9RH'}{70H^3}dX \tag{4.14}$$

$$\Delta P_2 = -\frac{1}{\omega}\int_0^{\omega}\frac{13R^2(4H'^2-3H'')}{539000H^3} - \frac{3R^2}{5H^3}\left(\frac{H'B_b}{H^2} - \frac{B_b'}{H}\right)^2\left(B_b + \frac{B_b^2}{H}\right)^2 - \frac{H'^2+HH''}{10H^3} - \frac{B_b'(H'+B_b')}{H^3}dX \tag{4.15}$$

where X is defined as $X= \epsilon x/h_m$; H is the dimensionless aperture defined as $H=h/h_m$, H' and H'' are the first and second derivatives of H with respect to X; R is the Reynolds number defined as $R=\rho q/\mu$; B_b is the dimensionless bottom wall function defined as $B_b=b_b/h$.

4.2.3 Non-linear Reynolds equation

The equivalent hydraulic aperture h_T of the wedge can be defined by multiplying h_m by an extra modification factor:

$$h_T = h_m \cdot F_p \tag{4.16}$$

where F_p is a modification factor based on the perturbation solution (PS) given by $F_p^3=\Delta p_m/\Delta p$. Essentially, the equivalent hydraulic aperture of each local wedge within a fracture can be obtained from equation (4.16). Incorporating inertial effects can encourage more flow for diverging wedge-shaped cell whereas flow is more discouraged for the converging cases (see Figure 4.8). Note the limitation of the PS as discussed by Basha and El-Asmar (2003); Wang et al. (2019), where an increasingly greater error in the PS is associated with the increase of R. Therefore, an assumption is made that the equivalent hydraulic aperture for each local wedge-shaped cell, when incorporating inertial effects using equation (4.16), should be within the size of inflow and outflow apertures under the creeping flow condition. With equation (4.16), the proposed non-linear flow model can thus be written in the form:

$$\frac{\partial}{\partial x}\left[{h_T}^3(x,y)\frac{\partial p}{\partial x}\right] + \frac{\partial}{\partial y}\left[{h_T}^3(x,y)\frac{\partial p}{\partial y}\right] = 0 \tag{4.17}$$

Equation (4.17) is in a similar form to the Reynolds equation except that the original measured apparent aperture h is replaced by h_T to incorporate the varying local fracture geometry and inertial effects. Equation (4.17) can thus be seen as a nonlinear version of the Reynolds equation (NRE) and is solved iteratively in this work using an approach similar to that described in Moreno et al.(1988) due to the nonlinearity of F_p.

4.3 Model validation

4.3.1 Flow simulation in three-dimensional rock fractures

A single fracture (F0.0) was created from an intact granite block using the Brazilian indirect tensile loading and the fracture surface morphology was obtained using an advanced stereotopometric scanning system as described in Xiong et al.(2018), with both fracture surfaces having a dimension of 150 mm×150 mm. The spatial variations of the fracture apertures are shown in Figure 4.3a and the corresponding statistical distribution is shown in Figure 4.3b, together with the probability density functions. To account for the effect of surface contact on flow behaviours, two additional cases were considered where the fracture was assumed to be under compression in the direction normal to the fracture plane with normal relative displacements of 0.3 mm and 0.5 mm directly applied to the obtained fracture geometry of F0.0. These two cases with different contact areas were denoted as F0.3 and F0.5, respectively. In total, three different rock fractures were used in this study for the purpose of validation and some of their statistics are listed in Table 4.1. The spacing of the scanned grid was 0.1 mm in both the x and y direction, with an accuracy of ±25 μm. In this study, the grid spacing was optimized to 1 mm to reduce the computational workload for solving the NSE in complex 3D geometry with highly detailed surface topography (Zimmerman et al. 2004; Zou et al. 2017) while retaining the main geometric effect on flow behaviours. A comparison of the results of flow simulations and experiments shows close agreement with a mean absolute error of 3% as found in Xiong et al.(2018), indicating that the essential fracture geometry information has been well captured.

Table 4.1 Fracture geometry statistics*

	F0.0	F0.3	F0.5
Mean aperture h_m (mm)	1.67	1.37	1.18
Aperture standard deviation σ (mm)	0.70	0.69	0.68
Relative roughness σ/h_m (-)	0.42	0.50	0.58
Contact ratio C_r (%)	1.64	3.81	7.03
$<\omega/h_m>$ (-)	0.16	0.21	0.25
$<\epsilon>$ (-)	0.24	0.23	0.23
$<\|c/h_m\|>$ (-)	0.20	0.27	0.32

*$<\omega/h_m>$ describes the average of ω/h_m in all wedge-shaped cells; $<\epsilon>$ is the average perturbation parameter; and $<|c/h_m|>$ is the average of absolute c/h_m of all wedge-shaped cells.

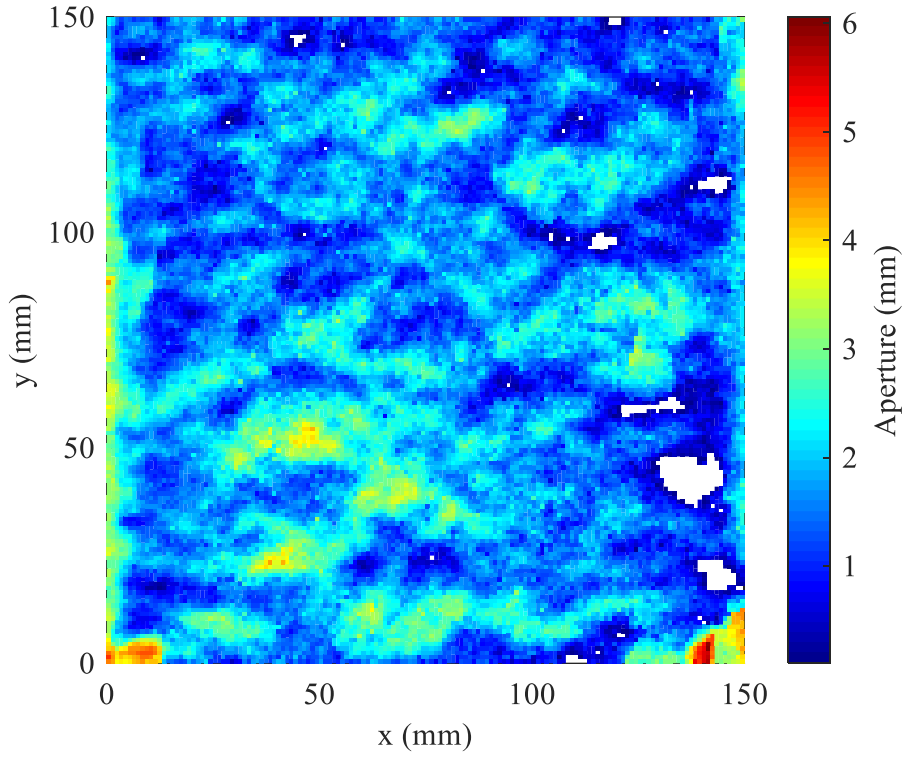

(a)

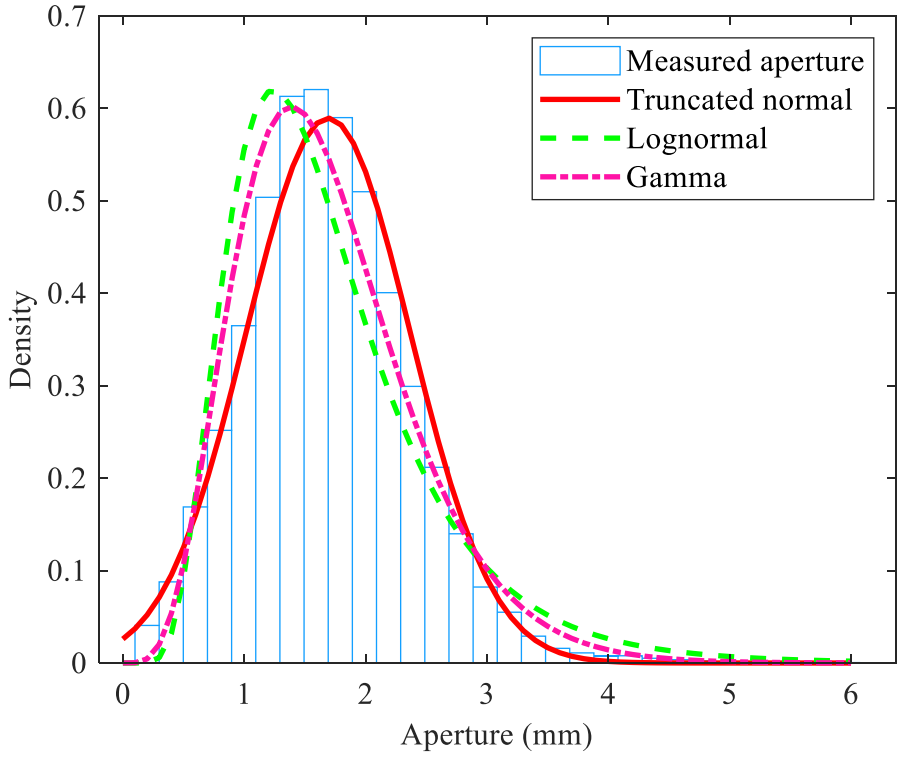

(b)

Figure 4.3 Aperture distribution of F0.0 for (a) spatial aperture variation where white areas are surface contact areas and (b) probability density function of the measured aperture field fitted with truncated normal, lognormal and gamma distributions.

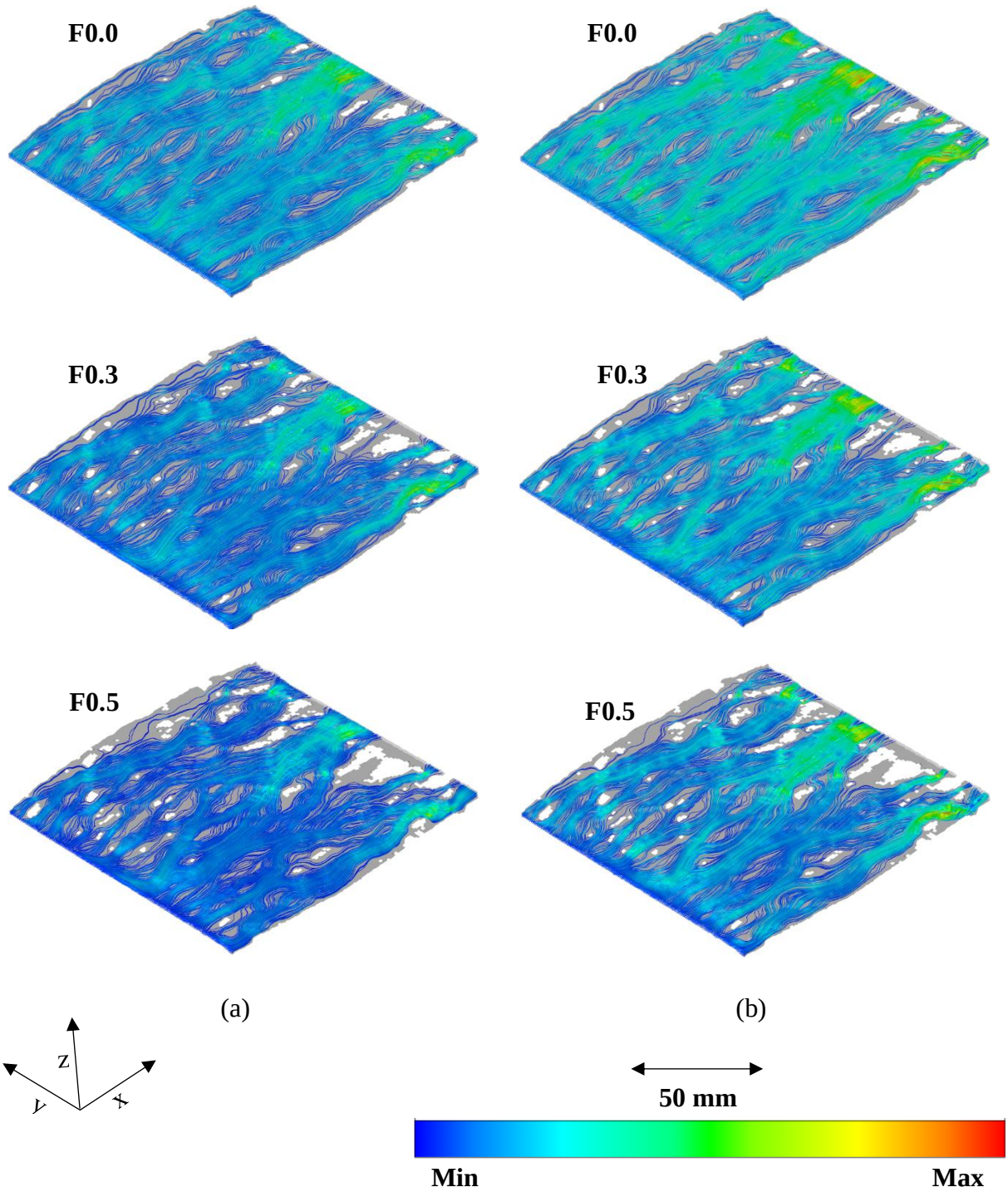

Figure 4.4 Flow streamlines of the three fracture cases for (a) R=1 and (b) R=20, where blue represents the minimum velocity and red is the maximum velocity. The grey areas are fracture voids with little flow and white areas are surface contact areas. The inflow q for all simulations is along the x direction.

Flow simulations in this work were conducted by solving numerically the 3D NSE with computational flow dynamics (CFD) code FLUENT in ANSYS. No-flux and non-slip boundary conditions were set for fracture walls. Water (at 15°C) was considered in this study with a density ρ=999.1 kg/m^3 and a dynamic viscosity μ=0.00114 kg/m·s. The mesh scheme was optimized to reduce the mesh-related effect on flow simulations. In general, over 1.5 million hexahedron mesh elements were constructed for each fracture. The inflow boundary was assigned a constant mass flow rate and the outflow boundary was set with a constant pressure condition. The mass flow rate was progressively increased in the flow simulations, corresponding to R ranging from 0.1 to 20.

To demonstrate the general flow paths within the fractures, flow streamlines are plotted in Figure 4.4 using 1000 equally spaced sampling points at the inflow boundary along the three fractures tested in this study for R=1 and R=20. As illustrated in Figure 4.4, the flow pattern of F0.0 is generally consistent with the aperture distribution shown in Figure 4.3a, where the main flow paths and high velocity zones occur in large aperture locations. A comparison of the distributions of streamlines of F0.0, F0.3 and F0.5 shows that the streamlines become more tortuous as more contact areas are introduced. For F0.0, the streamlines spread more uniformly along the inflow boundary and on the fracture plane, whereas they become more concentrated and tortuous for F0.5. As expected, the surface contact has a strong impact on the general flow behaviours as it alters the flow paths by forcing the fluid to travel around the contact areas. In addition, contact areas are generally surrounded by small apertures and therefore relatively little flow is expected to pass through the available channels near the contact areas. Consequently, the majority of the flow is forced to travel in limited but well-connected tortuous channels with larger apertures as more surface contact areas are present, leading to stronger and well-documented channelling effects for flow in rock fractures.

4.3.2 Model performance

As mentioned in the previous section, fixed mass flow rates were assigned to the inflow boundary of all fractures in flow simulations to attain the corresponding R for each case, as shown in Figure 4.5. The pressure at the inflow boundary can then be directly obtained from flow simulations and the pressure difference Δp is calculated accordingly. From the simulation results, Δp demonstrates a non-linear increase as R increases from 0.1 to 20, which suggests a non-linear decrease in fracture transmissivity with greater inertial effects. In addition, the degree of flow non-linearity is further enhanced as the contact area increases, as caused by

more tortuous flow paths and the formation of eddies near the contact region. To demonstrate the robustness of the proposed NRE in describing this flow non-linearity in realistic 3D rock fractures, the pressure differences evaluated from equation (4.17) are compared with those from flow simulations at different R, as shown in Figure 4.5. The deviation is defined as the relative error in estimating the fracture transmissivity:

$$D = \frac{T_{model} - T_{real}}{T_{model}} \times 100\% \tag{4.18}$$

where T_{model} is the fracture transmissivity obtained from the NRE and T_{real} is the fracture transmissivity obtained from numerical simulations.

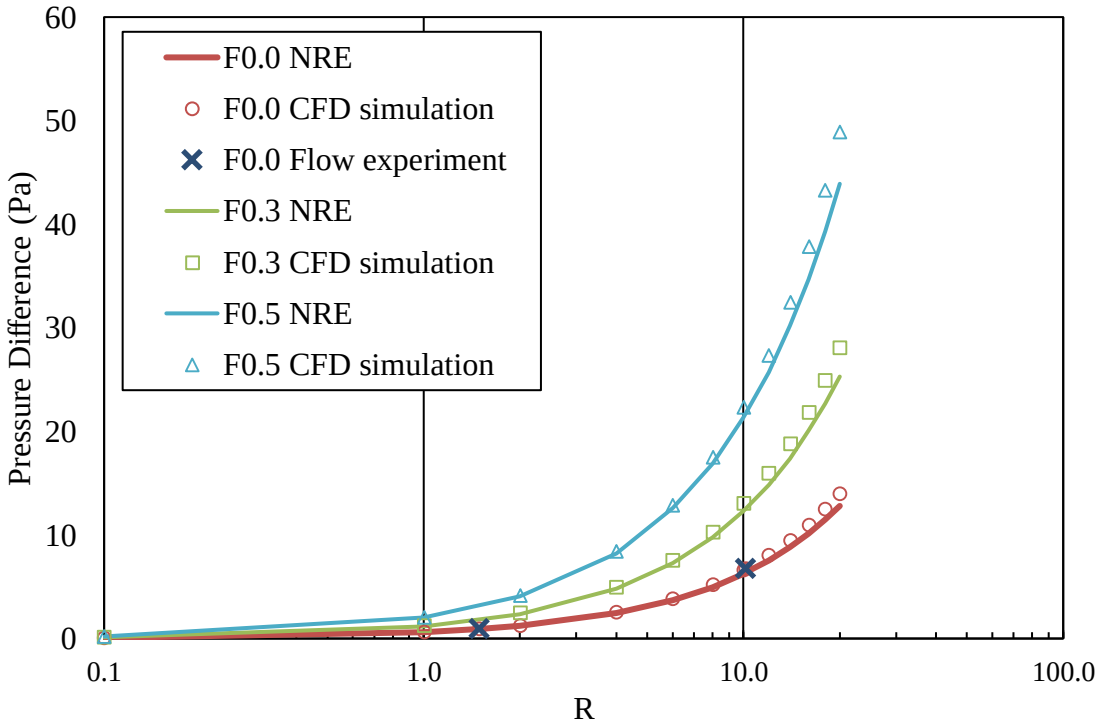

Figure 4.5. The pressure difference Δp between the inflow and outflow boundaries of tested fractures for R ranging from 0.1 to 20, obtained from flow simulations, experiments and the proposed NRE.

In general, the two are in close agreement for all three cases, with the deviation D_s ranging from 1.9% to 10.3% with a mean of 5.7%. For F0.0, D_s ranges from 4.6% to 8.6% and the mean deviation $<D_s>$ is 6.0%. A slightly higher $<D_s>$ of 6.2 % is observed for F0.3 with D_s in the range of 4.0% to 9.9%. F0.5 has the lowest $<D_s>$ of 4.9% in this case and the range of D_s is from 1.9% to 10.3%. The distribution of D_s with $0.1<R<20$ for all three cases can be found in Figure 4.6. In Figure 4.5, two flow test results given in Xiong et al. (2018) for F0.0 at R=1.5 and R=10.1 were also displayed. The corresponding deviations are 5.9% and 6.6%, respectively,

suggesting reasonably accurate estimates of real fracture transmissivity from the proposed flow model.

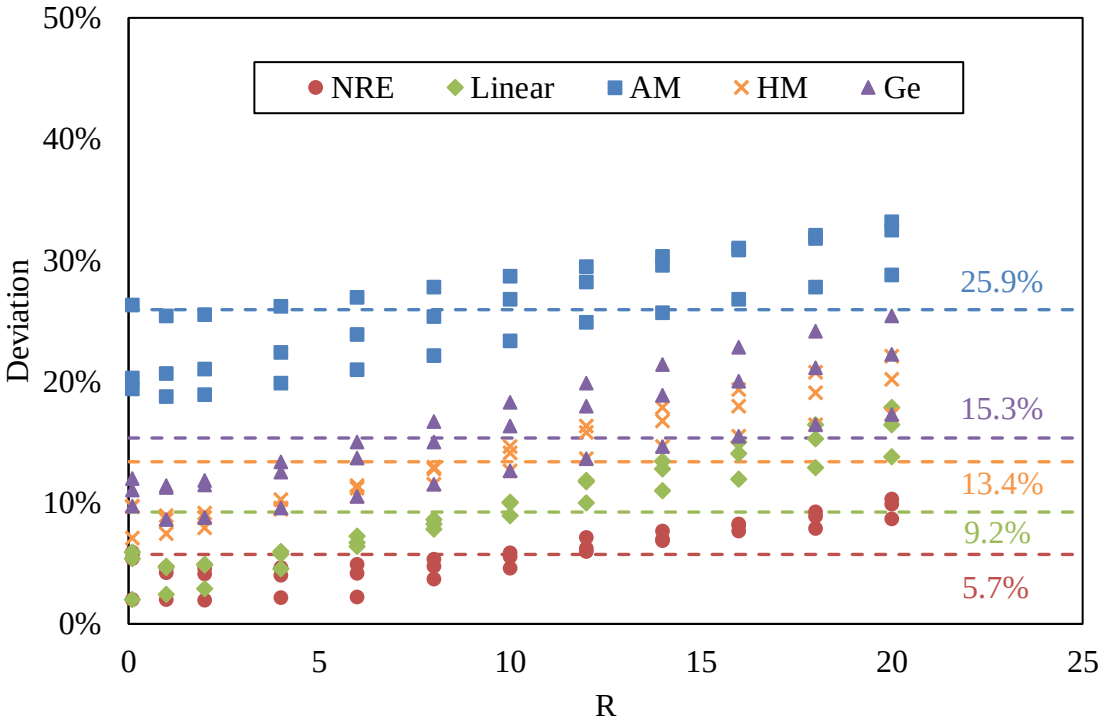

Figure 4.6. Deviation from flow simulations D_s for the proposed NRE, linear version of NRE, arithmetic mean (AM) (Bear 1979; Nicholl et al. 1999), harmonic mean (HM) (Bear 1979; Nicholl et al. 1999) and the model of Ge (1997), where the mean deviations of these models are 5.7%, 9.2%, 25.9%, 13.4% and 15.3%, respectively, as represented by dashed lines.

Further assessments of the NRE were made by comparing the values of D_s with those obtained from previously proposed flow models including the modified Reynolds equation in Ge (1997) and Reynolds equation with two average schemes for local transmissivity (arithmetic mean AM and harmonic mean HM) (Bear 1979; Nicholl et al. 1999). D_s from the linear version of equation (4.17) (i.e. setting R=0 for F_p) is also calculated as an additional comparison to demonstrate the difference in estimating the fracture transmissivity when neglecting inertial effects. Overall, the highest deviation is observed for AM with a mean of 25.9% and a maximum of 33.2%. Both the HM and Ge model deviate by less than 15% when R is less than 6; however, the deviation rises to 25.4% and 22.2%, respectively, as R increases to 20. Among all the tested linear models, the linear version of equation (4.17) demonstrates the lowest D_s with $\langle D_s \rangle$ of 6.1% for R less than 10 when the flow non-linearity is weak. D_s from the NRE and its linear version are virtually identical for R less than 1, which is in agreement with the results of Zimmerman et al. (2004) that flow can be considered to have

linear behaviour in the Darcy flow regime when R<1. The proposed NRE outperformed other models in the entire range of R with the lowest $\langle D_s \rangle$ of 5.7%. $\langle D_s \rangle$ of the NRE is 4.1% for the weak inertial regime and becomes 7.5% when entering the strong inertial flow regime.

4.4 Discussion

4.4.1 Flow in pore-scale wedges

The flow behaviours in pore-scale wedges are mainly affected by wedge geometry (i.e. aperture variation and wedge asymmetry) and flow dynamics (i.e. Reynolds number). The zero-order PS, equation (4.13), is effectively the Reynolds approximation that merely considers the effect of aperture variation on flow. The first-order term of the PS, equation (4.14), has incorporated inertial effects, which have opposite impacts for diverging and converging cases (Basha and El-Asmar 2003); whereas the second-order term of the PS, equation (4.15), takes into account additionally the effect of wedge asymmetry. When the wedge geometry becomes the same as fracture with two parallel planar walls, the derived PS becomes the classic CL solution and F_p=1.

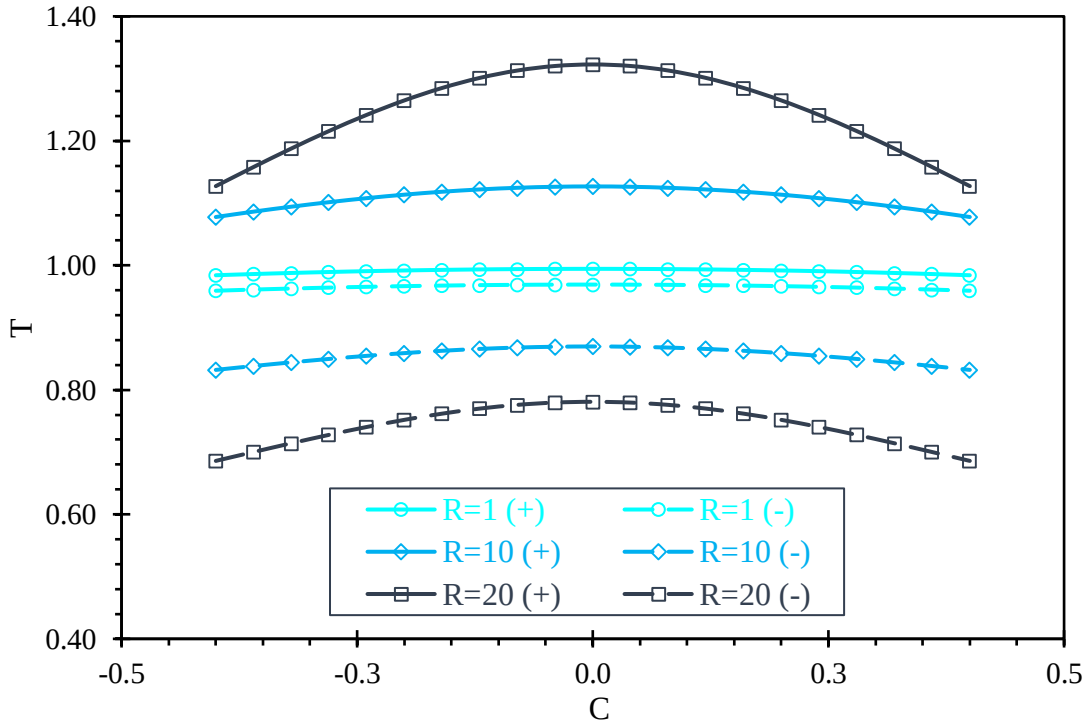

Figure 4.7 Effect of C on the normalized transmissivity T obtained from the PS (obtained transmissivity is normalized by the transmissivity from the CL using the arithmetic mean aperture), where the solid and dashed lines are for diverging (+) and converging (-) cases, respectively.

The degree of wedge asymmetry in this study is described by C ($C=c/h_m$) and to evaluate its effect on flow behaviours, ϵ and ω/h_m are fixed at 0.1 and 0.2, respectively. As shown in Figure 4.7, T decreases as the absolute value of C increases (i.e., as the degree of asymmetry increases). At R=10, as the absolute value of C changes from 0 to 0.3, T decreases from 1.13 to 1.08 for cases of diverging wedges and from 0.87 to 0.83 for converging ones. This suggests that flow is increasingly discouraged as the degree of wedge asymmetry increases and the effect becomes more pronounced with greater R. It is also evident that the effect of C on wedge transmissivity is symmetrical for both cases of diverging and converging wedges, meaning that the same effect on flow behaviour can be expected for the same degree of wedge asymmetry, regardless of whether C is positive or negative. T from the zero-order and first-order PS is independent of C as no asymmetry effect is considered.

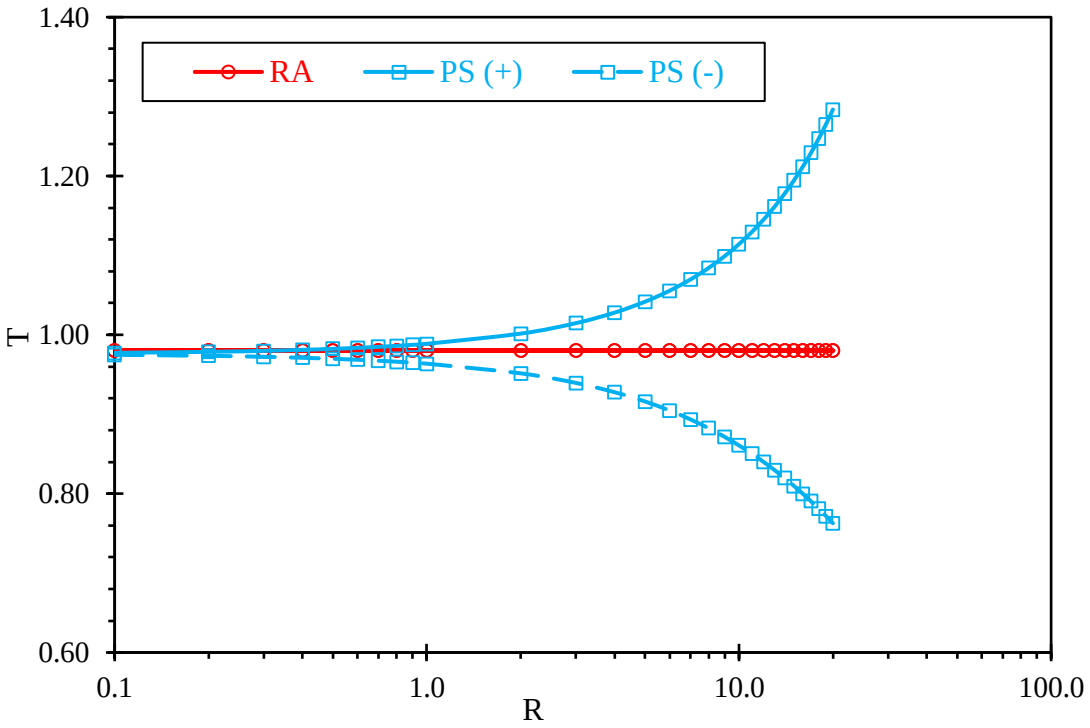

Figure 4.8 Effect of R on T obtained from the Reynolds approximation (RA) and PS, where the solid and dashed lines are for diverging (+) and converging (-) cases, respectively.

The effect of Reynolds number R on transmissivity T for Reynolds approximation (RA) and PS is illustrated in Figure 4.8, where R ranges from 0.1 to 20, with ϵ, ω/h_m and C fixed at 0.1, 0.2 and 0.3, respectively. As shown in Figure 4.8, inertial effects can have opposite effects on flow for diverging and converging cases. For converging wedges, more energy is dissipated due to the viscous effect as R increases, resulting in a decrease of T from 0.97 to 0.76 as R increases from 0.1 to 20; whereas for the diverging case, T increases from 0.97 to1.28 for the

same range of R due to the fact that inertial effects encourage more flow with weak viscous effect (Basha and El-Asmar 2003; Wang et al. 2019). From Figure 4.8, the transmissivity obtained from the perturbation solution T_{PS} appears to be symmetrical for diverging and converging cases. However, on close examination, T_{PS} increases by 32% for diverging wedges while it decreases by 22% for the converging ones in the same range of R. The transmissivity from the Reynolds approximation T_{RA} remains the same for different R as the inertial effects are ignored during the derivation of the Reynolds equation.

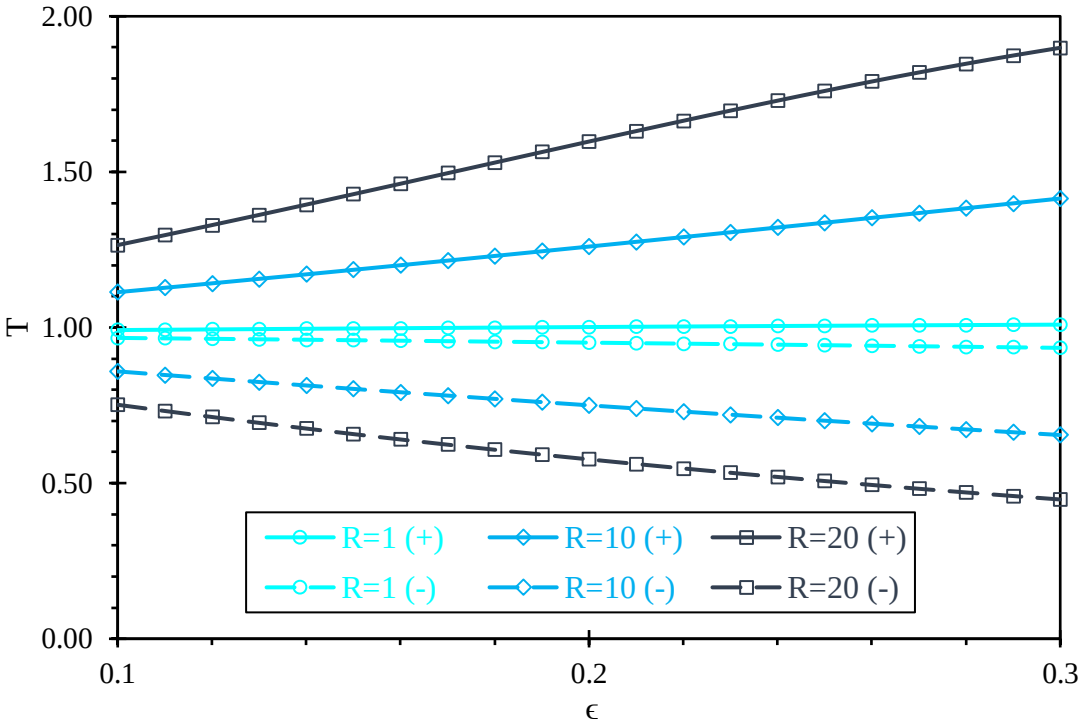

Figure 4.9 Effect of ϵ on T obtained from the PS, where the solid and dashed lines are for diverging (+) and converging (-) cases, respectively.

Figure 4.9 shows the effect of ϵ on T obtained from the PS, where ϵ ranges from 0.1 to 0.3 with ω/h_m and C both fixed at 0.2. T increases for diverging wedges but decreases for converging ones as ϵ increases from 0.1 to 0.3. For R=10, T for diverging wedges increases from 1.11 to 1.41 in the examined range of ϵ, whereas T decreases from 0.86 to 0.65 for converging wedges. In addition, the effect of ϵ on T is progressively enhanced as R increases, indicating that greater errors are produced for adopting the cubic law assumption when the aperture variation and inertial effects become more significant.

4.4.2 Limitations

The main limitation of this study arises from the PS in describing the flow behaviours of wedge-shaped fractures. The premise of its validity lies in the assumptions that the variation of aperture along the fracture length direction is gentle to modest and the dominant flow is in the fracture length direction (hence the perturbation parameter ϵ is small). This assumption can be violated as the degree of aperture variation increases. However, the feature of gradual aperture change is mostly considered and reported for rock fractures (e.g. Zimmerman et al., 1992; Basha and El-Asmar, 2003; Sisavath et al., 2003; Wang et al., 2019) and therefore the validity of the assumption is warranted in most cases. In addition, the perturbation method provides an approximate analytical solution to the problem where more higher-order terms need to be incorporated due to high Reynolds number. The error associated with the second-order perturbation solution is of the third-order of ϵ and is therefore estimated to be small for fractures with gradual aperture changes. The comparison study with the CFD simulation in Wang et al. (2019) shows a mean absolute discrepancy of 1.6% for similar wedge-shaped cells when the inertial effects are moderate.

Another limitation of the proposed NRE results from using 2D wedges to represent 3D fracture void geometries, i.e., assuming no variation of fracture aperture in the third dimension for each local cell. In reality, flow demonstrates much more complex behaviour in 3D voids that may include whirling backflows and transverse flow, particularly for high Reynolds number, whereas more regular rotational flow with closed streamlines occurs typically in 2D representations (Zou et al. 2017). This limitation appears in most existing analytical flow models that solve the flow using aperture fields (e.g. Brown, 1987; Ge, 1997; Konzuk and Kueper, 2004; Wang et al., 2018). Future work may focus on accounting for the contribution of local 3D pore-scale flow to the overall flow nonlinearity, and the transmissivity estimation of the entire fracture.

4.5 Conclusions

In this study, a non-linear flow model, NRE, has been proposed to improve the flow estimation for rock fractures with complex void geometry (rough fracture walls with surface contacts) and in flow regimes with moderate inertial effects. The NRE is based on a two-dimensional perturbation solution that can accurately estimate the transmissivity at local wedge-shaped cells by considering the effects of cell geometry and flow inertia. From the derived perturbation solution, it is found that flow through local wedge-shaped cells is mainly affected by the ratio

of aperture variation to mean aperture, the ratio of aperture variation to length, the degree of wedge asymmetry and the Reynolds number. With the derived solution, flow can then be solved for the entire fracture with varying transmissivity at locations within the fracture. To examine the performance of the proposed model, flow simulations in rock fractures with different relative surface roughness and contact ratios were performed for Reynolds numbers ranging from 0.1 to 20, which considers three main flow regimes (from weak to strong inertial effects). It has been found that results from the proposed model agree well with simulation results, showing that the pressure difference increases non-linearly as the Reynolds number increases, and demonstrates that the proposed model can well capture the non-linear behaviour of flow. In general, the absolute deviation of the proposed model from simulation results, in terms of the estimated transmissivity, is in the range of 2.0% to 10.3% with a mean deviation of 5.7% for all examined fracture cases. In addition, there is an absolute deviation of less than 5.0% between the results from the proposed model and those of flow experiments. In general, the proposed NRE captures well the flow non-linearity in rock fractures with complex void geometry under flow regimes with weak to moderate inertial effects. This provides a more accurate description of flow behaviours in rock fractures and can be used to study further the flow-related problems.

Acknowledgments

This work received support from a joint scholarship provided by the China Scholarship Council (CSC) and The University of Adelaide (No. 201506430003).

References

Basha, H.A., El-Asmar, W.: The fracture flow equation and its perturbation solution. Water Resour. Res. 39, 1365 (2003). doi:10.1029/2003WR002472

Bear, J.: Hydraulics of groundwater. McGraw-Hill. New York,NY,USA. (1979)

Berkowitz, B.: Characterizing flow and transport in fractured geological media: A review. Adv. Water Resour. 25, 861–884 (2002). doi:10.1016/S0309-1708(02)00042-8

Brown, S., Caprihan, A., Hardy, R.: Experimental observation of fluid flow channels in a single fracture. J. Geophys. Res. 103, 5125 (1998). doi:10.1029/97JB03542

Brown, S.R.: Fluid flow through rock joints: the effect of surface roughness. J. Geophys. Res. 92, 1337–1347 (1987). doi:10.1029/JB092iB02p01337

Brush, D.J., Thomson, N.R.: Fluid flow in synthetic rough-walled fractures: Navier-Stokes, Stokes, and local cubic law simulations. Water Resour. Res. 39, 1085 (2003). doi:10.1029/2002WR001346

Ge, S.: A governing equation for fluid flow in rough fractures. Water Resour. Res. 33, 53–61 (1997). doi:10.1029/96WR02588

Hasegawa, E., Izuchi, H.: On Steady Flow through a Channel Consisting of an Uneven Wall and a Plane Wall Part 1. Case of No Relative Motion in Two Walls. Bull. JSME. 26, 532–542 (1983). doi:10.1248/cpb.37.3229

Hunt, A.G., Sahimi, M.: Transport and Reaction in Porous Media: Percolation Scaling, Critical-Path Analysis, and Effective-Medium Approximation. Rev. Geophys. (2017). doi:10.1002/2017RG000558

Kitanidis, P.K., Dykaar, B.B.: Stokes flow in a slowly varying two-dimensional periodic pore. Transp. Porous Media. 26, 89–98 (1997). doi:10.1023/A:1006575028391

Konzuk, J.S., Kueper, B.H.: Evaluation of cubic law based models describing single-phase flow through a rough-walled fracture. Water Resour. Res. 40, 1–17 (2004). doi:10.1029/2003WR002356

Lee, S.H., Lee, K.K., Yeo, I.W.: Assessment of the validity of Stokes and Reynolds equations for fluid flow through a rough-walled fracture with flow imaging. Geophys. Res. Lett. 41, 4578–4585 (2014). doi:10.1002/2014GL060481

Lomize, G.M.: Filtratsiia v Treshchinovatykh Porod (Water Flow in Jointed Rock) (in Russian), (1951)

Mallikamas, W., Rajaram, H.: An improved two-dimensional depth-integrated flow equation for rough-walled fractures. Water Resour. Res. 46, 1–13 (2010). doi:10.1029/2009WR008779

Moreno, L., Tsang, Y.W., Tsang, C.F., Hale, F. V., Neretnieks, I.: Flow and tracer transport in a single fracture: A stochastic model and its relation to some field observations. Water Resour. Res. 24, 2033–2048 (1988). doi:10.1029/WR024i012p02033

Nazridoust, K., Ahmadi, G., Smith, D.H.: A new friction factor correlation for laminar, single-phase flows through rock fractures. J. Hydrol. 329, 315–328 (2006). doi:10.1016/j.jhydrol.2006.02.032

Neuzil, C.E., Tracy, J. V.: Flow through fractures. Water Resour. Res. 17, 191–199 (1981). doi:10.1029/WR017i001p00191

Nicholl, M.J., Rajaram, H., Glass, R.J., Detwiler, R.: Saturated flow in a single fracture: Evaluation of the Reynolds equation in measured aperture fields. Water Resour. Res. 35, 3361–3373 (1999). doi:10.1029/1999WR900241

Olsson, R., Barton, N.: An improved model for hydromechanical coupling during shearing of rock joints. Int. J. Rock Mech. Min. Sci. 38, 317–329 (2001). doi:10.1016/S1365-1609(00)00079-4

Oron, A.P., Berkowitz, B.: Flow in rock fractures: The local cubic law assumption reexamined. Water Resour. Res. 34, 2811–2825 (1998). doi:10.1029/98WR02285

Pyrak-Nolte, L.J., Cook, N.G.W., Nolte, D.D.: Fluid percolation through single fractures. Geophys. Res. Lett. 15, 1247–1250 (1988). doi:doi:10.1029/GL015i011p01247

Renshaw, C.E.: On the relationship between mechanical and hydraulic apertures in rough-walled fractures. J. Geophys. Res. 100, 24629–24636 (1995). doi:10.1029/95JB02159

Sisavath, S., Al-Yaaruby, a., Pain, C.C., Zimmerman, R.W.: A Simple Model for Deviations

from the Cubic Law for a Fracture Undergoing Dilation or Closure. Pure Appl. Geophys. 160, 1009–1022 (2003). doi:10.1007/PL00012558

Snow, D.T.: A parallel plate model of fractured permeable media. Ph.D. thesis, Univ. of Calif., Berkeley. (1951)

Tsang, Y.W., Tsang, C.F.: Channel model of flow through fractured media. Water Resour. Res. 23, 467–479 (1987). doi:10.1029/WR023i003p00467

Tsang, Y.W., Witherspoon, P.A.: Hydromechanical Behavior of a Deformable Rock Fracture Subject to Normal Stress. 86, 9287–9298 (1981)

Walsh, J.B.: Effect of pore pressure and confining pressure on fracture permeability. Int. J. Rock Mech. Min. Sci. Geomech. Abstr. 18, 429–435 (1981). doi:http://dx.doi.org/10.1016/0148-9062(81)90006-1

Wang, Z., Xu, C., Dowd, P.: A Modified Cubic Law for single-phase saturated laminar flow in rough rock fractures. Int. J. Rock Mech. Min. Sci. 103, 107–115 (2018). doi:10.1016/j.ijrmms.2017.12.002

Wang, Z., Xu, C., Dowd, P.: Perturbation Solutions for Flow in a Slowly Varying Fracture and the Estimation of Its Transmissivity. Transp. Porous Media. 128, 97–121 (2019). doi:10.1007/s11242-019-01237-7

Witherspoon, P.A., Wang, J.S.Y., Iwai, K., Gale, J.E.: Validity of Cubic Law for fluid flow in a deformable rock fracture. Water Resour. Res. 16, 1016–1024 (1980). doi:10.1029/WR016i006p01016

Xiong, F., Jiang, Q., Ye, Z., Zhang, X.: Nonlinear flow behavior through rough-walled rock fractures: The effect of contact area. Comput. Geotech. 102, 179–195 (2018). doi:10.1016/j.compgeo.2018.06.006

Xu, C., Dowd, P.A., Tian, Z.F.: A simplified coupled hydro-thermal model for enhanced geothermal systems. Appl. Energy. 140, 135–145 (2015). doi:10.1016/j.apenergy.2014.11.050

Xu, C., Fidelibus, C., Dowd, P., Wang, Z., Tian, Z.: An iterative procedure for the simulation of the steady-state fluid flow in rock fracture networks. Eng. Geol. 242, 160–168 (2018). doi:10.1016/j.enggeo.2018.06.005

Yeo, I.W., De Freitas, M.H., Zimmerman, R.W.: Effect of shear displacement on the aperture and permeability of a rock fracture. Int. J. Rock Mech. Min. Sci. 35, 1051–1070 (1998). doi:10.1016/S0148-9062(98)00165-X

Zimmerman, R., Bodvarsson, G.: Hydraulic conductivity of rock fractures. Transp. Porous Media. 23, 1–30 (1996). doi:10.1007/BF00145263

Zimmerman, R.W.: Fluid Flow in Rock Fractures. In: Proc. 11th Int. Conf. on Computer Methods and Advances in Geomechanics. pp. 89–107. , Turin, Italy (2005)

Zimmerman, R.W., Al-Yaarubi, A., Pain, C.C., Grattoni, C.A.: Non-linear regimes of fluid flow in rock fractures. Int. J. Rock Mech. Min. Sci. 41, 1–7 (2004). doi:10.1016/j.ijrmms.2004.03.036

Zimmerman, R.W., Chen, D.W., Cook, N.G.W.: The effect of contact area on the permeability of fractures. J. Hydrol. 139, 79–96 (1992). doi:10.1016/0022-1694(92)90196-3

Zou, L., Jing, L., Cvetkovic, V.: Shear-enhanced nonlinear flow in rough-walled rock fractures.

Int. J. Rock Mech. Min. Sci. 97, 33–45 (2017). doi:10.1016/j.ijrmms.2017.06.001

Chapter 5: Thesis Summary

5.1 Conclusions

This work provides analyses of linear and non-linear flow behaviours by considering local fracture geometries at pore-scale to develop flow models at the scale of a single rock fracture. A modified cubic law has been developed to improve the linear flow prediction of the standard cubic law by incorporating the effects of flow tortuosity, aperture variation and local roughness. To model the flow non-linearity, approximate analytical solutions to the two-dimensional Navier-Stokes equations are derived under both the pressure boundary condition (PBC) and flow rate boundary condition (FBC) using the perturbation method. The derived solutions are validated against numerical simulations by applying them to the geometry of symmetric wedges and fractures with sinusoidal profiles. The FBC solution demonstrates an improved flow estimation over the PBC solution, due to a more accurate quantification of inertial effects. The derived FBC solution is then extended to cover asymmetric cases for a more realistic representation of the pore-scale fracture geometry. A non-linear version of the Reynolds equation is developed based on the extended FBC solution to provide a more accurate flow prediction and to capture the feature of flow non-linearity, which is not sufficiently considered in previous flow models for rock fractures with the complex void geometry.

5.2 Limitations

The fundamental limitation of the modified cubic law and non-linear version of the Reynolds equation, developed in this research, is in using the two-dimensional pore-scale geometry to approximate the realistic local fracture geometry in three-dimensions. Although the error produced in this approach can be constrained to a reasonable level with fine measurements of the fracture void geometry, three-dimensional flow obviously demonstrates quite different behaviours and some of the physical phenomena observed in three-dimensions (e.g., complex three-dimensional whirling flow) may not occur in two-dimensions, especially for flow in the strong inertial regime.

In addition, as a one-dimensional cubic law based model, the proposed modified cubic law is not able to incorporate the flow channelling effect in two-dimensions. Hence, the performance of the modified cubic law may not be warranted in cases where strong channelling effects are present due to a variable aperture field.

Another limitation in the non-linear Reynolds equation developed in this research is associated directly with the validity of the perturbation solution that constitutes the basis of the non-linear Reynolds equation. As mentioned in Chapter 3, the perturbation solution is derived to the second-order to account for aperture variation, aspect ratio, inertial effects and geometry asymmetry. However, as inertial effects become stronger, more higher-order terms need to be included to maintain an accurate quantification of the flow behaviours at pore-scale.

This thesis focuses mainly on flow behaviours at the scale of a single rock fracture and aims to provide flow models with improved performance in estimating fracture hydraulic properties. However, rock masses often contain fractures that intersect with each other to form complex fracture networks. Thus, the performance of the proposed models in simulating fluid flow in fracture networks can be affected by e.g., fracture intersections, and further evaluations on the model performance in such cases are needed.

5.3 Future work

The thesis has provided detailed analyses of the geometrical and kinematical effects on flow behaviours in a single rock fracture with complex void geometry. A modified cubic law and non-linear version of the Reynolds equation are developed to improve the flow estimation in rough rock fractures. For many subsurface projects in fractured rocks, fluid flow is often coupled with mechanical, thermal and/or chemical processes. As the two flow models are generally dependent only on the fracture void geometry, in the future work, both models may be conveniently used as the flow governing equations to study a series of coupled processes, providing that the contribution to the alteration of fracture void geometry from each process is well quantified.

The mathematical models presented in this work can also be further improved. The modified cubic law can potentially be extended to account for flow channelling effects by introducing a robust path searching method to find the main two-dimensional flow paths within a three-dimensional rock fracture. A direct improvement to the derived perturbation solution is to include more higher-order terms and more general boundary conditions (e.g., permeable walls), although the complexity associated with the derivation process and solution formulation is expected to increase. For the non-linear version of the Reynolds equation, the focus of the future work should be on providing an accurate quantification of flow through more realistic pore-scale geometry to improve the overall flow estimation at the scale of a fracture.